Application of Soft Computing Techniques in Power System Security Analysis

Thesis submitted by

Saborni Das

Reg. No.: 101711503007

(Index No.: D-7/E/446/16)

Doctor of Philosophy (Engineering)

Department of Power Engineering

Faculty Council of Engineering and Technology

Jadavpur University

Kolkata, India

June 2021

JADAVPUR UNIVERSITY

KOLKATA-700032, INDIA

INDEX NO.: D-7/E/446/16

1. Title of the thesis:

Application of Soft Computing Techniques in Power System Security Analysis

2. Name, Designation & Institution of the Supervisor /s:

Dr. Mousumi Basu, Professor, Dept. of Power Engineering, Jadavpur University, Salt Lake Campus, Kolkata-700098.

3. List of Publication:

[1] **Das, S.**, & Basu, M. (2020). Day-ahead optimal bidding strategy of microgrid with demand response program considering uncertainties and outages of renewable energy resources. Energy, 190, 116441.

[2] **Das, S.**, Hazra, A., & Basu, M. (2018). Metaheuristic optimization based fault diagnosis strategy for solar photovoltaic systems under non-uniform irradiation. Renewable energy, 118, 452-467.

[3] Hazra, A., **Das, S**., & Basu, M. (2017). An efficient fault diagnosis method for PV systems following string current. Journal of Cleaner Production, 154, 220-232.

[4] Hazra, A., **Das, S.**, & Basu, M. (2018). Heat transfer search algorithm for non-convex economic dispatch problems. Journal of The Institution of Engineers (India): Series B, 99(3), 273-280.

[5] Hazra, A., **Das, S.**, Basu, M., & Laddha, A. (2019). Multi area power dispatch strategy considering economic and environmental aspects using NDSGA II. International Journal of Hybrid Intelligence, 1(4), 308-325.

[6] Ganguly, D., **Das, S.**, Hazra, A., Laddha, A., & Basu, M. (2019). Improved real coded genetic algorithm-based short-term hydrothermal generation planning. International Journal of Hybrid Intelligence, 1(2-3), 118-146.

[7] Hazra, A., **Das, S.**, Laddha, A., & Basu, M. (2020). Economic Power Generation Strategy for Wind Integrated Large Power Network Using Heat Transfer Search Algorithm. Journal of The Institution of Engineers (India): Series B, 1-7.

4. List of Patents: Nil

5. List of Presentations in National/International/Conferences/Workshops:

[1] **Das, S.**, Hazra, A., Basu, M., & Laddha, A. (2017, September). Optimized hydel-thermic operative outlining using grey-wolf optimizing technique. In 2017 IEEE International Conference on Power, Control, Signals and Instrumentation Engineering (ICPCSI) (pp. 1753-1758). IEEE.

[2] Hazra, A., **Das, S.**, Sarkar, P., Laddha, A., & Basu, M. (2017, March). Optimal allocation and sizing of multiple DG and capacitor banks considering load variations using water cycle algorithm. In 2017 4th International Conference on Power, Control & Embedded Systems (ICPCES) (pp. 1-6). IEEE.

[3] Hazra, A., **Das, S.**, Basu, M., & Laddha, A. (2018, December). Optimal Torque Control of Parallel Hybrid Power Train based Hybrid Electric Vehicle. In 2018 8th IEEE India International Conference on Power Electronics (IICPE) (pp. 1-6). IEEE.

[4] Hazra, A., **Das, S.**, Basu, M., & Laddha, A. (2017, December). Optimized power operational strategies through DISGEN in a railway rake up keeping depot. In 2017 IEEE Transportation Electrification Conference (ITEC-India) (pp. 1-6). IEEE.

[5] Laddha, A., **Das, S.**, Hazra, A., & Basu, M. (2017, November). Implementation of social spider optimization for optimized hydel-thermic operational delineation. In 2017 IEEE PES Asia-Pacific Power and Energy Engineering Conference (APPEEC) (pp. 1-6). IEEE.

[6] Ganguly, D., **Das, S.**, Hazra, A., Basu, M., & Laddha, A. (2017, November). Optimalized hydel-thermic operative planning using IRECGA. In 2017 Third International Conference on Research in Computational Intelligence and Communication Networks (ICRCICN) (pp. 68-73). IEEE.

JADAVPUR UNIVERSITY

KOLKATA-700032, INDIA

"Statement of Originality"

I, **Saborni Das**, registered on 4th July 2016 do hereby declare that this thesis entitled "**Application of Soft Computing Techniques in Power System Security Analysis**" contains literature survey and original research work done by the undersigned candidate as part of Doctoral studies.

All information in this thesis have been obtained and presented in accordance with existing academic rules and ethical conduct. I declare that, as required by these rules and conduct, I have fully cited and referred all materials and results that are not original to this work.

I also declare that I have checked this thesis as per the "Policy on Anti Plagiarism, Jadavpur University, 2019", and the level of similarity as checked by iThenticate software is 6%.

Signature of Candidate: Saborni Das

Date: 29.06.2021

Moumita Basu

Professor
Dept. of Power Engineering
Jadavpur University, Salt Lake Campus
Kolkata-700 098

Certified by Supervisor (s):
(Signature with date, seal)

JADAVPUR UNIVERSITY

KOLKATA-700032, INDIA

Certificate from the Supervisor/s

This is to certify that the thesis entitled "**Application of Soft Computing Techniques in Power System Security Analysis**" submitted by **Smt. Saborni Das**, who got her name registered on 4th July, 2016 for the award of Ph. D. (Engineering) degree of Jadavpur University is absolutely based upon her own work under the supervision of **Prof. Mousumi Basu** and that neither her thesis nor any part of the thesis has been submitted for any degree/diploma or any other academic award anywhere before.

Mousumi Basu

Professor
Dept. of Power Engineering
Jadavpur University, Salt Lake Campus
Kolkata-700 098

29.06.2021

_____

Signature of the Supervisor and

Date with Official Seal

Dedicated to

My Parents

&

Family Members…

Acknowledgement

I take this opportunity to express my sincere gratitude for my supervisors, Prof. Dr. Mousumi Basu for her guidance, patience, and encouragement during the whole period of my PhD journey. During the course of the PhD work, she continuously provided me with enthusiasm, vision and wisdom. The guidance received from her cannot be acknowledged with few words. Her unconditional love, moral support and lucid illustrations of the technical matters have made my PhD journey memorable.

I am extremely thankful to all the members of the respected Doctoral Committee for the valuable internal reviews they provided regarding the work which was pivotal in giving a perfect blend to the thesis.

I am also grateful to the Head of the Power Engineering Department for providing the necessary departmental laboratory and library facilities during my course of work. I would like to extend my heartfelt gratitude to all faculty and non-teaching staffs of this department for their helpful attitude and constant encouragement.

The work of this dissertation has been supported and funded by the PURSE-II Program, Department of Science & Technology, Government of India. and I acknowledge the support that was provided by them.

I want to thank all my beloved lab mates Dr. Abhik Hazra, Ashish Laddha, and all other seniors and juniors who have helped me through this journey. The best part of having such people in my lab has been that they have always made me feel insecure with their outstanding research capabilities and thus I was compelled to push myself further so that I could achieve my goal.

Most importantly, I want to pay my deepest gratitude to my parents Mrs. Ashima Das and Mr. Jugal Chandra Das and my parents-in-law Mrs. Mamata Saha and Mr. Manik Saha for their endless support, care and love with lots of blessings. My brothers Pinaki and Ranajit, sisters Mahua and Jayita, auntie and uncle deserve my wholehearted thanks for providing their constant support and selfless love.

I owe gratefulness to a very special person, my husband, Mr. Amit Saha for his continued and unfailing love, support and understanding during my pursuit of Ph.D degree that made the completion of thesis possible. I appreciate my baby, my little boy Ahnik for abiding my ignorance and the patience he showed during my thesis writing. Words would never say how grateful I am to all of you. I consider myself the luckiest in the world to have such a lovely and caring family, standing beside me with their love and unconditional support.

Finally, I would like to thank God and the role of millions of countrymen who do not have much to eat or wear and who could have been fed and clothed with the money used for supporting my research and many others like mine.

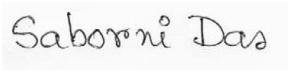

Saborni Das

Jadavpur University

List of Figures

List of Tables

Abstract

For the last two decades, global as well as regional energy scenarios have been experiencing various challenges due to rapid exhaustion of conventional fossil fuels and subsequent high-level penetration of integrated renewable energy resources into the modern power system.

Prompt population expansion, social-economic development, and technical advancement, ecological pandemonium make mankind to rethink on the strategic utilization of residual fossil fuels and integration of renewable energy resources which are of stochastic and intermittent in nature. All these issues significantly dispute the secure planning, operation and management of the power system. Thus, analysis of the overall technical, ecological and economic security of power systems with renewable energy resources has become challenging and widely trending in present years.

Power system security analysis deals with sudden interruptions or contingencies in the system. A power system, in normal operating condition, may face contingency conditions, such as component outages or faults in generating units and other power system components, uncertainties or sudden changes in renewable energies and load demand from the forecasted values and so on.

Initially deterministic approaches were being exercised for power system security analysis. But the stochastic system behaviors are unaccounted for in such methodologies and their practice does not reflect actual scenarios of the underlying phenomenon. Consequently, different soft computing techniques were gradually being adopted for power system security studies. This dissertation is oriented towards some research advancements in this area.

The power system security tradeoffs that are presented here incorporate component outages and uncertainty issues of power system and their solution using soft computing techniques.

Module level outage is considered in case of open circuit and short circuit fault diagnosis of photovoltaic system using soft computing techniques. Identification of outages of photovoltaic modules, determination of type of module faults and tracing the location of the faulty modules in a photovoltaic array are effectively performed using improved real-coded genetic algorithm.

Another study incorporates outage scenarios of renewable components in case of day-ahead bidding in microgrid. The study also focuses on uncertainties related to load demand, renewable energy generations and outage schedules and their distributions during day-ahead bidding planning. To deal with outages of renewable generations different probability distribution functions are adopted. Demand response program is formulated considering outage-based contingencies. Chaos theory is introduced to generate stochastic scenarios of uncertain variables. The reserve and penalty costs for erroneous estimation of renewable energies are cited to design more secure economic bidding. To deal with uncertainties two-stage stochastic programming is adopted. This stochastic bidding problem is structured as a mixed integer nonlinear optimization problem and is solved using soft computing based LINDOGlobal solver.

Table of Contents

Chapter 1

Introduction

1.1 Power system security

One of the major interdisciplinary applications of the reliability engineering is found in the dominion of power system. Roy Billinton is considered as a pioneer as well as the father of power system reliability [1]. According to Billinton *et al*, it considers *all aspects of the ability of the power system to perform its intended function of providing an adequate supply of electrical energy to customers efficiently with a reasonable assurance of continuity and quality* [2]. The studies of power system reliability can be segregated into two main domains, *viz.*, adequacy and security. The adequacy analysis focuses on the evaluation of adequate facilities prevailing within the power system to meet all the system operational constraints and consumer load demand. However, it deals only with static conditions and does not account for system dynamic disturbances and transient conditions. Conversely, the security analysis focuses on the power system contingencies and uncertainties. It is defined as the ability of the system to restore, manage and operate under stable conditions undergoing component outages or a major change (uncertainty) in the system. Hence, power system security analysis can be represented in twofold aspect: component outages and uncertainties.

1.1.1 Component outages

Component outages play a major role in case of the pre-event planning and the post-event recovery of the concerned power system. However, the task of exact prediction of the states of components is highly challenging and difficult. Component outages are subdivided into two modes: the independent outages and the dependent outages. The independent outages of the power system components can be further categorized as follows: the forced outages, the planned outages, the semi-forced outages, the partial and the multiple failure modes. The forced outages are comprised of the repairable failures

and the non-repairable failures. Non-repairable failures involve failure by aging and by chance. The aging-based failures of components necessitate risk evaluation once the components reach at the end stages of their shelf lives. The dependent outages are generally classified based on common causes, component grouping, station originated, cascading phenomenon and environment dependent failures. The dependent outages generally entail outages of more than one power system component. The dependent outages further cause much more severe and frequent consequences than the independent outages [2].

1.1.2 Uncertainties

At present, uncertainties in power systems is an ongoing security issues, particularly in the modern renewable integrated power systems. The task to accurately presume the current and the future states of power systems parameters is very difficult because of many underlying uncertainty issues which are exposing the systems to repeated potential disturbances. The power systems must deal with lots of uncertain parameters such as loads, electricity prices, photovoltaic (PV) power generation, wind power generation, outage forecast, plug-in electric vehicles and load growth which need appropriate uncertainty modeling and management at different stages of planning and operation within an integrated power system framework. Typical forms of uncertainty issues are as shown as in Figure 1.1 [3].

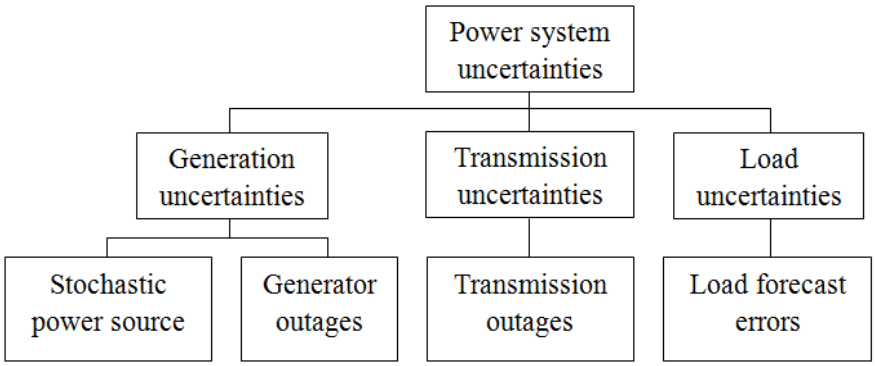

Figure 1. 1 Typical power system uncertainties.

1.2 Motivation & importance of the study

Security analysis has been quietly studied in power system associated mainly with conventional energy sources. However, future projection of energy scenario indicates extensive infiltration of renewable energy resources in most of the power systems around the world. But, high level integration of renewable energy resources brings about, additional social, technical, and economic challenges jeopardizing the power system security. Most likely,

1. Renewable energy is to some extent random and sporadic due to the uncertainty in the resources (wind speed, solar irradiation, wave speed, availability of biomass etc).
2. Extremely harsh environmental condition and remoteness of the distributed generation (DG) plants make system more prone to unplanned component outages and various faults frequently.
3. Renewable power systems generally are installed at far of locations and, they require vast installation area. All these make it difficult for regular maintenance, human patrolling, and result into costly monitoring.
4. The renewable generation depends on climatic condition and forecasting and results into uncertainty, unavailability, and power quality issues.
5. Harsh weather and pollution degrade and corrode renewable power systems components very soon.
6. Injection of renewable systems in the existing power system involves many technical complexities, incorporates additional faults.
7. The co-existence of grid connected, and grid disconnected modes amplifies the complexity of the power system.
8. Installation and maintenance costs of renewable systems are very high as compared to conventional power system.

Hence, studies of security analysis of integrated power systems with an intense focus to renewable energy resources are highly relevant in such situation.

For power system security analysis, initially the deterministic approaches, *viz.*, n–1 contingency security criterion were customarily used. However, over or under

redundancy is extremely difficult to avoid for the cases based exclusively on such methodologies. The stochastic behaviors of the systems are left disregarded in such approaches and consequently their usages may not reproduce actual scenarios of the underlying events. Consequently, the techniques that include probabilistic features were gradually being adopted. These resulted in qualitative and quantitative indices for better management of system intermittency and confident decision making throughout different stages of power system planning and operation respectively. Statistical review of the past performances and probabilistic estimation of the future performances in the planning, operation and management of a power system render a realistic vision of the security analysis being carried out. Moreover, to tackle any sort of noise in the inputs, uncertainties in the system and to achieve solution in real time, wide range of soft computing techniques are gaining popularity for various applications in power system security analysis. The term soft computing technique was coined by Lotfi A. Zadeh. According to him, the soft computing techniques *aim to exploit the tolerance for imprecision and uncertainty to achieve tractability, robustness, and low solution cost.* Its major components are optimization, neural computing, and fuzzy logic [4].

In this context, this dissertation presents an overview of power systems security analysis using soft computing techniques and touches upon some of the following research advancements in this realm.

1. **Component outages.** The dissertation focuses on various component outage events and their solution strategies accordingly. PV module outages due to open circuit and short circuit faults and their diagnosis using soft computing optimization techniques will be studied. Here, identification of outages of PV modules, differentiation of fault types and tracing the fault location in a PV array are considered. Another study of optimum day-ahead energy bidding planning for microgrid aims to incorporate of outages of renewable systems in the bidding model.
2. **Uncertainties.** The uncertainties related to renewable energy generations, load demand, and outages of renewable systems and their forecasts are considered in the study of optimum day-ahead energy bidding planning for microgrid. Different

methods those can minimize the effects of uncertainties and outages on day-ahead bidding are studied in the dissertation.

1.3 Recent advancements and challenges

Numerous compendia of literature contributed to different state of art in the vast domain of power system security analysis. In this section, we review relevant research advancements on the fault diagnosis of PV system, day-ahead bidding of microgrid and their challenges correspondingly.

1.3.1 Fault diagnosis of PV system

Sustained policy supports and cost reductions are continuously boosting strong renewable energy growth. It is expected that total installed renewable capacity is on target to surpass natural gas by 2023 and coal by 2024. Solar energy alone will account for 60% of all renewable energy additions through 2025 [5].

However, several security issues of PV technologies persist and are hindering the widespread industrialization of the PV energy sector. Numerous anomaly conditions such as mechanical damages, aging degradation, and electrical faults in various components of PV system (cell, module, array/ string, bypass diode, other system apparatus) have been stated [6]. These significantly mortify the performance and efficiency of the whole system. Electrical faults and outages that significantly degrade electrical output in a PV system are mostly short circuit (SC) fault and open circuit (OC) fault. To deal with SC faults and OC faults in PV systems, profound studies on fault diagnosis are being carried out nowadays.

Module level fault diagnosis techniques for SC faults and OC faults in PV system are generally founded on threshold evaluation, domain alteration, categorization, evaluation of state and amalgamation among the aforesaid methods [6], [7]. These methodologies generally investigate outputs and different operating states of PV system and afterward compare the measured data with the simulated data, or the PV electrical yields attained either from the simulated PV system or the reference data supplied by various well-developed algorithms or practices.

In several works [8]-[10], voltage and current indicators were compared with the threshold standards for detection of faulted PV array to recognize and categorize OC and SC or bypassed module faults. In the study [11], a simple analytical comparison between simulated and measured power outputs was made with the intention to reduce the figure of installed sensors. This technique only determined the number of faulted modules in PV array. Fault diagnosis idea, presented in [12], modeled a procedure founded on supervising and comparison of simulated and measured both AC and DC power outputs to classify the PV array faults and inverter faults. Although it traced the open circuited PV array but was unable to trace the position of detached modules in PV array. Expenditure reduction by means of minimization of sensor number was also regarded in [13] to find the quantity of module level OC and SC faults and make a distinction between the fault behaviors with partial shading. This method was founded on monitoring of voltage of PV array and evaluation of such with personalized trained set of data. Though, for unlike PV system set ups and ambient settings, diverse training sets of data are required. Preparation of such training data is cumbersome. Various other comparison dependent PV fault detection methodologies employed experimented and simulated current-voltage characteristics of PV systems [14-18]. Although threshold limits for comparison purpose were not talked about. In the work [18], only OC kind fault was diagnosed. Conversely, several current-voltage characteristics-based detection practices presented in [19]-[22] specified threshold limits. In [20] a set of threshold errors was defined to detect the fault events in PV array, but the technique was unable to differentiate between SC fault and partial shading. The work in [21] presented threshold assessment fault identification experiencing variable cloud conditions. Authors of the work [22] used artificial neural network (ANN) along with the threshold assessment to classify the faults showcasing identical set of characteristics. But locations of faults were not conferred in the above mentioned current-voltage characteristics based PV fault detection techniques. Further studies too employed ANN for PV fault diagnosis. Triple layered feed forward type ANN was used for the diagnosis of SC fault position of PV array in the work [23]. One more work [24] demonstrated the deployment of enhanced wavelet ANN algorithm. In the study [25], ANN is united with analytical techniques to identify the faults in PV array. However, the position of faulted PV modules in a array

remain untraceable using the proposed ANN based fault diagnosis techniques. Other smart methods, for instance machine learning (ML), also were used for module failure detection purpose. Support vector machine dependent method for the discovery of only SC fault was described in the work [26]. In the study [27], graph-based semi-supervised ML was introduced to perceive and categorize OC and line to line faults considering the array current and voltage output, temperature, and irradiation data. All the proposed ANN and ML based diagnosis approaches need training data to be labeled as normal, SC or OC conditions. However, labeling the data is quite costly and intricate. In addition, these methodologies did not portray location data of the defective modules. The authors in their study [28], depicted a different scheme based on measurement of earth capacitance (MEC) to trace the detachment in a array and the time domain reflectometry (TDR) to discover module degeneration. Other works [29]-[33] also exploited TDR for identification of the OC faults and the SC faults in PV system. But both the TDR and MEC only work offline. However online techniques for fault diagnosis are extremely desirable to assess malfunction during operating condition of PV system. Several additional fault diagnosis methods employed sophisticated apparatus, for example thermal imaging, infrared thermographs, photoluminescence, and electroluminescence. In [34], thermal sensor-based cameras were implemented to perceive the characteristics of temperature distribution of PV array under the OC fault and the SC fault occurrence. But with time, gradual quality drop in the thermal images (because of device aging and dilapidation) of PV system with time poses accuracy problem and other technical challenges [35]. Additionally, elevated installation expenses of the thermal camera equipment bound their wide applications in case of fault analysis.

The compendium of research works gives an insight of the extensive interests in diverse fault diagnosis schemes of PV system. It is clearly distinguished that nearly all of the fault diagnosis approaches presented in the aforesaid literatures have shown some intricacies to absolutely diagnose the SC faults and the OC faults while simultaneously identifying the positions of faulty PV modules in the array. Some methods can detect only the SC faults, while some can find the OC faults only. Few can differentiate the faulty or the healthy PV array. Few of them are only able to perceive the figure of the OC faults and the SC faults in a PV array. Some can only discriminate between the OC faults

and the SC faults. Although, most studies can identify faulty PV array, but every distinct method alone countenance difficulty to concurrently detect and identify the location of flawed modules in a PV array. A PV array in any large-scale PV plant is generally consisted of thousands of PV modules [36]. Consequently, tracing the faulty PV modules by only human monitoring and calibration of a PV array is chaotic, incompetent and time consuming. Although in few works, attentions have been given to the detailed detection of locations of faulty PV modules in an array, the techniques are offline [28-33], costly and intricate [34-35].

The above milieu portraits the need of adept fault diagnosis stratagems which can identify short and open circuited PV modules and the respective fault locations even during the operating state of PV systems, over and above, which are simple, robust, economic, and reliable.

1.3.2 Day-ahead bidding of microgrid

Microgrid with the combination of intelligent technologies has become the central part of any smart grid. It aims to supply efficient electricity of enhanced power quality to off-grid autonomous end user sites with better convenience, reliability, and economic way. Microgrid continues to transform with elevated incorporation of modern technologies, distributed energy sources, competent energy storage units and significant consumer partaking through demand response program (DRP) or demand side management [37], [38]. A smart microgrid assists bidirectional interface between microgrid operator or customer and utility grid. However, unknown uncertainties inclusion in decision variables (e.g., market price of electricity, load demand, and decision of customer) amplifies the complexity of energy management of microgrid [39]. Furthermore, uncertain climate condition, volatile and intermittent renewable energy resources and the related outages intensify the challenges of microgrid operator to precisely forecast the decision variables and to manage and to plan the electricity bids in the day-ahead energy market [40], [41]. Therefore, it is extremely crucial for microgrid operator to schedule well-organized energy management program and implement optimum bidding strategy, in order that the revenue from the partaking in the real time energy market are maximized with least risk

due to forecasting of future tendency of load consumption, renewable generation and electricity prices.

With the intention of profit maximization in the electricity market and the reliability augmentation of power system, microgrid operators accentuate to devise the paramount bidding policy by means of different heuristic approaches and stochastic programming (SP), which have been widely executed in literature [42]-[55] and validated using various sophisticated tools and commercial power system software [56].

Bidding strategy presented in the work [42] used Q-learning to maximize the revenue of utility customers. A dispersed load shedding scheme has been implemented as DRP [42]. However, this proposed machine learning dependent bidding approach [42] has not taken uncertainties for consideration as decision variables. The ref. [43] has considered uncertainties regarding PV and wind turbine (WT) power, the intra-day and online energy market prices using probability distribution functions (PDFs) and resolved bidding strategy problem of microgrid by means of stochastic programming. Different scenarios were generated using neuro-fuzzy tree modeling [43]. Ref. [43] did not precisely express the problem as they ignored nonlinearities and supplementary constraints. A bidding strategy based on genetic algorithm was projected for PV incorporated microgrid system as presented in the study [44]. Here, Analog Ensemble kind sampling was employed to estimate the probability of future PV generation and to count uncertainty. In the work [45], a hybridized stochastic and robust optimization for bidding in combined electricity and reserve market was developed considering elastic ramping multiplier. The real time uncertain energy prices scenarios were produced using K-means cluster. A different study [46] also utilized robust optimization approach to model the uncertainties only in grid electricity prices. The scenarios of electricity prices were produced by subdividing the subsections inside lower and upper forecast boundaries. Penalty dependent time-of-use DRP were employed to reduce electricity cost amount during energy bidding by a grid coupled microgrid.

Few studies [47]-[54] disintegrated bidding tactic of microgrid into dual-phase optimization problem. Scenario production and diminution of uncertain attributes are

accomplished in the first phase. While in later phase optimum bids, allied revenues, and operational schedule of microgrid systems are decided. Ref. [47], presented mixed integer nonlinear programming (MINLP) for solving dual-phase bidding optimization. Latin hypercube sampling (LHS) was used to generate day-ahead power scenarios. SP was employed to handle uncertainties in load demand, wind velocity and solar radiation. In the study [48] bi-stage SP was also exploited for scheduling generation and maximization of profit during optimal bidding planning of microgrid. The scenarios of system uncertainties were created using Monte Carlo simulation (MCS). A different dual-phase SP based optimal bidding plan was framed as depicted in the study [49] and then solved with mixed-integer linear programming. Here, consequences of uncertainty in renewable generation and energy price were treated by means of robust optimization and minimization of unbalanced energy in online market. The scenarios were generated in stochastic manner. The authors in work [50] modeled linear programming for dual phase bidding strategy implementation in AC/DC microgrid to reduce the cost of operation and control heating and cooling program of the joint heat and electricity unit. Uncertainties regarding energy prices, load and the ambient temperature were dealt with scenario hierarchies. The scenarios were generated stochastically. 'Conditional value at risk' (CVaR) criterion was commenced for a dual-phase stochastic bidding planning in the work [51] to assess the efficacy of the results. To produce the scenarios of uncertain load demand, wind velocity and solar insolation LHS was employed. A stochastic bidding with double auction framework was projected in ref. [52], where dual-phase SP was utilized to reduce cost of operation and to boost energy yielding capacity of microgrid during the bidding. The uncertain scenarios of power output and the load profile were exploited via MCS. The binary auction bidding system in the work [53] aimed at maximization of social wellbeing of both electricity purchaser and retailer of a PV incorporated microgrid. However, no uncertainty associated issue was mentioned in this work. Instead, stochastic scenarios were framed. A hierarchical marketplace was fabricated in the ref. [54]. At initial phase the effects of scenarios of uncertain renewable output were generated with risk controlled MCS and at subsequent phase market bided amount was decided with the intention of profit maximization of microgrid operator. To avoid dealing uncertainties using opportunistic or robust mechanisms, the work [55]

projected theory of information gap assessment to cope up with the risk of the uncertainties throughout bidding planning of microgrid. The scenarios of this multi-objective optimal bidding problem were generated with MCS.

As stated above a variety of scenario generation methods were adopted regarding various uncertain attributes. Such as the work [42] employed machine learning. But, the process of training and labeling data is quite expensive and intricate. Ref. [43] used neuro-fuzzy logic, which too involves costly and complicated learning algorithm based on neural network. In the work [45], an unsupervised machine learning named K-means clustering was employed. Amid the allied complications of machine learning methods, assessment of the K-value is difficult. Moreover, it may not work for global clustering. Accordingly, the learning dependent scenario creation mechanisms necessitate expert and rigorous human efforts. Various sample making techniques, for instance LHS in the studies [47] and [51] and MCS in the ref. [48], [52] and [54], were implemented to model the scenarios. However, these techniques involve enormous samples of past data no less than 1000 [55]. Sampling of such massive data gives rise to accuracy issues and increases computational burden. So, diverse intricate reduction techniques are necessary. The management of such gigantic data and therefore the generation and reduction of scenarios are burdensome, complex and involve immense risk [49], [57], [58].

On the contrary, stochastic or random scenario generation [44], [49], [50], [53] and subdividing the forecast boundaries [46] were implemented in several studies. However, these methods do not abide by any ruling and work though the hit and the miss action. Hence, chance of losing a set of data is high. So, huge figure of scenarios is needed to produce. Following these concerns regarding scenario generation, an apposite chaotic mapping technique is introduced for mapping the entire uncertain scenarios [59]. Chaos theory is profoundly documented and aptly fitted for dynamic systems which are very sensitive to the initial setting [59]. Chaos is non-converging, non-repetitive and executes well inside restricted provisions. Chaos mapping is on the other hand more robust and ordered than stochastic scenario generation mechanisms. Moreover, chaotic sequences perform swiftly and are effortless to create and store, because lengthy sequences are

removed in the course of operation. In this work, tent mapping [60] is employed to produce chaos sequences.

The studies stated above characterized uncertain character of the day-ahead electricity prices, renewable generations, load, and additional decision variables using different PDFs or time series profiles founded on the historical and the predicted data. The sporadic behavior of renewable recourses, inaccessible and insensitive ambience of renewable integrated power systems result into frequent outages of renewable components. Moreover, the outage probabilities of renewable systems track several defined formulas or PDFs regarding the categories of failures, for example aging, weather based and repairable failure [61]-[62]. But, considering the aforesaid review on bidding of microgrid it is evident that none of the studies implemented the outage modeling of renewable energy systems or uncertainties related to outages in case of formulation of bidding plan for microgrid. Furthermore, the bidding tactics presented in [38], [43], [46], [55] incorporated DRP to merely release load during expensive periods or peak demand. However, DRP integration during sudden energy crisis or renewable generation outages can significantly secure microgrid reliability and reduce operation costs. Considering the facts, this work proposes an optimal day-ahead bidding strategy for microgrid taking into account both emergency and price dependent DRP formulation and the outages of renewable energy resources, uncertainties relating to outages.

1.4 Summary of main contributions

The works presented above represent advancements in the area of power system security analysis in case of fault diagnosis in PV system and bidding strategy planning of microgrid. They highlighted not only the component outages and uncertainty issues but also provided various solution mechanisms based on different soft computing techniques. The contributions of this study to the aforesaid advancements are discussed below.

1.4.1 Optimization based fault diagnosis of PV system

A new framework is proposed which addresses the aforementioned challenges in open and short circuit fault diagnosis of PV system. It is accomplished through novel

implementation of optimization techniques in the projected fault diagnosis method, which not only identifies faults, in addition traces the location and differentiates between short and open circuited PV modules in a functioning PV array experiencing heterogeneous irradiation and temperature condition.

Implementations of the optimization methods in the realm of PV fault diagnosis are present in literature [63]-[65]. Attempts were taken for the optimal positioning of voltage sensors in PV system [64] and extraction of parameters from I-V characteristic curves by means of optimization techniques for instance differential evolution and artificial bee colony [63]-[65] for fault identification. In these studies, optimization techniques were employed to perform peripheral objectives of PV fault diagnosis. However, this study directly employs metaheuristic optimization approaches for PV system fault diagnosis and utilizes their heuristic property to quantify, identify and locate the OC and the SC module faults.

The philosophy behind the projected mechanism is to search a certain fault pattern that results in an exclusive power outcome of PV array, as the power output of each PV module of a large-scale PV array, undergoing varied temperature and irradiation distribution, is dissimilar. This fact is subjugated here in the study to devise objective function. In essence, the fault diagnosis technique deploy metaheuristic as a search tool to identify the probable fault pattern of modules, number of faulted PV modules and the fault locations in the PV array for a particular temperature and irradiation condition prevailing at that moment, which may result in the identical array power outcome as the physically measured power output of that faulted PV array.

Thus, an implicit goal of the study is to discover the ability of optimization methodologies in the diagnosis of the OC faults and the SC faults in PV system. As of mathematical viewpoint, a faulted PV array is a multi-constrained, non-linear, and multi-modal system. Metaheuristic algorithms, for example the evolutionary rule and the swarm intelligence, are well customized methods to resolve such extremely constrained, non-linear, and multi-modal problems and to discover the global solution efficiently. Amongst evolutionary processes, Improved Real-Coded Genetic Algorithm (IRGA) [66]

is opted for optimization in the proposed study. Accordingly, the contributions of the work are presented as follows:

- A fault diagnosis methodology based on soft computing optimization is projected for PV system.
- Module outages due to open circuit and short circuit faults under non-uniform temperature and irradiation conditions are diagnosed.
- The faults are identified, differentiated and located simultaneously using the proposed method.

The proposed scheme is tested on a PV arrangement of 3kW placed in the lab facility of the power engineering department, Jadavpur University. To execute the experiment, Matlab simulation model replicating the existing PV system setup is fabricated and random state of affairs, which correspond to various probable fault combinations, are produced on the existing PV setup. The PV array power outcome functioning at maximum power point (MPP) is attained from the array inverter (DC side). The measured and simulated array power outputs are fed to an internally embedded Matlab code for the projected fault identification algorithm employing IRGA. Being soft computing based technique; the projected method does not require a lot expensive sensing devices or other complicated appliances. Moreover, it makes the online fault detection mechanism robust, economic and simple.

1.4.2 Optimal bidding plan of microgrid under outages and uncertainties

With the purpose of accomplishment of better bidding plan outline for renewable energy incorporated microgrid in the day-ahead electricity marketplace. The uncertainties regarding renewable systems and associated outages during microgrid operation are considered and solved by means of MINLP. The probabilities of renewable power outcomes uncertainties are decided by means of well-founded PDFs, for example, Lognormal PDF for PV system, Weibull PDF for WT system. Outages of renewable generators are evaluated via three major failure categories. They are weather contingent, aging and repairable failure. DRP based on emergency outage and time of use (TOU) is considered here to decide demand response resources. Besides, for the first time in case

of bidding stratagem development of microgrid, reserve cost for over-estimation and penalty cost for under-estimation of renewable outcomes are integrated to the original cost to promote microgrid operator to decide adequate dispatch scheduling during bidding in order that the energy imbalances in the real-time energy market is minimized. All the mentioned issues regarding renewable energy outages and the uncertainties accelerate risk for the microgrid operative authorities to take part in the aggressive and volatile bidding marketplace. To deal with these risks tow criterion, *viz.*, 'value at risk' (VAR) and the 'conditional VAR' are utilized during bidding optimization.

Case studies on a renewable integrated microgrid containing three gas turbines (GTs), a PV system, a WT system, and an energy storage system (ESS) have been exercised. Large number of technical and operational constraints and strict modeling of microgrid component led to an optimal bidding problem of MILNP format. The novel contributions provided by the work are as follows:

- Day-ahead bidding strategy for microgrid is planned considering outages and uncertainties
- Both emergency outage and price based DRP modelling are exercised.
- Tent mapping of chaos theory is implemented to map the entire intermittent scenarios of renewable systems, load, and outages inside confidence intervals.
- The reserve costs and the penalty costs for the over and the under estimation of renewable energy outputs are incorporated in cost modelling.
- A novel bidding objective function considering system outages and uncertainties and their risk management is formulated as mixed integer non-linear programming and is solved using soft computing based LINDOGlobal solver.

1.5 Dissertation organization

The rest of the dissertation is planned as follows. It begins by developing problem formulation in Chapter 2. In this chapter, the requisite mathematical formulations of above stated power system security problems containing analytical expressions, constraints and objective functions are developed. For the first problem, *viz.*, optimization based fault diagnosis of PV system, mathematical modeling of PV system, module outage

patterns, fitness functions and simulation based diagnosis blocks are modeled. For the second problem, *viz.*, optimal bidding plan of microgrid under outages and uncertainties, modeling of energy market, day ahead bidding strategy, uncertainties of renewable energy output, outages and load, tent chaos mapping within confidence interval, cost modeling of energy generation, DRP, objective functions and constraints and risk managements are presented.

In Chapter 3 various soft computing solution methodologies are discussed. Description of improved real-coded genetic algorithm and task flow of the same for open circuit and short circuit fault diagnosis of PV system are provided. Another soft computing technique, LINDOGlobal solver for the solution of MINLP is discussed for optimal bidding planning of microgrid experiencing uncertainties and outages.

The Chapter 4 presents the results and discussions for different case studies. For the performance assessment of the optimization-based fault diagnosis of PV system twelve sample cases are studied. Six scenarios are assessed for validation of the optimal bidding strategy of microgrid under uncertainties and outages. The relevant results are presented and limitations of the works are also discussed.

Lastly, the dissertation is concluded in Chapter 5. The chapter also highlights several potential avenues for future study in the field of power system security.

This page is left blank intentionally.

Chapter 2

Problem formulation

For the development of mathematical formulation of the power system security problems stated in the previous chapter requisite analytical expressions, constraints and objective functions must be modeled. Thus, problem formulations of the power system security problems are stated in this chapter.

2.1 Problem formulation of optimization-based fault diagnosis of PV system

2.1.1 PV system modeling

A PV array is made up of a number of PV modules. They are arranged in parallel or series or combinational connection electrically to generate power at a required voltage and current level. Each module in an array is generally shunted by a bypass diode in the reverse polarity to shun hotspot development during module OC faults. In a PV module, numerous solar cells are assembled in different series-parallel combination to achieve requisite current-voltage (I-V) characteristics and the power outcome P_{Module} as modeled in (2.1) and (2.2) respectively [67]. The equivalent circuit configuration of PV module containing N_s and N_p number of the series and the parallel connected cells respectively is depicted in Figure 2. 1.

$$I_{Module} = N_p I_{ph} - N_p I_s \left[exp \left\{ \frac{q}{AKT} \left(\frac{V_{Module}}{N_s} + \frac{IR_s}{N_p} \right) \right\} - 1 \right] - \frac{1}{R_{sh}} \left(\frac{N_p V_{Module}}{N_s} + IR_s \right) \quad (2.1)$$

$$P_{Module} = I_{Module} . V_{Module} \quad (2.2)$$

Here, I_{Module} is the module current and $V_{Module}$is the voltage output. I_{ph} represents the photocurrent. I_s symbolizes the diode reverse saturation current. q is the electron charge whose value is 1.6022×10^{-19} C. A represents ideality factor of the diode. The value

of Boltzmann constant K is 1.3807×10^{-23} JK^{-1}. R_s and R_{sh} are the series and shunt resistances. T is the module operational temperature T_{Module} that can be derived using ambient temperature $T_{Ambient}$ as formulated in (2.3) [68].

$$T_{Module} = T_{Ambient} + \frac{(NOCT-20)G_{Module}}{800} \tag{2.3}$$

Here, $NOCT$ is normal operating cell temperature (at 800 W/m^2 irradiation and 25°C air temperature). G_{Module} is the module irradiation level (W/m^2).

2.1.2 Realization of faults in PV model

Each PV module in an array may possibly experience one of the three circumstances at any instant: connected to the array or in healthy condition, shunted through a conductor (SC fault) and open circuited from the array (OC fault). The circumstances are as shown in Figure 2. 2.

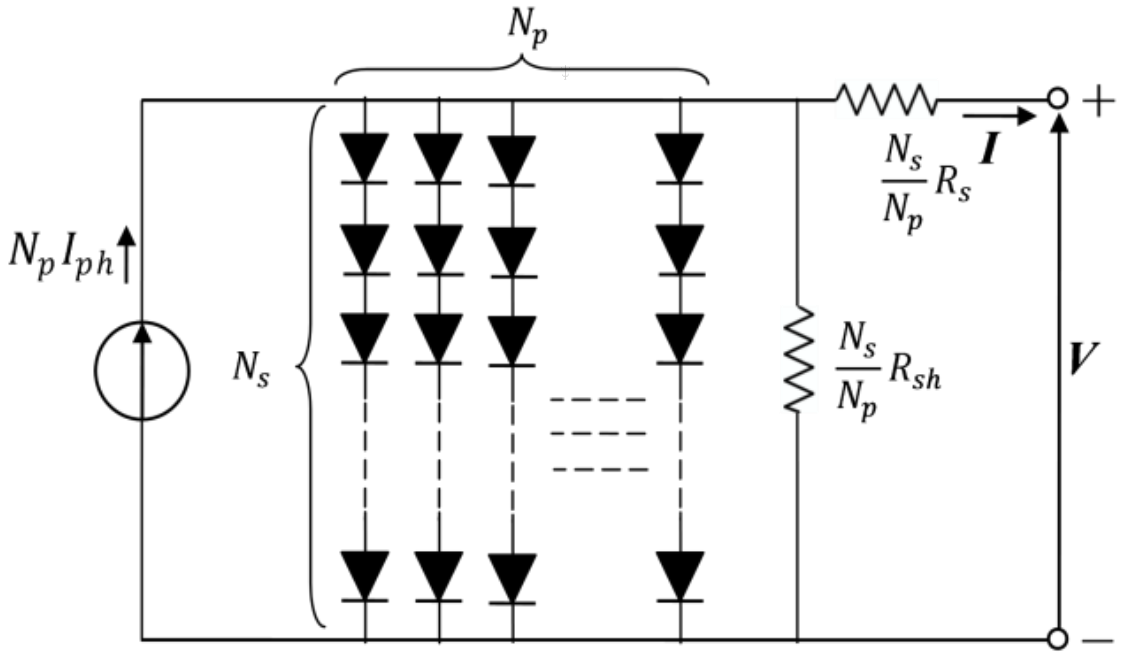

Figure 2. 1 The equivalent circuit configuration of PV module.

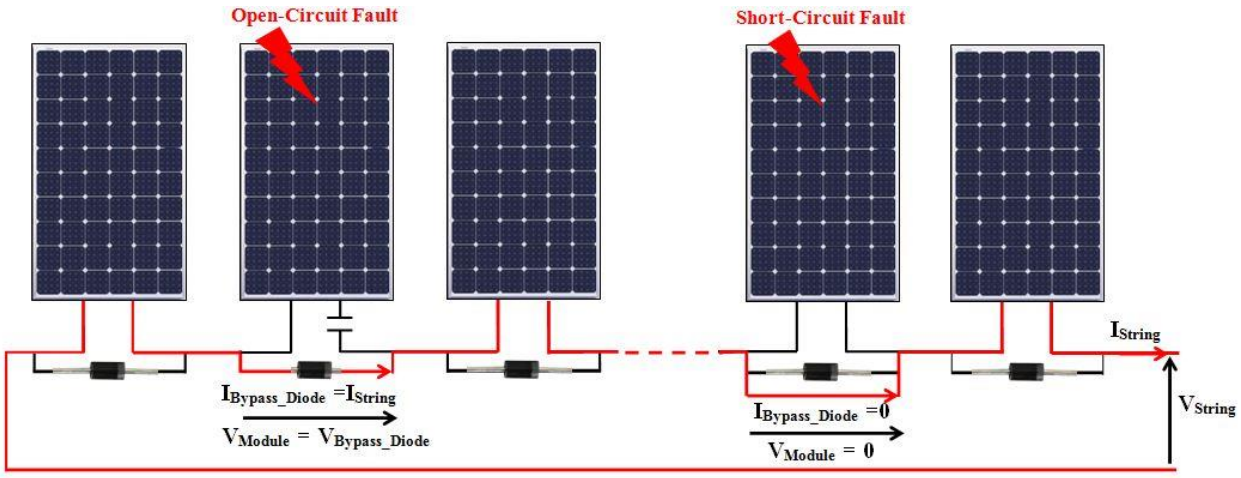

Figure 2. 2 OC fault, SC fault and healthy faulty modules in a PV array.

The abovementioned situations can be realized through the assumption of imaginary switches. One is connected in series manner (SOCs) and another is connected in parallel manner (SSCs) with every module as depicted in Figure 2. 3. A module having closed series connected switch (SOC) and opened parallel connected switch (SSC) represents no fault/ healthy condition of the PV module. Similarly, opened SOC and SSC correspond to an OC fault or open circuited module. Conversely, a closed SSC represents an SC fault or short circuited module.

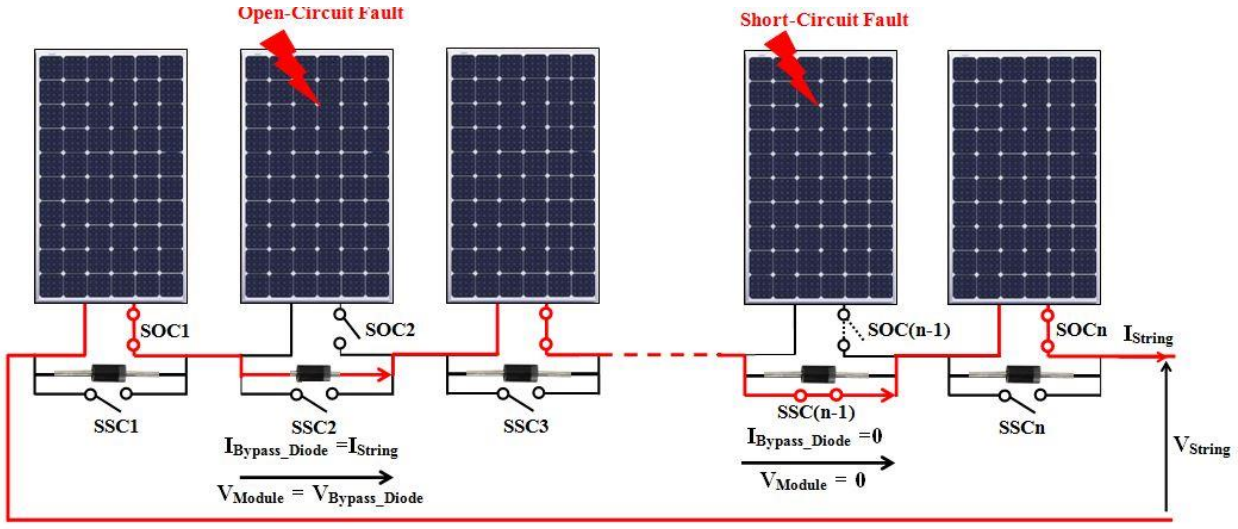

Figure 2. 3 Realization of healthy and faulty modules in a PV array of Figure 2. 2using imaginary switches SOCs & SSCs.

2.1.3 Formulation of objective function

Solar irradiation and temperature are generally distributed non-uniformly over the modules in a PV array, particularly in large-scale PV system. This results in diverse voltage, current and power generation in PV modules. This remarkably affects PV array electrical outcomes. Therefore, to obtain the maximum potential quantity of energy from PV system, incorporation of apposite maximum power point tracker (MPPT) into the array inverter is recommended [69].

The operating output voltage, current and the power yield of individual module can be computed from (2.1) and (2.2) using the measured module irradiation data, temperature data and the technical specifications of the concerned module. Occurrence of SC fault in a module makes the voltage to be zero across the module and contributes no power to the array. During open circuited PV module fault, voltage across the module terminals becomes negative due to forward bias voltage drop along the bypass diode. So, instead of power contribution to the PV array, power P_{Loss} gets lost in the bypass diode and it is calculated by (2.4).

$$P_{Loss} = I_{Array}.V_{Bypass\_diode} \tag{2.4}$$

Here, I_{Array} is the array current output. V_{Bypass_diode} represents the voltage drop along the bypass diode.

The power outcome from a PV array is therefore the summation of the contributed power from all the healthy PV modules minus the summation of power loss in bypass diodes which are connected across the open circuited PV modules. The MPPT thus trails an exclusive array voltage, current and power output for an array with particular fault category and fault location with particular distribution of heterogeneous irradiation and temperature along the PV modules in the array. This observable fact of PV system is analytically subjugated here to formulate the objective function. The objective function can be constructed using any one out of the three array parameters, viz., voltage, current and power, as their values are transformed and diverged from the values prevailed during

normal situation with the occurrences of faults. Operating logarithm on both sides of (2.2) gives (2.5).

$$\log_e P_{Module} = \log_e I_{Module} + \log_e V_{Module} \tag{2.5}$$

Differentiating both sides of (2.5) gives (2.6).

$$\frac{dP_{Module}}{P_{Module}} = \frac{dI_{Module}}{I_{Module}} + \frac{dV_{Module}}{V_{Module}} \tag{2.6}$$

Therefore, relative deviation is given by (2.7).

$$\frac{\Delta P_{Module}}{P_{Module}} = \pm\left(\frac{\Delta I_{Module}}{I_{Module}} + \frac{\Delta V_{Module}}{V_{Module}}\right) \tag{2.7}$$

From (2.7), it is seen that the relative divergence of output power of the module is equivalent to the summation of the relative divergence s of voltage and current output of that module. Hence it is evident that, during fault occurrences, the module output power and therefore the array output power is numerically more diverged from that of the array with healthy state than the generated voltage or current. This fact motivates to regard array power output for the formulation of objective function in this work.

During no fault condition or normal operation, the array power output P_{Array} can be expressed as (2.8).

$$P_{Array=} \sum_{i=1}^{N} P_i(T_i, G_i) \tag{2.8}$$

Here, i indicates the position of the PV modules in the array. N represents the total figure of PV modules connected in series manner in the array. T_i and $G_i$denote temperature and irradiation of the module at i^{th} position. $P_i(T_i, G_i)$, is the power contribution by the module at i^{th} position to the array.

In the state of the array containing a number of short circuited PV modules, by which the power contribution to the array is zero, the array power output can be represented as (2.9).

$$P_{Array=} \sum_{\substack{i=1, \\ i \neq sc}}^{N} P_i(T_i, G_i) \quad (2.9)$$

Subjected to, $0 \leq N_{sc} \leq N$.

Here, $sc \in \{sc_1, sc_2, sc_3, \dots, sc_{N_{sc}}\}$ represents the location set of the short circuited modules. N_{sc} denotes the total numeral of short circuited PV modules in the array.

During the occurrence of only OC faults, as the power loss takes place along the bypass diode shunted with the open circuited PV modules, the array power output can be evaluated as (2.10).

$$P_{Array=} \sum_{\substack{i=1, \\ i \neq oc}}^{N} P_i(T_i, G_i) - N_{oc} P_{Loss} \quad (2.10)$$

Subjected to, $0 \leq N_{oc} \leq N$.

Here, $oc \in \{oc_1, oc_2, oc_3, \dots, oc_{N_{oc}}\}$ signifies the location set of the open circuited PV modules. N_{oc} is the total figure of open circuited PV modules in the array.

Consequently, allowing for healthy condition and short circuit and open circuit faults in PV array, a general expression (2.11) of array output power can be evaluated combining (2.8), (2.9) and (2.10).

$$P_{Array=} \sum_{\substack{i=1, \\ i \neq sc \neq oc}}^{N} P_i(T_i, G_i) - N_{oc} P_{Loss} \quad (2.11)$$

Constraining, $(N_{sc} + N_{oc}) \leq N$,

And, $N_{sc} \geq 0$, $N_{oc} \geq 0$.

Now, assigning the value of $(N_{sc} + N_{oc}) = 0$ in (2.11), (2.8) is attained, which corresponds to array functioning at normal condition. Again, by substituting N_{oc} with the value '0' in (2.11), the expression for PV array output power (2.9) stating only short circuit faults is accomplished. Likewise, if (2.11) is assessed with $N_{sc} = 0$, then, the situation of occurrence of only OC faults and the PV array output power of (2.10) is obtained. Therefore, by assigning different values of N_{sc}, N_{oc}, and $(N_{sc} + N_{oc})$ in (2.11),

abiding by the constraints as $N_{sc} \geq 0$, $N_{oc} \geq 0$ and $(N_{sc} + N_{oc}) \leq N$, any operational combinations of PV module in the array (no fault, short circuited, open circuited or occurrences of both faults) can be explicitly expressed. Therefore, the equation (2.11) is regarded here as a universal expression for PV array power output undergoing any kind of situation.

To trace the real fault pattern, the absolute difference between the practically measured array output power ($P_{Measured}$) of the PV system and the evaluated array power output (P_{Array}) using equation (2.11) should be minimized. When the projected algorithm identifies the correct sc, oc, N_{sc} and N_{oc}, this difference theoretically converges to zero. Thus, the objective function $f(N_{sc}, N_{oc}, sc, oc)$ is designed as a minimization problem having the global optima equal to zero. The objective function is represented as in equation (2.12).

Minimize $f(N_{sc}, N_{oc}, sc, oc) = abs|P_{Measured} - P_{Array}|$ (2.12)

Subjected to, $(N_{sc} + N_{oc}) \leq N$

$N_{sc} \geq 0,$

$N_{oc} \geq 0.$

2.1.4 Proposed fault diagnosis scheme

The projected fault diagnosis method based on optimization can be staged as in Figure 2. 4. It portrays various blocks of the proposed diagnosis procedures and transfer of data amongst these blocks. These data are utilized to assess the objective function (2.12) and to execute the search process. IRGA is utilized in this work as the potent metaheuristic tool to execute the fault searching procedure.

Figure 2. 5 depicts the experimentation setup to perform the projected fault identification procedure which is composed of a roof top PV generator system, module irradiation and temperature data monitoring units, sensing devices for array output power, current and voltage, the MPPT controller- inverter set, computer interfaces, computing

machine for diagnosis platform and electrical load. The roof top PV generator system is a PV array comprising of 10 PV modules which are fabricated by the Websol Energy System Limited. Each module consists of 72 polycrystalline PV cells. The technical specifications of PV modules are tabulated in Table 2. 1. All the technical data are prepared at standard test condition (STC) (Irradiation- 1000 W/m^2, AM 1.5, 25°C Temperature). The generated output power from the PV array is fed to the electrical load via an MPPT controller-inverter set.

The electrical data of PV array are calibrated by means of sensors for array electrical parameters installed at the DC side or input side of the inverter. The entire the measured data attained from the monitoring units are transferred to the diagnosis platform through the computer interfaces. In the projected fault diagnosis approach, the computations on the measured data acquired from the computer interface are carried out using a computing device equipped with the Matlab software. A Matlab-Simulink soft replica, representing the practical PV test system, is designed to accomplish the intermediary evaluations requisite for the fault diagnoser block as shown in Figure 2. 4. Here, in this block, IRGA diagnoser subsystem holds an in-house coded soft computing source to execute IRGA for the proposed fault diagnosis. The simulated subsystem of the block PV Array is portrayed below in Figure 2. 6.

Table 2. 1 Technical specifications of the PV modules.

Parameter	Value
Maker	Websol Energy System Limited
Rated peak power (P_{MAX})	300 W
Voltage at maximum power (V_{MP})	36.2 V
Current at maximum power (I_{MP})	8.3 A
Open circuit voltage (V_{OC})	44.9 V
Short circuit current (I_{SC})	8.9 A
Total number cells in series (N_S)	72
Total number cells in parallel (N_P)	1
Maximum system voltage	1000 V
Module Efficiency	0.8

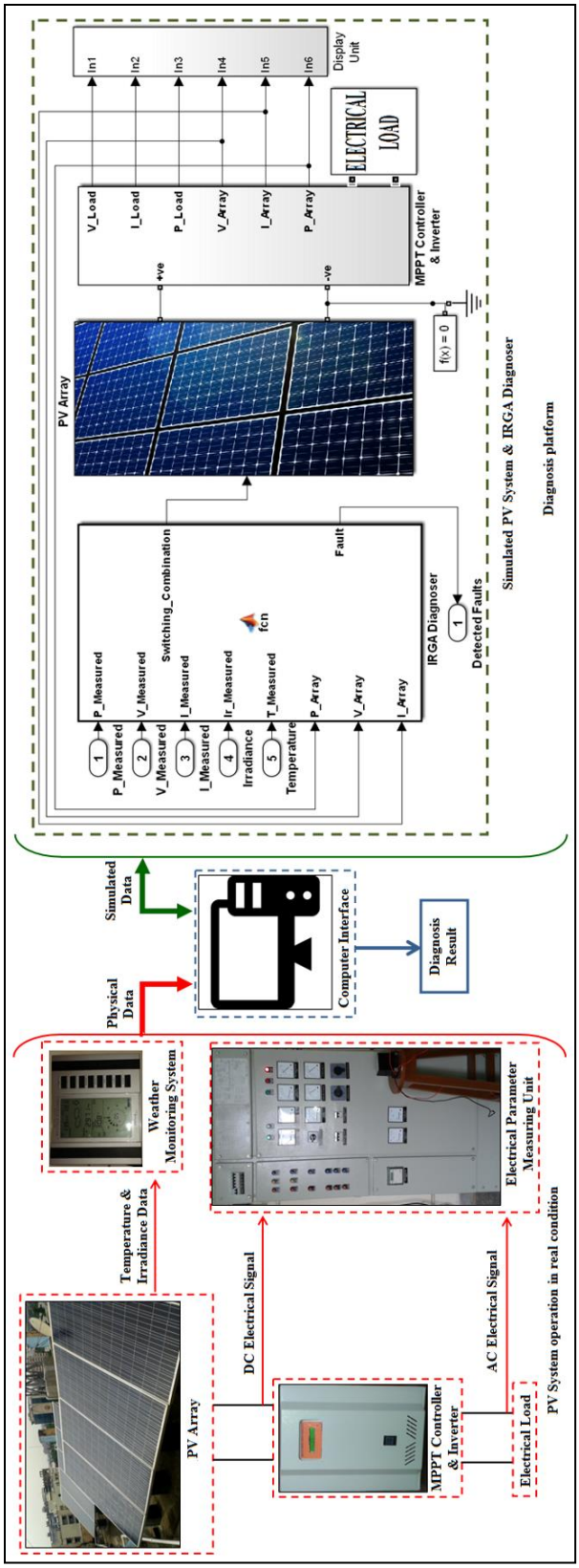

Figure 2. 4 Schematic diagram of the proposed fault diagnosis scheme.

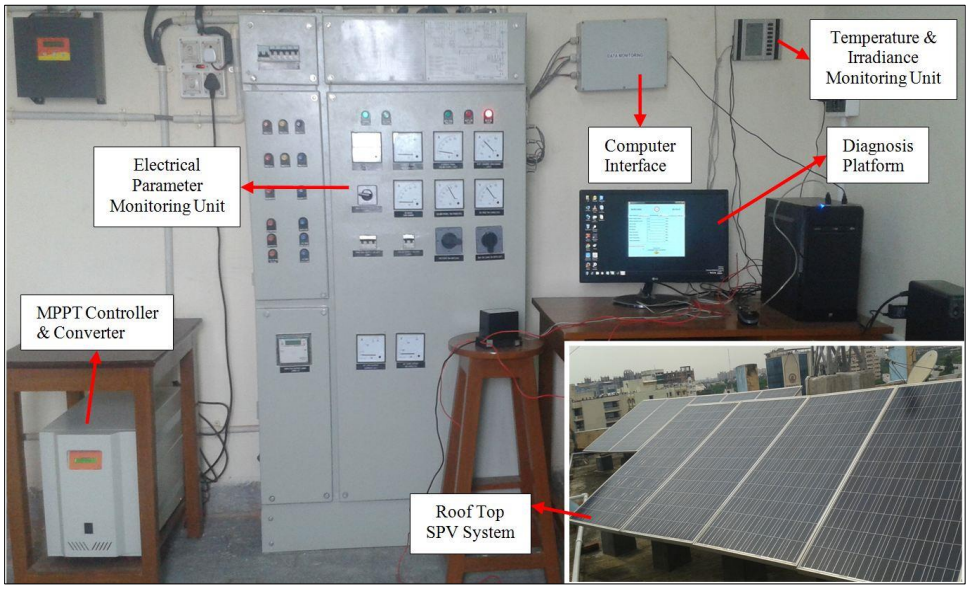

Figure 2. 5 Laboratory test setup for the proposed fault diagnosis scheme.

The simulated PV array subsystem, as shown in Figure 2. 6, incorporates the conception of switching of 10 SOCs and 10 SSCs switches as depicted in Figure 2. 3 to imitate the normal, the short circuited or the open circuited condition of the PV modules. The switches of the simulated PV system as shown in Figure 2. 6 are consigned the value '0' or '1' to signify the open or the closed state of the simulated switches respectively. Thus, assigning '1' to an SOC switch and '0' to an SSC switch associated to a PV module corresponds to a healthy PV module. Again, assigning '0' to an SOC switch and '0' to an SSC switch connected to a PV module corresponds to module OC condition. Again, assigning '1' to an SSC switch connected to a PV module signifies module SC condition. Usually, all the SOC switches are assigned '0' and SSC switches are assigned '1' to characterize a healthy PV array. During the incidences of faults, the fault diagnoser produces random decision variables (N_{sc}, N_{oc}, sc, oc). In accordance with the positions designated by the decision vector $sc \in \{sc_1, sc_2, sc_3, \dots, sc_{N_{sc}}\}$, the fault diagnoser assigns the value '1' to N_{sc} number of SSC switches at the respective locations of the modules in the simulated PV system as in Figure 2. 6. Concurrently, in accordance with the positions designated by the decision vector $oc \in \{oc_1, oc_2, oc_3, \dots, oc_{N_{oc}}\}$, the fault diagnoser assigns the value '0' to N_{oc} number of SOC switches at the respective

locations of the modules in PV system as in Figure 2. 6. Other switches (SSCs and SOCs) are assigned according to normal no-fault condition. Afterwards, the objective function (12) is estimated. As the value of $f(N_{sc}, N_{oc}, sc, oc)$ approaches to zero or to a very small value (ε) close to '0', the correct fault combination may be accomplished. The suboptimal values (between 0 and ε) of the objective function are obtained due to the precision, the accuracy and the tolerance error of the monitoring devices. In several cases, the PV array may produce the similar power even under dissimilar fault conditions having non-uniform irradiation and temperature allocation. However, it is impossible to also produce same current and voltage output alongside same output power for dissimilar fault patterns when the PV array is working at the maximum power point. Since, for dissimilar fault patterns having non-uniform irradiation and temperature distribution, the array P-V-I characteristics are all exclusive. So, to avert those kinds of placebo fault detections, the solutions attained by the optimizer should be cross verified by comparing the simulated current and voltage output of the PV array for that resulted fault pattern with that of the physically measured values of array voltage and current output.

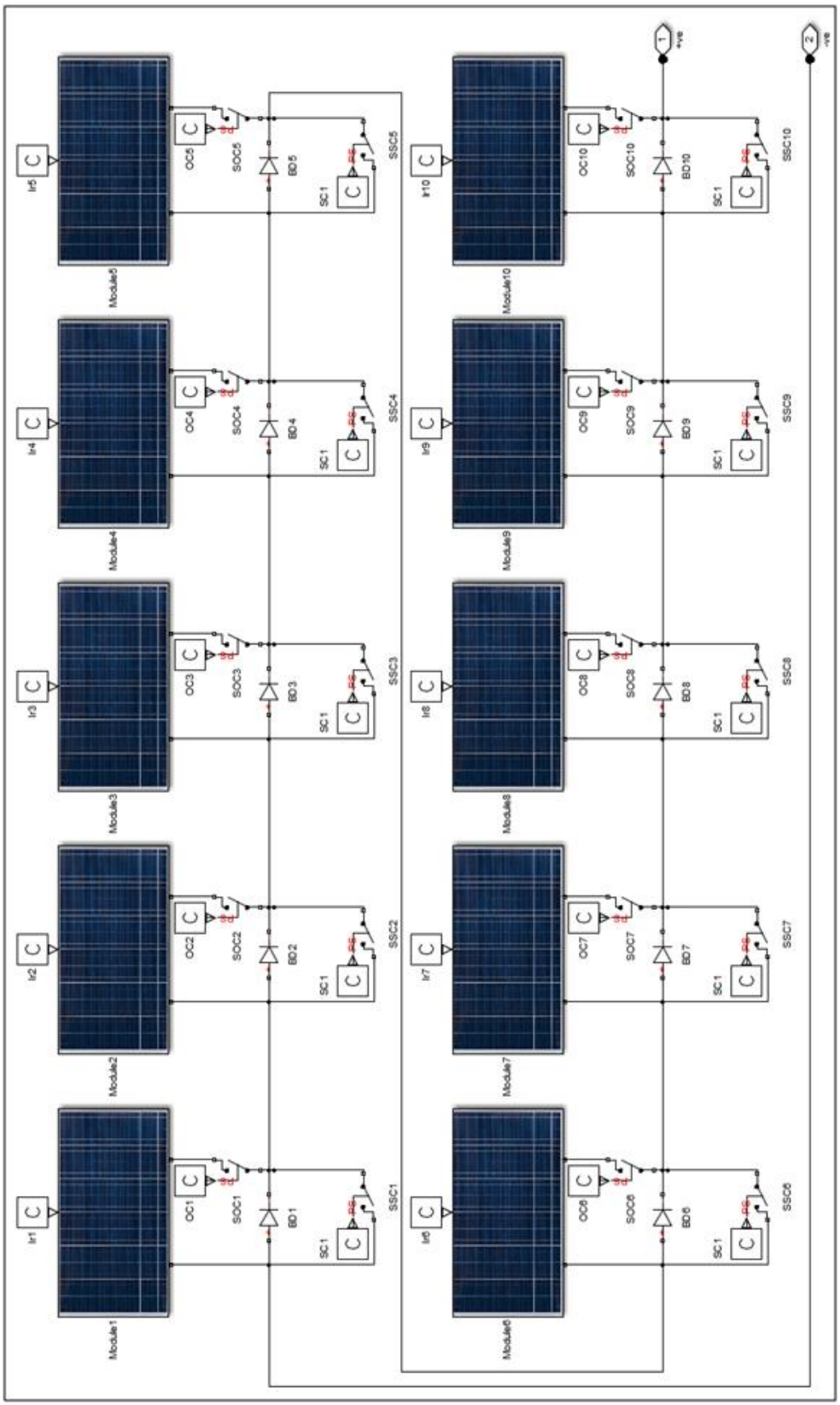

Figure 2. 6 Simulated PV array.

The logical flow chart of the proposed fault diagnosis scheme is given in Figure 2. 7.

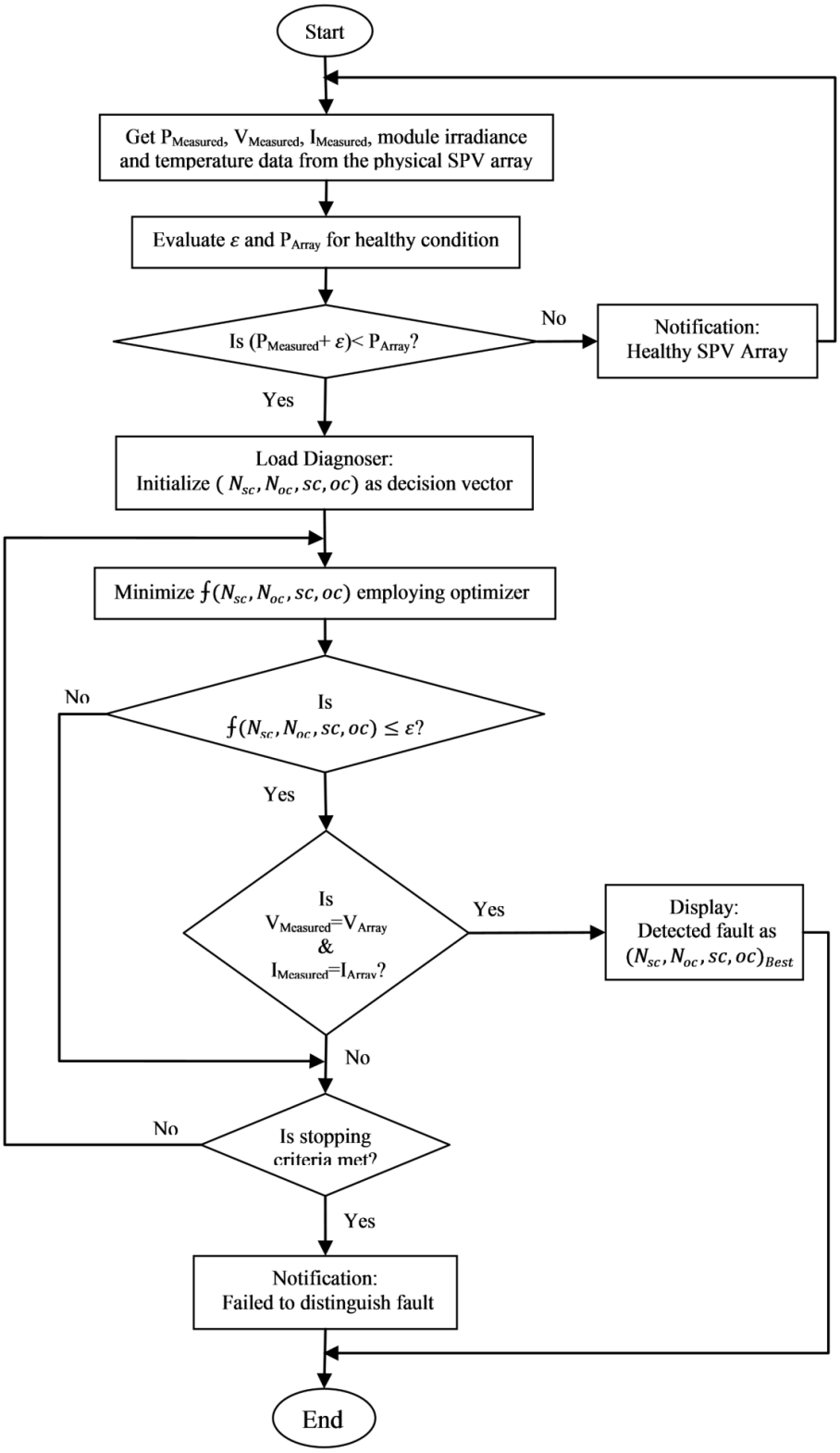

Figure 2. 7 The logical flow chart of the proposed fault diagnosis scheme.

2.2 Problem formulation of optimal bidding plan of microgrid under outages and uncertainties

2.2.1 Market model

To accomplish a beneficial and robust market behavior, the Microgrid Central Controller (MGCC) has to decide the quantity of bidding energy in the day ahead electricity market with the intention of maximization of microgrid revenues with least risk possibilities and optimum system operation. The decision must be made depending on the day ahead forecast of hourly energy prices, renewable energy generations, dispatchable and non-dispatchable load demands and controllable distributed generations. Conversely, the intermittency of renewable energy outputs, hourly load and renewable system outages make the optimal planning of bidding strategy and microgrid operation further challenging. Besides, limited installation capacity of microgrid cannot fulfill its load requirement at many times during the day (for example, at peak load periods, low renewable energy production or component outages of renewable energy systems) and brings in severe energy imbalances. Therefore, dual-settlement energy market structure consisting of day-ahead market and energy balancing market is adhered here. The day-ahead electricity market is a pool-based market. Here the MGCC executes clearing, identify accepted offers and bids and pays the electricity producers in accordance with the generation multiplied with the subsidiary price. Conversely, the balancing market is founded on dual-pricing market. Here deviations from the contracted bids are penalized. Producing less power than the scheduled amount is fined at a price higher than the day-ahead market price while excess generation is penalized at a price lower than the day-ahead market price [47].

2.2.2 Proposed bidding strategy

Figure 2. 8 presents the schematic outline of the solution mechanism for the stochastic optimal planning of microgrid bidding strategy. Day-ahead wind velocity, solar irradiation, weather condition and the load demand data are forecasted evaluating historical data and supplementary factors. The uncertainties regarding these parameters are formulated using various PDFs. In this work, Tent chaos mapping is employed to

produce the scenarios of intermittent wind velocity, solar irradiation, demand and failure outage probability (FOP) pattern. During optimal bidding planning, the final load demand, power output capacities of renewable systems and their failure rates have immense impact on DRP model, operation of the distributed generations in microgrid and finally on the bidding strategy of microgrid. Hence, the scenarios of uncertain input parameters should be created within the well-defined confidence intervals. Confidence intervals can be estimated according to probability distribution of the input variables and their historical data. Consequently, for scenario generation Tent mapping is used. Reserve price for the over estimation and penalty price for the under estimation of renewable energy outputs are included to recompense uncertainty errors regarding renewable resources. The microgrid risk management both in day-ahead and real-time electricity markets is assessed by means of weighted CVaR evaluation [39].

The strategy of the microgrid bidding is structured as a MINLP. Dual-phase stochastic programming is engaged here to manage uncertainties of parameters during microgrid bidding planning [39]. First phase settles on the hourly optimal energy bids preceding the contemplation of the uncertainties regarding load demand, renewable energy outputs and their outages. So, these variables at this phase are termed as the ‘here & now’ variables. The scheduling of generating units, energy storage systems and positive and negative imbalances are accomplished in the second phase considering first phase variables and uncertain scenarios. Hence, these variables are termed as “wait & see” variables. The risk management is attained through CVaR evaluation. The optimal results are further validated using the VSS calculation.

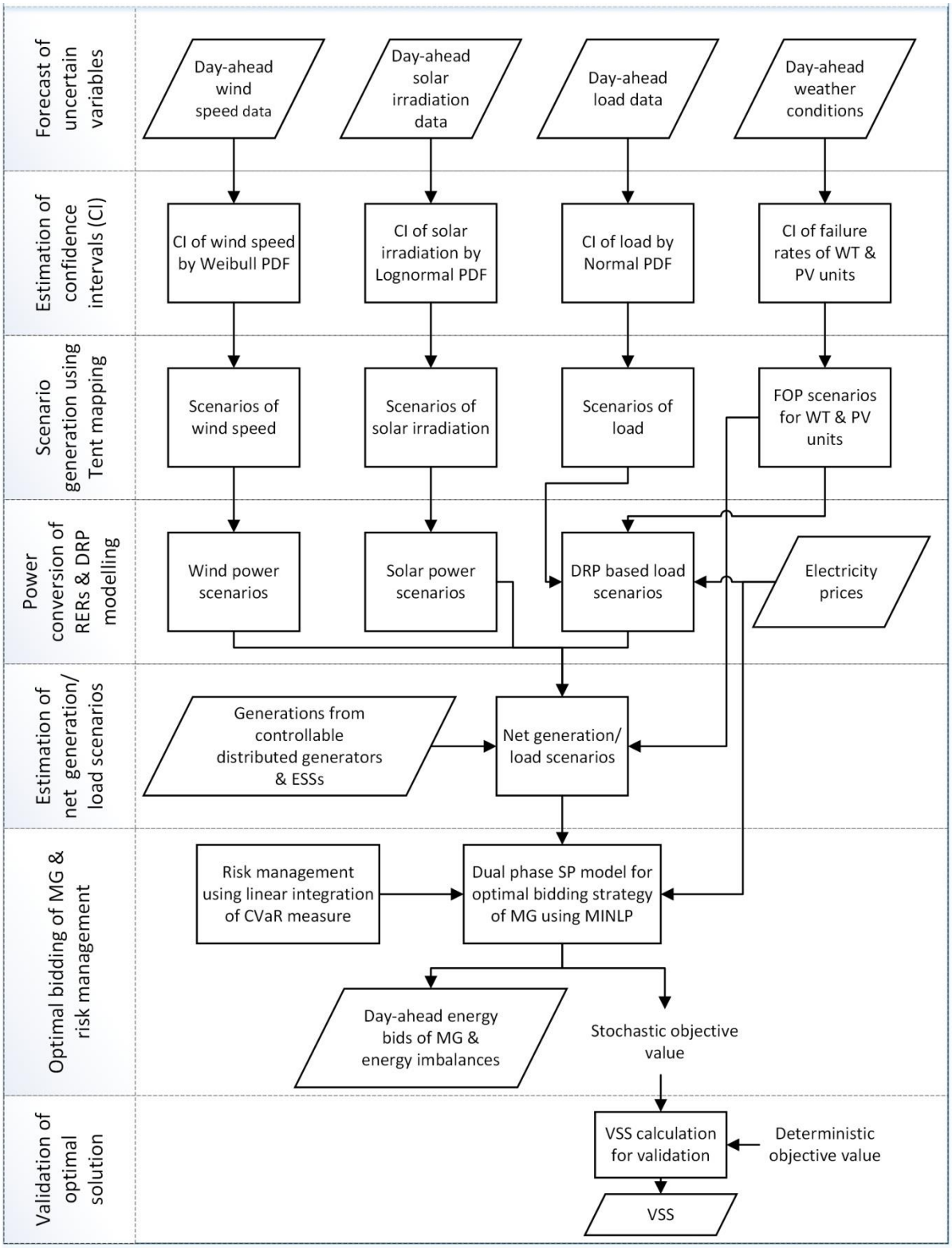

Figure 2. 8 Schematic outline of the proposed bidding strategy.

2.2.3 Uncertainty modeling

2.2.3.1 Probability distribution of renewable energy resources

The renewable energy resources are the most significant but intricate parts to incorporate in microgrid owing to their intermittency and uncertainty. The overestimation of the renewable power output requires huge reserve capacity margin and imbalances the steady state security of microgrid if the excess demand arises. On the other hand, underestimation results in wastage of the surplus energy. These imbalances add to the overall cost model of microgrid during bidding planning in energy market. Therefore, uncertainty modeling using Weibull, Lognormal, Gumbel, Beta and other PDFs has been employed in many researches to estimate reserve cost for the overestimation and penalty cost for the underestimation. Solar irradiation G and wind velocity v are well tracked by lognormal [70] and Weibull PDFs [71] respectively as represented in equations (2.13) and (2.14), when appropriate mean μ_G and standard deviation σ_G data for the lognormal PDF $f_G(G)$ and scale factor α and shape factor β of the Weibull PDF $f_v(v)$ are provided. The value of μ_G, σ_G, α and β for geographical region can be evaluated from solar irradiation and wind velocity pattern of the region for a long time period.

$$f_G(G) = \frac{1}{G \times \sigma_G \times \sqrt{2 \times \pi}} e^{-\left\{\frac{-(\ln G - \mu_G)^2}{2 \times \sigma_G^2}\right\}} \quad \text{for } G > 0 \tag{2.13}$$

$$f_v(v) = \left(\frac{\beta}{\alpha}\right) \times \left(\frac{v}{\alpha}\right)^{(\beta-1)} \times e^{-\left(\frac{v}{\alpha}\right)^{\beta}} \quad \text{for } 0 < v < \infty \tag{2.14}$$

2.2.3.2 Power probabilities of renewable energy resources

The equation (2.15) presents the probability $f_{PV}(P_{PV})$ of PV power output P_{PV}.

$$f_{PV}(P_{PV}) = f(G) \tag{2.15}$$

The power outcome from a PV system for an irradiation intensity G W/m^2 can be represented as in equation (2.16).

$$P_{PV} = \begin{cases} P_{PVr} \times \frac{G^2}{G_{STD} \times G_C} & \text{for } 0 < G < G_C \\ P_{PVr} \times \frac{G}{G_{STD}} & \text{for } G \geq G_C \end{cases} \quad (2.16)$$

Here, P_{PVr}, G_{STD} and G_C are respectively the rated power output of PV system, standard and certain irradiation. The power produced from WT system for v m/s wind velocity is estimated as equation (2.17).

$$P_{WT} = \begin{cases} 0 & \text{for } v < v_{in} \text{ and } v > v_{out} \\ (A + B \times v + C \times v^2) & \text{for } v_{in} \leq v \leq v_r \\ P_{WTr} & \text{for } v_r < v \leq v_{out} \end{cases} \quad (2.17)$$

Here, P_{WTr}, v_{in}, v_{out} and v_r represent the rated power output of WT system, cut-in, cut-out and the rated wind velocities respectively. The constants A, B, and C are modeled as the functions of v_{in} and v_r according to the subsequent equations (2.18)-(2.20).

$$A = \frac{1}{(v_{in} - v_r)^2} \times \left[v_{in} \times (v_{in} + v_r) - 4 \times v_{in} \times v_r \times \frac{(v_{in} - v_r)^3}{2 \times v_r} \right] \quad (2.18)$$

$$B = \frac{1}{(v_{in} - v_r)^2} \times \left[2 - 4 \times \frac{\left(\frac{4}{v_{in}} + v_r \right)^3}{2 \times v_r} \right] \quad (2.19)$$

$$C = \frac{1}{(v_{in} - v_r)^2} \times \left[4 \times (v_{in} + v_r) + \frac{(v_{in} + v_r)^3 - (3 \times v_{in} + v_r)}{2 \times v_r} \right] \quad (2.20)$$

Wind power probability for the discrete zones, i.e., for the first and the third cases of equation (2.17), are computed by equations (2.21) and (2.22) respectively.

$$f_{WT}(P_{WT})|_{P_{WT}=0} = 1 - e^{-\left(\frac{v_{in}}{\alpha}\right)^{\beta}} + e^{-\left(\frac{v_{out}}{\alpha}\right)^{\beta}} \quad (2.21)$$

$$f_{WT}(P_{WT})|_{P_{WT}=P_{WTr}} = e^{-\left(\frac{v_{in}}{\alpha}\right)^{\beta}} - e^{-\left(\frac{v_{out}}{\alpha}\right)^{\beta}} \quad (2.22)$$

The probability of WT power for the continuous region in second case of the equation (2.17) can be represented as equation (2.23).

$$f_{WT}(P_{WT}) = \frac{\beta \times (v_r - v_{in})}{\alpha^{\beta} + P_{WTr}} \times \left[v_{in} + \frac{P_{WT}}{P_{WTr}} \times (v_r - v_{in})\right]^{\beta-1} \times e^{-\left(\frac{v_{in} + \frac{P_{WT}}{P_{WTr}} \times (v_r - v_{in})}{\alpha}\right)^{\beta}} \quad (2.23)$$

2.2.3.3. Outage modeling of RERs

Insensitive environmental circumstances make renewable energy systems to countenance outages often. Modeling of outage is dependent on three failure factors, viz., repairable failure, aging failure and weather dependency failure [61], [62]. Repairable FOP ρ_{Repair} of a power system element is stated as equation (2.24). It is dependent on generating unit's yearly failure numbers F and mean time for repairmen $MTTR$ of the failure component.

$$\rho_{Repair} = \frac{F \times MTTR}{8760} \quad (2.24)$$

Aging outage probability of any component usually follows normal PDF [61], [62]. During T^{th} year of service time, the aging outage probability ρ_{Aging} can be modeled as equation (2.25) where, μ_{Aging} and σ_{Aging} are respectively the mean and the standard deviation of the normal PDF.

$$\rho_{Aging} = \frac{1}{\sigma_{Aging} \times \sqrt{2 \times \pi}} \times e^{-\frac{\left(T - \mu_{Aging}\right)^2}{2 \times \sigma_{Aging}{}^2}} \quad (2.25)$$

Though, in case of planning of bidding strategy for short period, aging factor hardly plays any role in evaluating outages of renewable energy systems, more aged machineries are more susceptible to weather dependent outages [61], [62]. Weather dependent outage probability $\rho_{Weather}$ is modeled using exponential distribution as portrayed in equation (2.26) for a time duration of Δt and forecasted failure rate λ. Microgrid operator decides the failure rate λ based on the forecasted weather condition.

$$\rho_{Weather} = 1 - e^{-\lambda \times \Delta t} \quad (2.26)$$

As multi-factor independent outages are involved for outage of any component, the outage rate of any component can be estimated using the conception of union set [61],

[62]. Hence the FOP ρ of a renewable energy system can be comprehended by equation (2.27).

$$\rho = \rho_{Repair} \cup \rho_{Aging} \cup \rho_{Weather} = \rho_{Repair} + \rho_{Aging} + \rho_{Weather} - \left(\rho_{Repair} \cap \rho_{Aging}\right) - \left(\rho_{Aging} \cap \rho_{Weather}\right) - \left(\rho_{Weather} \cap \rho_{Repair}\right) + \left(\rho_{Repair} \cap \rho_{Aging} \cap \rho_{Weather}\right) \quad (2.27)$$

2.2.3.4 Probability distribution of load

As stated in the studies [51], [72], normal PDF is the most apposite function to track load forecasting. The equation (2.28) presents load L distribution using normal PDF where μ_{Load} and σ_{Load} are respectively the mean and the standard deviation regarding normal PDF.

$$f_v(v) = \frac{1}{\sigma_{Load} \times \sqrt{2 \times \pi}} \times e^{-\frac{(L-\mu_{Load})^2}{2 \times \sigma_{Load}^2}} \quad (2.28)$$

2.2.4 Confidence interval

Truth estimation by means of confidence interval evaluation has been widely employed in recent power system applications, since it conveys richer information [73]. Let us assume, an uncertain parameter, y (for example, wind velocity, solar irradiation, failure rate or load demand) that has a sample set $X = \{x_t\}_{t=1}^{24}$ from $f_y(x_t)$, where $f_y(x_t)$ is PDF of the parameter y. Considering the point forecast of the parameter, the forecast error ε_t between point forecast x_t and real-time value $\hat{x}_t$ of parameter is indicated by the equation (2.29).

$$\varepsilon_t = (\hat{x}_t - x_t)/{x_t}^{max} \quad (2.29)$$

At a pre-specified confidence level σ, the conditional confidence interval or the upper and the lower bounds of the prediction errors$\left[{\varepsilon_t}^{min}, {\varepsilon_t}^{max}\right]$, can be evaluated as given in equations (2.30) and (2.31).

$$\varepsilon_t{}^{min} = infimum\left\{x_t \epsilon [0, x_t{}^{max}] \middle| \int_0^{x_t{}^{max}} \varepsilon_t \times f_y(x_t)\, dx_t \geq \frac{1-\sigma}{2}\right\} \quad (2.30)$$

$$\varepsilon_t{}^{max} = infimum\left\{x_t \epsilon [0, x_t{}^{max}] \middle| \int_0^{x_t{}^{max}} \varepsilon_t \times f_y(x_t)\, dx_t \geq \frac{1+\sigma}{2}\right\} \quad (2.31)$$

In accordance with the forecasted data of the input parameter, the minimum and the maximum value of the parameter can be estimated as equations (2.32) and (2.33) respectively.

$$\underline{x_t} = \hat{x}_t - x_t{}^{max} \times \varepsilon_t{}^{max}\,, \quad \varepsilon_t{}^{max} > 0 \quad (2.32)$$

$$\overline{x}_t = \hat{x}_t - x_t{}^{max} \times \varepsilon_t{}^{min}, \varepsilon_t{}^{min} < 0 \quad (2.33)$$

The arbitrary variable assigned for the existing parameter at the time period t is delimited within the confidence level as given in equation (2.34).

$$x_t \epsilon \left[\underline{x_t}, \overline{x}_t\right] \quad (2.34)$$

2.2.5 Scenario generation using Tent mapping

To achieve global optimum outcome for microgrid bidding planning with reasonable confidence level, the scenarios of uncertain input parameters are generated inside confidence interval by means of Tent chaos mapping. The chaos theory [59], because of its intrinsic ergodicity characteristic, can produce non-recurring values of parameters of a non-linear system restricted under deterministic setting by efficient dynamic parameter control mechanisms [52]. Therefore, chaotic sequence is an automatic sequence generator and generates sequences adaptively throughout the searching advancement of optimization algorithm. The uses of chaos sequence to control the value setting of optimization parameters and generate sequences adaptively have two advantages. First of all, as the trial and the tuning are not required, additional computational time and the extra space for fine-tuning of attribute settings are saved. Secondly, the adaptive generation process instead of random value generation causes diversity in parameter value setting. All these augments the efficacy and the convergence speed of optimization algorithm. The Tent mapping [60] is one of the well-established discrete-time scenario

generators of Chaos theory and can be modeled as equation (2.35), where, $ctrl$ is the control parameter for generation of chaotic sequence. Moreover, Tent mapping generates sequences with more even allocation from the beginning than any other chaos mapping methods and creates scenarios having identical probability. If N_s is total numeral of the generated scenarios, then the probability of incidences of s^{th} scenario is $\pi_s = 1/N_s$.

$$x_s = \begin{cases} ctrl \times x_{s-1}, & 0 < x_{s-1} \leq 0.5 \\ ctrl \times (1 - x_{s-1}), & 0.5 < x_{s-1} \leq 1 \end{cases}, \qquad \forall\, s \in N_s \tag{2.35}$$

2.2.6 Risk management through CVaR

Due to the uncertainties of the system parameters, the profit of microgrid because of prior scheduling has to countenance risk of decline of actual profit from the expected profit. The risk management in a competitive energy market acts an vital role during the operation and management of generating units of microgrid. To evaluate the risk two principal indicators, viz., the Value at Risk (VaR) and the Conditional Risk Value (CVaR) are employed. VaR is the largest profit p amid all the profits whose probabilities are less than or equal to (1-confidence level). Therefore, for the confidence level σ, the VaR_{σ} and the $CVaR_{\sigma}$ of the profit can be respectively calculated as shown in equations (2.36) and (2.37) [39]. Confidence level is customarily selected between 0.9 and 0.99.

$$VaR_{\sigma} = max\{p | probability(Profit \leq p) \leq (1 - \sigma)\} \tag{2.36}$$

$$CVaR_{\sigma} = expectation(Profit | Profit \leq VaR_{\sigma}) \tag{2.37}$$

Thus the $CVaR_{\sigma}$ considers the expected profit so that less than $(1 - \sigma) \times 100\%$ scenarios should have lowest profits. The CVaR is utilized as a risk management index in the projected bidding optimization problem, such that the expected profit among all possible scenarios is maximized.

2.2.7 Objective function and constraints

The aim of the projected bidding strategy planning is the maximization of the profit of microgrid with the optimum risk management. Accordingly, for profitable participation

in the day-ahead electricity market, the objective function is devised as the weighted sum of the microgrid profit $Profit_{MG}$ and $CVaR$ as presented in equation (2.38).

$$\text{Maximize, } f = (1-\omega) \times Profit_{MG} + \omega \times CVaR \tag{2.38}$$

Expected profit, the first term of the objective function, can be articulated as in equation (2.39).

$$Profit_{MG} = \sum_{t=1}^{24} Revenue_{Market_t} + \sum_{t=1}^{24} \sum_{s=1}^{N_s} \pi_{s,t} \times \left\{ Revenue_{Load_{s,t}} - \left(Cost_{GT_{s,t}} + Cost_{PV_{s,t}} + Cost_{WT_{s,t}} + Cost_{ESS_{s,t}} + Cost_{DRP_{s,t}} \right) + Compensation_{Imbalance_{s,t}} \right\} \tag{2.39}$$

Here, the first term $Revenue_{Market_t}$ of equation (2.39) symbolizes the revenue from the bidding in the day-ahead electricity market. $Revenue_{Load_{s,t}}$ stands for the expected revenue of microgrid acquired from selling the power to the local loads. The terms $Cost_{GT_{s,t}}$, $Cost_{PV_{s,t}}$, $Cost_{WT_{s,t}}$, $Cost_{ESS_{s,t}}$ and $Cost_{DRP_{s,t}}$ indicate respectively the generation costs from gas turbines, PV system, WT system and ESS unit and the incentives to the local loads for taking part in DRP. The term $Compensation_{Imbalance_{s,t}}$ signifies the adjustments for compensating the energy imbalance in the real-time market.

The second term of the objective function is formulated to maximize the CVaR as in depicted equation (2.40).

$$CVaR = VaR - 1/(1-\sigma) \times \sum_{s=1}^{N_s} (\pi_s \times \eta_s) \tag{2.40}$$

Here, VaR represents value-at-risk and η_s symbolizes an auxiliary variable. The values of VaR and η_s are estimated by $CVaR$ constraints.

2.2.7.1 Revenue model

The revenue from selling power to the energy market and the local consumers are formulated by equations (2.41) and (2.42) respectively.

$$Revenue_{Market_t} = r_{Grid_t} \times P_{Grid_t}, \quad \forall \ -P_{Grid}^{max} \le P_{Grid_t} \le P_{Grid}^{max}, \ t = 1{:}24 \tag{2.41}$$

$$Revenue_{Load_{s,t}} = r_{Load_t} \times P_{Load_{s,t}},\ \forall\, s = 1{:}\, N_s,\ t = 1{:}\,24 \tag{2.42}$$

The term P_{Grid_t} is the power transaction with the grid during bidding. It is constrained by the power transfer capacity P_{Grid}^{max} of line linking microgrid to the main grid. This power is exchanged at a rate of r_{Grid_t}. The local load $P_{Load_{s,t}}$ is traded at a retail price of r_{Load_t}.

2.2.7.2 GT cost model

The cost of the GTs is modeled as depicted in equation (2.43) where, $P_{GT_{i,t}}$ and c_{GT_i} are power output and energy rate of the i^{th} GT system respectively.

$$Cost_{GT_{s,t}} = \sum_{i=1}^{N_{GT}} \left(c_{GT_i} \times P_{GT_{i,s,t}}\right) \times S_{GT_{i,s,t}} \tag{2.43}$$

The term $S_{GT_{i,s,t}}$ is '1' if i^{th} GT system is scheduled on at t^{th} hour and '0' otherwise. Constraints (2.44)-(2.46) provide the minimum and the maximum generation constraints ${P_{GT_i}}^{max}$, minimum up time MUT_i and down time MDT_i constraints, ramp up R_{U_i} and ramp down R_{D_i} limits of the i^{th} GT system respectively.

$$0 \le P_{GT_{i,\mathrm{s},t}} \le {P_{GT_i}}^{max}, \quad \forall\, i \in N_{GT}, \mathrm{s} = 1{:}\, N_s,\ t = 1{:}\,24 \tag{2.44}$$

$$\begin{cases} \left(T_{On_{i,\mathrm{s},(t-1)}} - MUT_i\right) \times \left(S_{GT_{i,\mathrm{s},(t-1)}} - S_{GT_{i,\mathrm{s},t}}\right) \ge 0, \\ \qquad \forall\, i \in N_{GT}, \mathrm{s} = 1{:}\, N_s,\ t = 1{:}\,24 \\ \left(T_{Off_{i,\mathrm{s},(t-1)}} - MDT_i\right) \times \left(S_{GT_{i,\mathrm{s,t}}} - S_{GT_{i,\mathrm{s},(t-1)}}\right) \ge 0, \\ \qquad \forall\, i \in N_{GT}, \mathrm{s} = 1{:}\, N_s,\ t = 1{:}\,24 \end{cases} \tag{2.45}$$

$$\begin{cases} \left(P_{GT_{i,\mathrm{s},(t+1)}} - P_{GT_{i,\mathrm{s},t}}\right) \le R_{U_i}, \quad \forall\, i \in N_{GT}, \mathrm{s} = 1{:}\, N_s,\ t = 1{:}\,24 \\ \left(P_{GT_{i,\mathrm{s},t}} - P_{GT_{i,\mathrm{s},(t+1)}}\right) \le R_{D_i}, \quad \forall\, i \in N_{GT}, \mathrm{s} = 1{:}\, N_s,\ t = 1{:}\,24 \end{cases} \tag{2.46}$$

2.2.7.3 PV cost model

The operational cost of PV system as depicted in equation (2.47), comprises of the direct cost, the reserve cost for the overestimation and the penalty cost for the underestimation

on scheduled solar power and are modeled as respectively in (2.48)- (2.50). The reserve cost and the penalty cost are the function of lognormal PDF of the concerning PV systems.

$$Cost_{PV_{s,t}} = \sum_{j=1}^{N_{PV}} \left[C_{PV_{j,s,t}}\left(P_{PV_{j,s,t}}\right) \times S_{PV_{j,s,t}} + O_{PV_{j,s,t}}\left(P_{PV_{j,s,t}}\right) + U_{PV_{j,t}}\left(P_{PV_{j,s,t}}\right) \right] \quad (2.47)$$

Where, $S_{PV_{j,s,t}} = \begin{cases} 1, & \rho_{PV_{j,s,t}} < F_{PV} \\ 0, & otherwise \end{cases}$

The $S_{PV_{j,s,t}}$ is '1' if j^{th} solar system is scheduled on at t^{th} hour and '0' otherwise. The PV system is scheduled on when FOP $\rho_{PV_{j,s,t}}$ of PV system does not exceed the pre defined FOP limit F_{PV}.

$$C_{PV_{j,s,t}}\left(P_{PV_{j,s,t}}\right) = d_{PV_j} \times P_{PV_{j,s,t}} \quad (2.48)$$

$$O_{PV_{j,s,t}}\left(P_{PV_{j,s,t}}\right) = o_{PV_j} \times \int_0^{P_{PV_{j,s,t}}} \left(P_{PV_{j,s,t}} - x\right) \times f_{PV}(x)dx \quad (2.49)$$

$$U_{PV_{j,t}}\left(P_{PV_{j,s,t}}\right) = u_{PV_j} \times \int_{P_{PV_{j,s,t}}}^{P_{PVr}} \left(x - P_{PV_{j,s,t}}\right) \times f_{PV}(x)dx \quad (2.50)$$

d_{PV_j}, o_{PV_j} and $u_{PV_j}$are the per system direct, reserve and penalty costs of j^{th} the PV systemt respectively.

2.2.7.4 WT cost model

The operational cost of WT system as presented in (2.51), is comprised of the direct cost, the reserve cost for the overestimation and the penalty cost for the underestimation on scheduled wind power and are evaluated as in (2.52) -(2.54) respectively.

$$Cost_{WT_{s,t}} = \sum_{k=1}^{N_{WT}} \left[C_{WT_{k,s,t}}\left(P_{WT_{k,s,t}}\right) \times S_{WT_{k,s,t}} + O_{WT_{k,s,t}}\left(P_{WT_{k,s,t}}\right) + U_{UWT_{k,s,t}}\left(P_{WT_{k,s,t}}\right) \right] \quad (2.51)$$

Where, $S_{WT_{k,s,t}} = \begin{cases} 1, & \rho_{WT_{k,s,t}} < F_{WT} \\ 0, & otherwise \end{cases}$

The $S_{WT_{k,s,t}}$ is '1' if k^{th} WT system is scheduled on at t^{th} hour and '0' otherwise. The WT system is scheduled on when FOP $\rho_{WT_{k,s,t}}$ of WT system stays within the pre specified FOP limit F_{WT}.

$$C_{WT_{k,t}}\left(P_{WT_{k,t}}\right) = d_{WT_k} \times P_{WT_{k,t}} \tag{2.52}$$

$$O_{WT_{k,t}}\left(P_{WT_{k,t}}\right) = o_{WT_k} \times \int_{P_{WT_{k,t}}^{min}}^{P_{WT_{k,t}}} \left(P_{WT_{k,t}} - y\right) \times f_{WT}(y)dy \tag{2.53}$$

$$U_{WT_{k,t}}\left(P_{WT_{k,t}}\right) = u_{WT_k} \times \int_{P_{WT_{k,t}}}^{P_{WT_{k,t}}^{max}} \left(y - P_{WT_{k,t}}\right) \times f_{WT}(y)dy \tag{2.54}$$

d_{WT_k}, o_{WT_k} and $u_{WT_k}$are the per unit direct, reserve and penalty costs of k^{th} WT system respectively.

2.2.7.5 ESS cost model

The operational cost usually maintenance cost of ESS, is believed to be to a linear function of the absolute amount of charged/discharged capacity $P_{ESS_{s,t}}$ as shown in equation (2.55). The operation of ESS is constrained by the maximum charging power $P_{Charge}^{max}$and discharging power $P_{Discharge}^{max}$ limits as (2.56) and (2.57), minimum energy storage capacity E^{min} and maximum energy storage capacity E^{max} as (2.58). The dynamic energy model for ESS is represented by equation (2.59).

$$Cost_{ESS_{s,t}} = b_{ESS} \times \left|P_{ESS_{s,t}}\right| + c_{ESS} \tag{2.55}$$

$$P_{Charge_{s,t}} \leq P_{Charge}^{max}, \ \forall\, s = 1{:}\, N_s, t = 1{:}\, 24 \tag{2.56}$$

$$P_{Discharge_{s,t}} \leq P_{Discharge}^{max}, \quad \forall\, s = 1{:}\, N_s, t = 1{:}\, 24 \tag{2.57}$$

$$E^{min} \leq E_{s,t} < E^{max}\ , \qquad \forall\, s = 1{:}\, N_s, t = 1{:}\, 24 \tag{2.58}$$

$$E_{s,t} = E_{s,(t-1)} + \left(\zeta \times P_{Charge_{s,t}} - \frac{P_{Discharge_{s,t}}}{\tau}\right) \quad (2.59)$$

Here, b_{ESS} and c_{ESS} are the cost coefficients of ESS system. $P_{Charge_{s,t}}$ and $P_{Discharge_{s,t}}$ are the charging and discharging power of ESS at t^{th} hour for s^{th} scenario respectively. ζ and τ are the charging and the discharging efficiencies of the ESS respectively.

2.2.7.6 DRP model

DRP evens out the load demand curve and curtails probable operational cost of microgrid. Besides, the DRP is remodeled in this work in such a manner that, it also facilitates load shifting from the vulnerable outage periods to the off-peak or inexpensive periods. The operational cost is minimized as microgrid procures a lesser amount of energy in outage periods as well as peak periods. In this study, both the price based and the incentive based DRP formulation is considered [74].

A. Price based DRP

Price based DRP is formulated in accordance with TOU program [75], [76]. Here some percentage of loads is reallocated from the expensive or peak periods to cheap or off-peak periods maintaining the total amount of daily load to be fixed. The demand-side load consumption reduction by consumers taking part in the price based DRP in a day-ahead energy market at any hour t is represented in equation (2.60) [50].

$$PDRP_{s,t} = L_{Base_{s,t}} \times \sum_{t'=1}^{24} \left(E_{t,t'} \times \frac{r_{Load_{t'}} - r^0_{Load_{t'}}}{r^0_{Load_{t'}}}\right) \quad (2.60)$$

Here, $L_{Base_{s,t}}$ represents the base load before DRP integration. $r^0_{Load_{t'}}$ and $r_{Load_{t'}}$ are the electricity tariffs before and after pertaining the price based DRP. $E_{t,t'}$ signifies the elasticity of demand applying to t^{th} and t'^{th} hours. The elasticity in load demand can be estimated by a variety of mechanisms based on the survey analysis from consumers and real data [77].

B. Incentive based DRP

Incentive remuneration is offered to the energy consumers who are partaking in the incentive based DRP. Unlike the price based DRP, here the response rates are not correlated to the consumers' response to electricity price alterations but are connected to other significant parameters for example the failure of system components, weather conditions and their effects on generation outages. In this work the incentive based DRP takes account of emergency DRP [78]. Throughout any emergency hour t the reduction in load consumption is rewarded with lofty incentives as guided by emergency based DRP in real time market as specified in equation (2.61) [78].

$$IDRP_{s,t} = L_{Base_{s,t}} \times \sum_{t'=1}^{24} \left(E_{t,t'} \times \frac{c_{DRP_{t'}}}{r^0_{Load_{t'}}} \right) \quad (2.61)$$

Here, $c_{DRP_{t'}}$ symbolizes the incentive reward payments to the customers at hour t [$/MWh]. Therefore, the percentage in load change $DRP_{s,t}$ from $L_{Base_{s,t}}$ during DRP integration at t^{th} hour is set by equation (2.62). $DRP_{s,t}$ is delimited by the limit DRP^{max} as in equation (2.63) and (2.64).

$$DRP_{s,t} = PDRP_{s,t} + IDRP_{s,t} - Inc_{s,t} \quad (2.62)$$

$$\left| DRP_{s,t} \right| \leq DRP^{max}, s = 1{:}\, N_s, t = 1{:}\, 24 \quad (2.63)$$

$$\sum_{t=1}^{24} \left(DRP_{s,t} \times L_{Base_{s,t}} \right) = 0 \quad (2.64)$$

Here, $Inc_{s,t}$ presents the consumption rise by the customers taking part in DRP at any hour t. The DRP customized load $L_{s,t}$ is presented by equation (2.65).

$$L_{s,t} = \left(1 - DRP_{s,t}\right) \times L_{Base_{s,t}} \quad (2.65)$$

2.2.7.7 Energy imbalance compensation

The probable energy imbalance P_{Imb_t} which must be remunerated in the real-time energy market is formulated as equation (2.66). The positive imbalance price $r_{PI_t}$and the negative imbalance price r_{NI_t} are controlled by the upward or the downward regulations as determined by the MGCC or the TSO as shown in (2.67).

$$Compensation_{Imbalance} = \sum_{t=1}^{24}\left[r_{I_t} \times P_{Imb_t}\right] \tag{2.66}$$

$$r_{I_t} = \begin{cases} r_{PI_t} \leq r_{Grid_t}, & P_{Imb_t} > 0 \\ r_{NI_t} > r_{Grid_t} & P_{Imb_t} < 0 \end{cases} \quad \forall\, t = 1{:}\,24 \tag{2.67}$$

2.2.7.8 Supply-demand balance

The constraint, balance of supply-demand as depicted in equation (2.68) makes sure that the total power generated by the renewable systems, the GTs, power acquired from the ESSs and the negative power imbalance (when, $P_{Imb_t} < 0$)(which has to be procured from the real-time electricity market) has to be equal to the summation of the DRP customized local loads, the power transacted with the main grid and the positive power imbalance (when, $P_{Imb_t} > 0$)(which has to be traded in the real-time market).

$$\sum_{i=1}^{N_{GT}}\left[P_{GT_{i,s,t}} \times S_{GT_{i,s,t}}\right] + \sum_{j=1}^{N_{PV}}\left[P_{PV_{j,s,t}} \times S_{PV_{j,s,t}}\right] + \sum_{k=1}^{N_{WT}}\left[P_{WT_{k,s,t}} \times S_{WT_{k,s,t}}\right] + P_{Discharge_{s,t}} = L_{s,t} + P_{Charge_{s,t}} + P_{Grid_t} + P_{Imb_{s,t}} \tag{2.68}$$

2.2.7.9 CVaR constraints

In order to evaluate the CVaR, the subsequent linear constraint [55] is included in the objective function as depicted in equation (2.69). These are used to calculate the value at risk.

$$VaR - Profit_{MG_s} \leq \eta_s\,, \qquad \forall\, \eta_s \geq 0 \tag{2.69}$$

2.2.8 Value of stochastic solution

Value of the stochastic solution (VSS) [55] is an adept measure to efficiently validate and compare the performance of the stochastic programming models over deterministic ones. Firstly, the stochastic problems are resolved using their associated deterministic first phase variables. Then VSS is estimated as equation (2.70) where, $f_{Deterministic}$ is the deterministic solution obtained from the first phase and $f_{Stochastic}$ represents the objective value attained from the stochastic optimization.

$$VSS = f_{Stochastic} - f_{Deterministic} \tag{2.70}$$

2.3 Summary

To achieve the solutions of the stated power system security issues using soft computing approaches, the concerned systems, their security problems and objective functions should be formulated precisely maintaining all the constraints.

Firstly, problem formulation for optimization-based fault diagnosis has been provided. PV system, fault pattern realization and objective function to diagnose the open circuit and short circuit test have been modeled. The fault diagnosis scheme has also been described where improve real coded genetic algorithm (IRGA) is employed for the optimization of the objective function. The detailed description of the IRGA based fault diagnosis of PV system is provided in the next chapter.

Next, the problem formulation of optimal bidding strategy for microgrid under outages and uncertainties has been presented. Market model, bidding strategy considering uncertainty of the microgrid, scenario generation and objective function considering risk management has been structured. The precise modeling of the constraints and fitness function for optimal bidding strategy for microgrid under outages and uncertainties led to an complex mixed integer non-linear programming for which LINDOGlobal solver is used for the solution purpose. A comprehensive depiction of LINDOGlobal solver for MINLP based optimal bidding plan of microgrid under uncertainties and outages is presented in the subsequent chapter.

This page is left blank intentionally.

Chapter 3

Soft computing approaches for problem solution

3.1 Improved real-coded genetic algorithm for fault diagnosis of PV system

The real-coded genetic algorithm (RGA) amalgamated with simulated binary style crossover and polynomial style mutation [79]-[82] is employed to resolve the proposed fault diagnosis problem. For the implementation of improved real-coded genetic algorithm, one-to-one level challenge is introduced in RGA to enhance the convergence pace and the solution quality. Here, each offspring candidate competes with the matching ancestor candidate one-to-one. The IRGA can be segmented functionally in five sub-stages, viz., the initialization, the selection of the parent population, the crossover, the mutation and the selection between the parent and the offspring [66]. A comprehensive depiction of segment wise solution process employing IRGA in fault diagnosis of PV system is presented in the following sections.

In this work, the IRGA attempts to search for a switching pattern which can accurately imitate the plausible SC fault and OC fault pattern in the PV system for inconsistent irradiation and temperature patterns throughout the array. Here, the variable or decision vector (N_{sc}, N_{oc}, sc, oc) is defined as a candidate. The elements of the candidate range from the value 0 to N, the total number of modules in the PV array. Subsequently, the optimizer allots '0' or '1' to the switches SOCs and SSCs corresponding to the produced candidates as discussed in section 2. After that, the array output power (P_{Array}) from the simulated PV system is calculated accordingly. Once the right candidate or correct fault pattern is achieved by the IRGA, the objective function (12) value converges. The task flow of the proposed fault diagnosis procedure for OC and SC faults in PV system using IRGA is as follows.

A. Initialization. The initial population $(N_{sc}, N_{oc}, sc, oc)_k$ of candidates or decision variables is chosen at random within limits as in (3.1).

$$\left.\begin{array}{l} k \in N_{pop} \\ (N_{sc} + N_{oc}) \in \{U(0, N)\} \\ sc: \{sc_1, sc_2, sc_3, \dots, sc_{N_{sc}}\} \\ oc: \{oc_1, oc_2, oc_3, \dots, oc_{N_{oc}}\} \\ a \in \{1, \dots, N_{sc}\} \\ b \in \{1, \dots, N_{oc}\} \\ sc_a \in \{U(0, N)\} \\ oc_b \in \{U(0, N)\} \end{array}\right\} \quad (3.1)$$

Here, N_{pop} stands for the population size. $(N_{sc}, N_{oc}, sc, oc)_k$ is the k^{th} population. Elements of sc and oc are mutually exclusive. $U(0, N)$ represents a uniform random integer ranging over $[0, N]$.

The objective function value $f(N_{sc}, N_{oc}, sc, oc)_k$ of each population is computed.

B. Selection of parent population. The binary tournament style selection process is employed for select the compatible parents within the mating pool [66]. For this, two chromosomes are arbitrarily selected from the generated population. Their objective function values are then compared. The champion chromosomes are reserved in the mating pool. This procedure runs in repetitive manner until the mating pool is filled with the chromosomes.

C. Simulated Binary Crossover (SBC). The course of generating the offspring $(N_{sc}, N_{oc}, sc, oc)'_1$ and $(N_{sc}, N_{oc}, sc, oc)'_2$ from two mating parents $(N_{sc}, N_{oc}, sc, oc)_1$ and $(N_{sc}, N_{oc}, sc, oc)_2$ by utilizing SBX operator is depicted as follows.

a. Generate a random number *n* between 0 and 1.

b. Fetch a parameter γ by exploiting polynomial PDF as (3.2).

$$\gamma = \begin{cases} (n\alpha)^{\frac{1}{\eta_c+1}}, & if\ n \le \frac{1}{\alpha} \\ \left(\frac{1}{2-n\alpha}\right)^{\frac{1}{\eta_c+1}}, & otherwise \end{cases} \tag{3.2}$$

Here $\alpha = 2 - \beta^{-(\eta_c+1)}$ and β can be computed as (3.3).

$$\beta = 1 + \frac{2}{(N_{sc},N_{oc},sc,oc)_2 - (N_{sc},N_{oc},sc,oc)_1} \times \min\Big[\big((N_{sc},N_{oc},sc,oc)_1 - (N_{sc},N_{oc},sc,oc)^{\min}\big), \big((N_{sc},N_{oc},sc,oc)^{\max} - (N_{sc},N_{oc},sc,oc)_2\big)\Big] \tag{3.3}$$

The parameter η_c stands for distribution index for the SBX and can gain any non-negative value. An infinitesimal value of η_c allows the creation of offspring far away from the parents and a great value limits the generation of offspring relatively close to the parent populations.

c. The intermediate populations are calculated as (3.4) and (3.5).

$$(N_{sc},N_{oc},sc,oc)_{p1} = 0.5\,[\big((N_{sc},N_{oc},sc,oc)_1 + (N_{sc},N_{oc},sc,oc)_2\big) - \gamma\big(\big| (N_{sc},N_{oc},sc,oc)_2 - (N_{sc},N_{oc},sc,oc)_1\big|\big)] \tag{3.4}$$

$$(N_{sc},N_{oc},sc,oc)_{p2} = 0.5\,[\big((N_{sc},N_{oc},sc,oc)_1 + (N_{sc},N_{oc},sc,oc)_2\big) + \gamma\big(\big| (N_{sc},N_{oc},sc,oc)_2 - (N_{sc},N_{oc},sc,oc)_1\big|\big)] \tag{3.5}$$

D. Polynomial Mutation. The polynomial PDF is employed as the mutation operator to create an offspring in the vicinity of a parent population as stated as follows:

a. Randomly generate a number *n* between 0 and 1.

b. Calculate the parameter σ as (3.6).

$$\sigma = \begin{cases} [2n + (1-2n)(1-\varphi)^{(\eta_m+1)}]^{\frac{1}{\eta_m+1}} - 1, & if\ n \le 0.5 \\ 1 - [2(1-n) + 2(n-0.5)(1-\varphi)^{(\eta_m+1)}]^{\frac{1}{\eta_m+1}}, & otherwise \end{cases} \tag{3.6}$$

Here, $\varphi = \frac{min|(\,(N_{sc},N_{oc},sc,oc)_p - (N_{sc},N_{oc},sc,oc)^{\min}),(\,(N_{sc},N_{oc},sc,oc)^{\min} - (N_{sc},N_{oc},sc,oc)_p)|}{(\,(N_{sc},N_{oc},sc,oc)^{\max} - (N_{sc},N_{oc},sc,oc)^{\min})}$. The parameter η_m symbolizes the distribution index for the mutation and attain any non-negative value.

c. Evaluate the mutated offspring as (3.7) and (3.8).

$$(N_{sc},N_{oc},sc,oc)'_1 = (N_{sc},N_{oc},sc,oc)_{p1} + \sigma(\,(N_{sc},N_{oc},sc,oc)^{\max} - (N_{sc},N_{oc},sc,oc)^{\min}) \quad (3.7)$$

$$(N_{sc},N_{oc},sc,oc)'_2 = (N_{sc},N_{oc},sc,oc)_{p2} + \sigma(\,(N_{sc},N_{oc},sc,oc)^{\max} - (N_{sc},N_{oc},sc,oc)^{\min}) \quad (3.8)$$

The perturbation can be altered by varying η_m and p_m with the iterations as (3.9) and (3.10).

$$\eta_m = \eta_{m\,\min} + iter \quad (3.9)$$

$$p_m = \frac{1}{N_{choice}} + \frac{iter}{iter_{\max}}(1 - \frac{1}{N_{choice}}) \quad (3.10)$$

Here $\eta_{m\,\min}$ represents the user's definite lowest value for η_m. The p_m is probability of mutation, and N_{choice} represents the number of choice variables.

d. Compute the objective function value of each offspring.

E. Selection between parent and offspring. Assortment of each parent $(N_{sc},N_{oc},sc,oc)_k$ by comparing its objective function value to the matching offspring $(N_{sc},N_{oc},sc,oc)'_k$ is performed. The population with lower objective function value between parent and offspring is carried on for the subsequent iteration as (3.11).

$$(N_{sc},N_{oc},sc,oc)_i = \begin{cases} (N_{sc},N_{oc},sc,oc)'_k, & if\ f(\,(N_{sc},N_{oc},sc,oc)'_k) \le f(\,(N_{sc},N_{oc},sc,oc)_k) \\ (N_{sc},N_{oc},sc,oc)_k, & otherwise \end{cases} \quad (3.11)$$

The process is simulated until the convergence, or the iteration limit is reached. The computational outline for the projected fault diagnosis employing IRGA is as follows.

Fault diagnosis algorithm.

Step 1. Acquire $P_{Measured}$, $V_{Measured}$, $I_{Measured}$, module irradiation and temperature data from physical PV system.

Step 2. Estimate ε and P_{Array} from module irradiation and temperature data for no fault or normal condition at MPP.

Step 3. If ($P_{Measured}$+ ε)< P_{Array}, initialize IRGA. Set, N_{pop}, η_c, itr_max.
Else, generate a notification: "Healthy PV array".

Step 4. Generate the parent population $(N_{sc}, N_{oc}, sc, oc)_k$, such that,
$k \in N_{pop}$, $(N_{sc} + N_{oc}) \in \{U(0,N)\}$, $sc \in \{sc_1, sc_2, sc_3, \dots, sc_{N_{sc}}\}$, $oc \in \{oc_1, oc_2, oc_3, \dots, oc_{N_{oc}}\}$, $a \in N_{sc}$, $b \in N_{oc}$, $sc_a \in \{U(0,N)\}$, $oc_b \in \{U(0,N)\}$. Evaluate the objective function value $f_k((N_{sc}, N_{oc}, sc, oc)_k)$. Set iteration count (itr) equals to 1.

Step 5. Choose parent population $(N_{sc}, N_{oc}, sc, oc)_k$ based on the objective function.

Step 6. Create two offspring $(N_{sc}, N_{oc}, sc, oc)'_1$ and $(N_{sc}, N_{oc}, sc, oc)'_2$ from two selected parents $(N_{sc}, N_{oc}, sc, oc)_1$ and $(N_{sc}, N_{oc}, sc, oc)_2$ by operating the simulated binary crossover and the polynomial mutation by equations (3.2) to (3.10) and evaluate the objective function value $f_i((N_{sc}, N_{oc}, sc, oc)'_k)$ of each offspring.

Step 7. Perform an selection between each parent $(N_{sc}, N_{oc}, sc, oc)_k$ and matching offspring $(N_{sc}, N_{oc}, sc, oc)'_k$ based on the objective function.

Step 8. Select the survivor between the parent and the matching offspring with smaller objective function value $f_i(N_{sc}, N_{oc}, sc, oc)_k$ so that,

$$(N_{sc}, N_{oc}, sc, oc)_k = \begin{cases} (N_{sc}, N_{oc}, sc, oc)'_k, & if\ f((N_{sc}, N_{oc}, sc, oc)'_k) \le f((N_{sc}, N_{oc}, sc, oc)_k) \\ (N_{sc}, N_{oc}, sc, oc)_k, & otherwise \end{cases}.$$

Step 9. If $f_i((N_{sc}, N_{oc}, sc, oc)_k) \le \varepsilon$, go to step 10.
Else go to step 12.

Step 10. Get V_{Array} and I_{Array} for $(N_{sc}, N_{oc}, sc, oc)_k$.

Step 11. If $V_{Measured}$=V_{Array} and $I_{Measured}$=I_{Array}, display the detected fault pattern and go to step 15.
Else go to step 11.

Step 12. itr=itr+1.

Step 13. If itr=itr_max, go to step 14.
Else go to step 5.

Step 14. Produce a warning notification: "Failed to distinguish fault".

Step 15. Terminate.

3.2 LINDOGlobal solver for MINLP optimal bidding plan of microgrid under uncertainties and outages

The precise modeling of the constraints and components in the microgrid incorporating outages and uncertainties led to an enormous complex MINLP optimal bidding problem (equations 2.38-2.69) as they consist of following traits [83].

1. It contains both discrete (P_{GT}, S_{GT}) and continuous (P_{Grid}, P_{ESS}) decision variables.
2. The objective function and the constraints are non-linear involving potential non-convexities.
3. The problem consists of both equality and inequality constraints.

Traditional nonlinear optimization solvers seldom get trapped at suboptimal points or local solutions for such complex MINLP with numerous integers and floating-point variables. This situation can be avoided using the global soft computing solvers. Hence, the proposed MINLP problem is solved using the Linear, Interactive, and Discrete Optimizer global (LINDOGlobal) solvers in GAMS to attain the global solutions [84], [85]. LINDOGlobal is an advanced commercial solver. The LINDOGlobal solver technique employs branch-and-cut approaches to break up a nonlinear programming model into several sub problems to relax the non-convex problem into multiple convex problems. Each sub problem is analyzed and returns any of the following findings accordingly: a) not have a optimal or feasible solution, or b) an optimal solution to the sub problem is found, in case the sub problem is appeared to be convex, or c) the sub problem need further division into two or more sub problems which are subsequently placed in the branch list. Provided suitable tolerances, after a finite number of iterations a solution of provable global optimal is achieved. The operation flow of LINDOGlobal solver is shown in Figure 3.1.

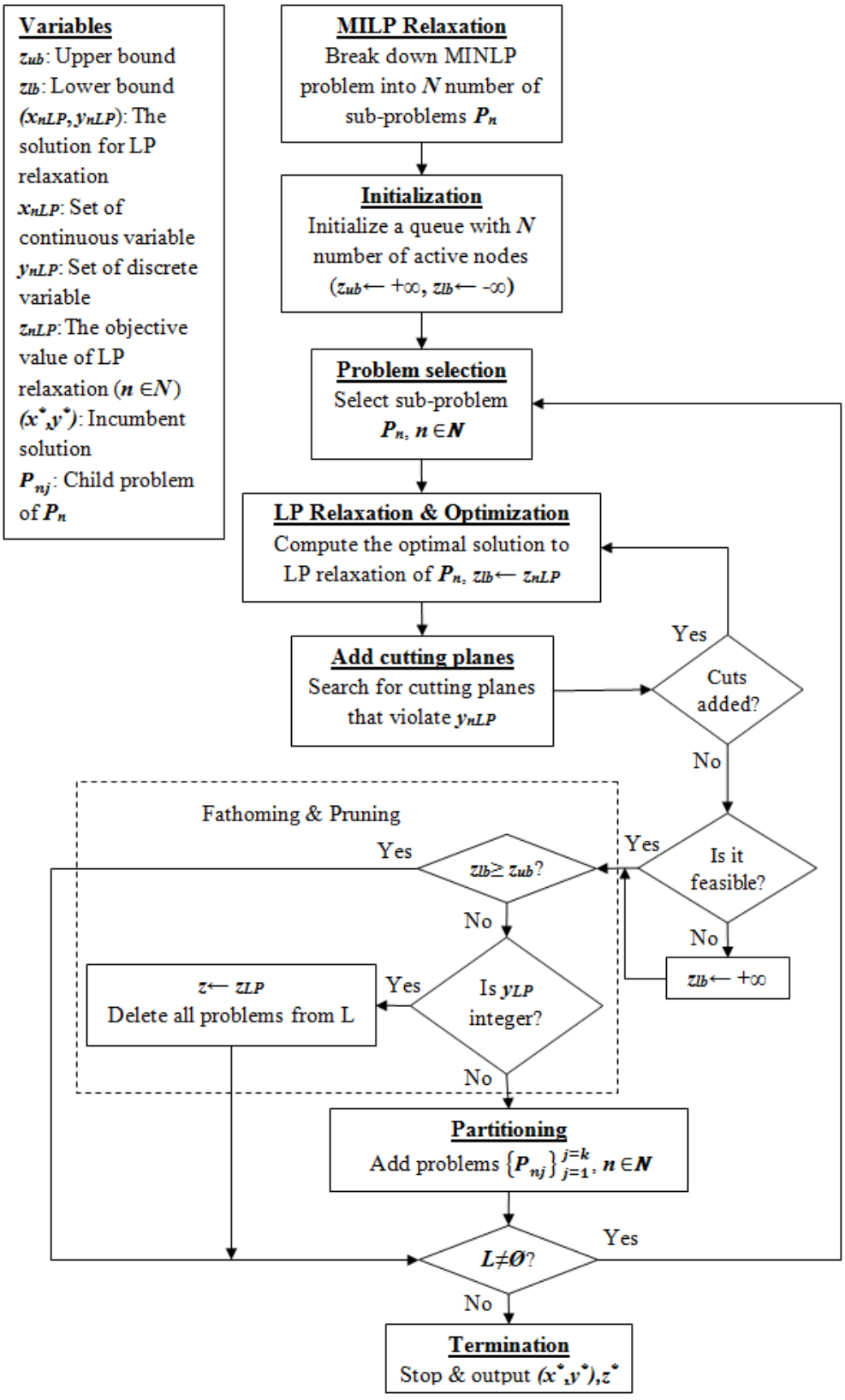

Figure 3. 1 Flowchart of LINDOGlobal solver.

3.3 Summary

Two soft computing approaches have been stated here for the solution of the concerned power system security problems.

Improved real coded genetic algorithm has been implemented to solve the fault diagnosis in PV system. Initialization, parent selection, binary crossover, polynomial mutation and winner selection are modeled to diagnose the probable open circuit and short circuit faults in PV system. The implementation yields diagnosis results, such as faulted PV modules, type and location of fault, which are presented in Chapter 4.

LINDOGlobal optimization technique to solve MINLP problems has also been discussed. This method is employed to plan the optimum strategy for day-ahead bidding of microgrid considering outages and uncertatainties. To find the global solution for this MINLP type optimal bidding plan of microgrid using LINDOGlobal solver GAMS software is used and generated results are presented and discussed in the next chapter.

This page is left blank intentionally.

Chapter 4

Result and discussion

4.1 Performance assessment of optimization-based fault diagnosis of PV system

4.1.1 Illustrative implementation

To assess the performance of the projected fault diagnosis methodology, it is tested on a PV system as displayed in Figure 2. 5. MATLAB R2013a platform is used to develop fault diagnosis numerical studies. As an online fault diagnosis mechanism, the time operation and data processing is limited within 5sec. After each 5sec time interval, online calibrated data are updated and fed to the diagnoser. If the algorithm get $P_{Measured}$ is lesser than $P_{Simulated}$, the optimizer initiates searching for the plausible fault pattern. N_{pop}, η_c and *itr_max* are initialized respectively as 50, 0.4 and 100. Allowing for $\pm 0.1\%$ overall error in the measuring devices, ε is calculated as 0.1% of $P_{Measured}$ for each execution.

Knowing that inconsistent irradiations over the PV array can significantly alter the temperature allotment and the electrical outputs, diverse module irradiation (Gn) and module temperature (Tn) setting are adopted as input for precise verification of the anticipated fault diagnosis algorithm. Furthermore, the situation of resemblance in the array output power, either from a healthy PV system under heterogeneous irradiation and a faulty PV array, or from the PV arrays undergoing two dissimilar faulty patterns, are taken into account. Thus, for appropriate validation of the projected methodology, a number of experiments are performed with diverse fault patterns experiencing varieties of inconsistent irradiation and temperature distribution. These fault combinations undergoing ranges of varied ambient situations are intentionally established in the physical PV test system. The modules are serially numbered as 1, 2, ..., 10 counting, starting from the negative terminal of the PV array as displayed in Figure 2. 6. The

Nominal Operating Cell Temperature (NOCT) is considered as 48°C and the ambient temperature is measured as 25°C at the instant of the experimentation.

To assess the efficacy of the fault identification approach in dissimilar operating conditions of the PV system, four sets of heterogeneous irradiation and temperature conditions (C1, C2, C3 and C4) are created and are tabulated as in Table 4. 1. Irradiation is varied randomly at four levels, viz., 800-1000 W/m^2 (High irradiation level), 600-800 W/m^2 (Medium irradiation level), 0-600 W/m^2 (Low irradiation level) and finally 0-1000 W/m^2 (Highly non-uniform irradiation level). For experimental validation of the diagnosis stratagem, the programmed algorithm is tested using these data under numerous experiments (E1, E2, ... , E12). For each set of the PV system conditions, the fault diagnosis procedure is tested thrice following different fault combinations. One test case for every set is evaluated for the healthy state of the PV array. Other two test cases correspond to different combinations of OC and SC faults. E6 presents incidences of only SC faults in the combination, while E8 presents the occurrences of only OC faults. Therefore, twelve (4x3) number of consecutive sample cases are considered for the validation the proposed strategy through diverse test conditions. The procedural data of the examined fault combinations, which are physically created throughout these experiments, are tabulated in Table 4. 2.

Table 4. 1 Module irradiation levels and corresponding module temperature data.

Operating conditions		Positions of modules									
		1st	2nd	3rd	4th	5th	6th	7th	8th	9th	10th
C1	G1 (W/m^2)	830	879	860	826	887	818	933	802	915	968
	T1 (°C)	54.1	55.8	55.1	54	56	53.6	57.7	53.1	57	58.9
C2	G2 (W/m^2)	647	670	714	612	699	728	644	767	794	741
	T2 (°C)	47.6	48.45	50	46.4	49.5	50.5	47.5	51.8	52.8	50.9
C3	G3 (W/m^2)	304	167	448	142	574	372	360	104	54	153
	T3 °C	35.6	30.8	40.7	30	45.1	38	37.6	28.6	26.9	30.4
C4	G4 (W/m^2)	451	283	790	364	532	712	871	129	650	975
	T4 °C	40.8	35	52.7	37.7	43.6	50	55.5	29.5	47.8	59.1

Table 4. 2 Examined faults and procedural data from physical measurement.

Experiment	Condition	Actual Fault Position		$P_{Measured}$	$V_{Measured}$	$I_{Measured}$
		OC	SC	(W)	(V)	(A)
E1	C1	Nil[a]	Nil[a]	2239.30	324.93	6.89
E2	C1	1,8,9	2,5	1070.50	155.20	6.90
E3	C1	4	6,7	1557.10	225.65	6.90
E4	C2	Nil[a]	Nil[a]	1787.60	334.25	5.34
E5	C2	3,5	1,10	1041.30	196.54	5.30
E6	C2	Nil[a]	1, 2, 3	1254.60	235.22	5.33
E7	C3	Nil[a]	Nil[a]	446.40	168.56	2.66
E8	C3	2,6,9	Nil[a]	347.70	131.99	2.63
E9	C3	3,4,7	1,9	189.90	60.62	3.14
E10	C4	Nil[a]	Nil[a]	972.30	245.53	3.96
E11	C4	7,10	4,8	669.30	170.14	3.93
E12	C4	8	6	824.60	208.75	3.95

[a] Nil represents normal operation (no fault).

This diagnosis design operates based on the analysis of the electrical parameters of a PV array. The electrical characteristics of the PV array are produced by means of Matlab simulator according to the irradiation and temperature data and the fault patterns to be examined. The simulated P-V-I characteristics of E1, E2 and E3 experiments, which are undergoing condition C1, are presented in Figure 4. 1. Figure 4. 2 presented the P-V-I characteristics of E4, E5 and E6 experiencing condition C2. Likewise, Figure 4. 3 and Figure 4. 4 demonstrate the P-V-I characteristics of E7, E8 and E9 experiencing condition C3 and P-V-I characteristics of E10, E11 and E12 experiencing condition C4 respectively. It can be studied that for dissimilar fault combinations under dissimilar conditions, the patterns of the P_V-I characteristics curves are dissimilar. Moreover, the behaviors and magnitudes of the array power output contrast greatly between two different fault combinations.

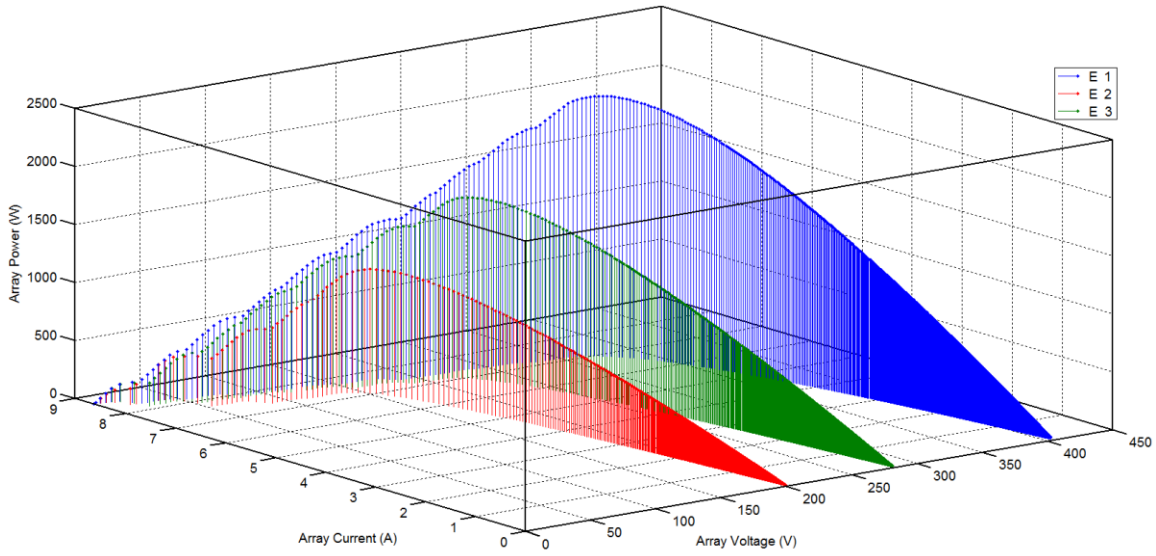

Figure 4. 1 Simulated P-V-I characteristics of E1, E2 and E3.

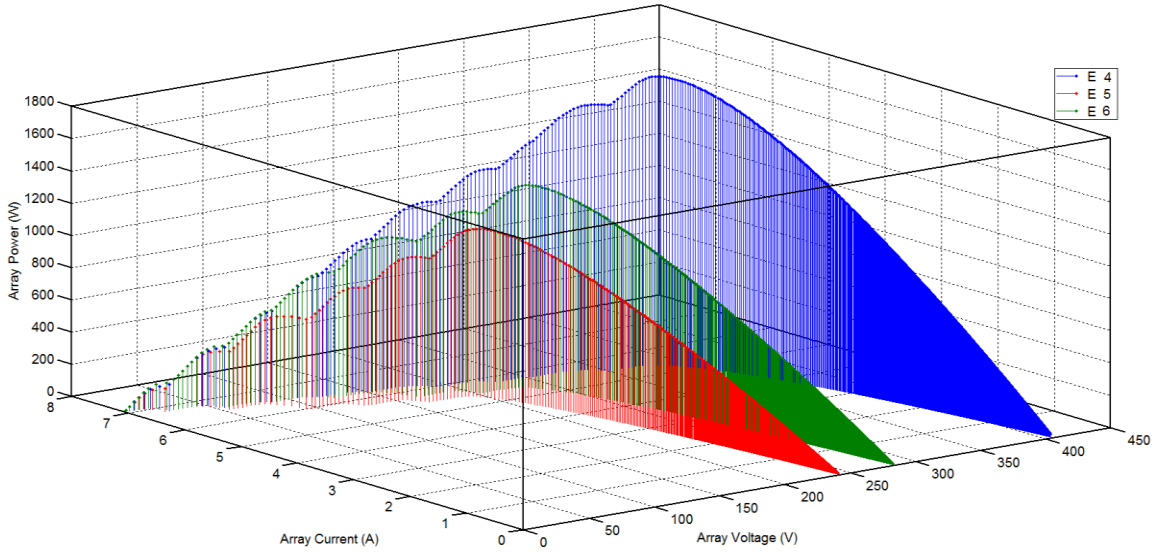

Figure 4. 2 Simulated P-V-I characteristics of E4, E5 and E6.

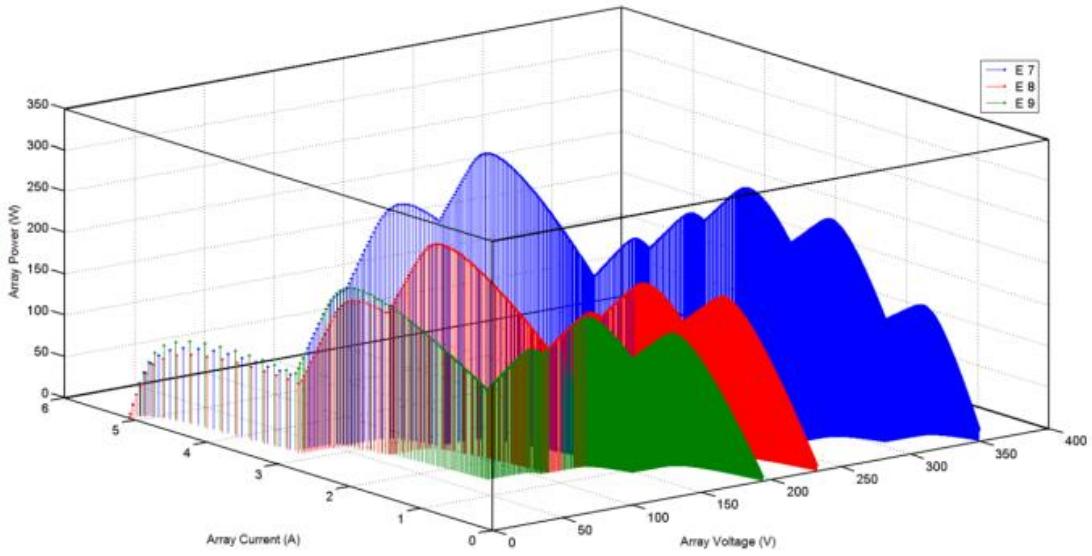

Figure 4. 3 Simulated P-V-I characteristics of E7, E8 and E9.

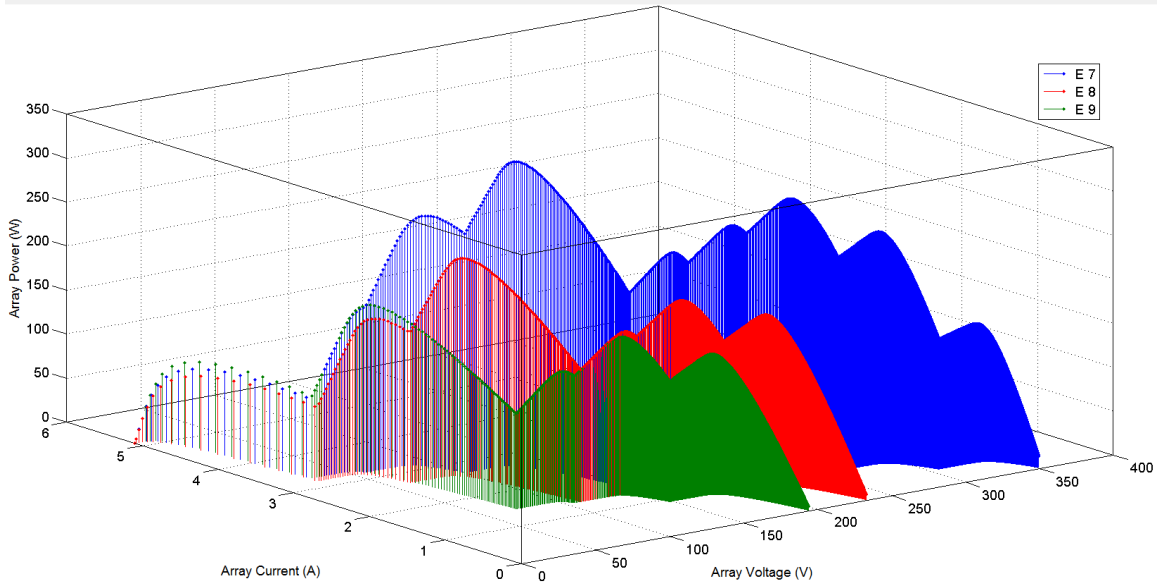

Figure 4. 4 Simulated P-V-I characteristics of E10, E11 and E12.

Figure 4. 5 depicts the variations of simulated PV array power outputs with simulated array output voltage for all the fault combinations. Correspondingly, Figure 4. 6 displays the variations of simulated PV array power outputs with simulated array current outputs for all the fault combinations. The specific marker positioned on each curve in Figure 4. 5 and Figure 4. 6 indicate the MPP array powers regarding the MPP array voltages and MPP array currents respectively for the listed fault combinations as presented in Table 4.2.

.

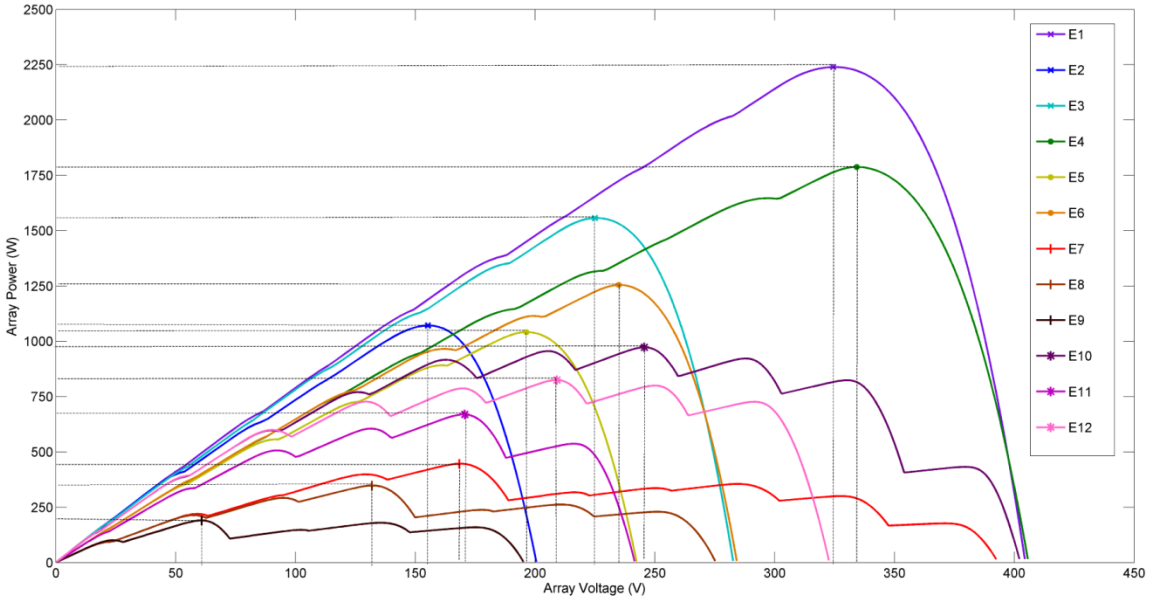

Figure 4. 5 Simulated P-V characteristics of E1 to E12.

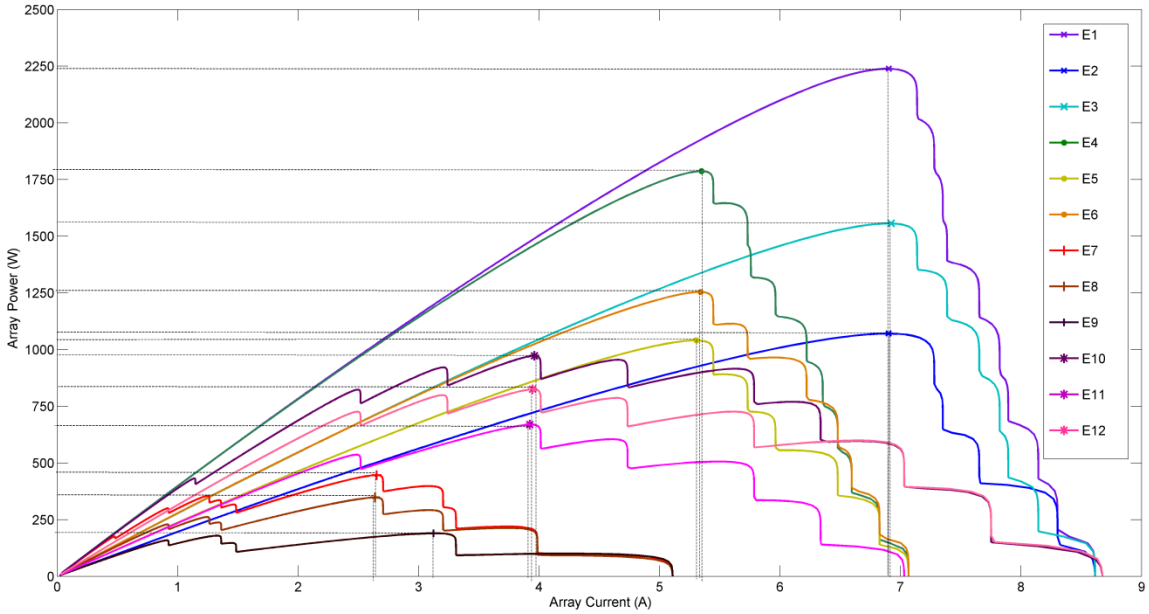

Figure 4. 6 Simulated P-I characteristics of E1 to E12.

Ten rounds of executions (Ex1-Ex10) for each test case (E1-E12) are performed. According to Table 4.2, in the cases of E1, E4, E7 and E10, the array runs in healthy or no-fault condition. For the entire executions of these cases, the diagnoser achieves success and notify "Healthy PV array". The execution outcomes of each experiment and relevant response time for the rest of the cases are presented in Table 4. 1 to Table 4. 10.

The variation propensity of objective function in the iterative progression is imperative for the investigation of convergence property of the projected optimization-based algorithm. The convergence curves for all the executions of the experiments E2, E3, E5, E6, E8, E9, E11 and E12 are depicted as in Figure 4. 7- Figure 4. 12.

Table 4. 3 Results obtained by the diagnoser in case of E2.

Executions of E2	P_{Array} (W)	V_{Array} (V)	I_{Array} (A)	$f(N_{sc}, N_{oc}, sc, oc)$ (W)	ε	Detected Fault Position		Response Time (sec)
						OC	SC	
Ex 1	1070.6770	155.2102	6.8982	0.1770	1.0706	1,8,9	2,5	3.104
Ex 2	1070.6770	155.2102	6.8982	0.1770	1.0706	1,8,9	2,5	3.224
Ex 3	1070.6770	155.2102	6.8982	0.1770	1.0706	1,8,9	2,5	3.512
*Ex 4	1073.9761	155.4492	6.9088	3.4761	1.0706	1,8,9	3,5	4.997
Ex 5	1070.6770	155.2102	6.8982	0.1770	1.0706	1,8,9	2,5	3.296
Ex 6	1070.6770	155.2102	6.8982	0.1770	1.0706	1,8,9	2,5	3.008
*Ex 7	1068.9470	155.0848	6.8926	1.5530	1.0706	1,7,8	2,5	5.001
Ex 8	1070.6770	155.2102	6.8982	0.1770	1.0706	1,8,9	2,5	3.032
Ex 9	1070.6770	155.2102	6.8982	0.1770	1.0706	1,8,9	2,5	3.006
Ex 10	1070.6770	155.2102	6.8982	0.1770	1.0706	1,8,9	2,5	2.798

* represents "Failed to distinguish fault".

Table 4. 4 Results obtained by the diagnoser in case of E3.

Executions of E3	P_{Array} (W)	V_{Array} (V)	I_{Array} (A)	$f(N_{sc}, N_{oc}, sc, oc)$ (W)	ε	Detected Fault Position		Response Time (sec)
						OC	SC	
Ex 1	1557.0673	225.6459	6.9004	0.0327	1.5571	4	6,7	2.627
Ex 2	1557.0673	225.6459	6.9004	0.0327	1.5571	4	6,7	2.684
*Ex 3	1558.809	225.7721	6.9043	1.709	1.5571	4	6,9	4.999
Ex 4	1557.0673	225.6459	6.9004	0.0327	1.5571	4	6,7	2.836
Ex 5	1557.0673	225.6459	6.9004	0.0327	1.5571	4	6,7	3.311
Ex 6	1557.0673	225.6459	6.9004	0.0327	1.5571	4	6,7	2.874
Ex 7	1557.0673	225.6459	6.9004	0.0327	1.5571	4	6,7	2.988
Ex 8	1557.0673	225.6459	6.9004	0.0327	1.5571	4	6,7	2.779
Ex 9	1557.0673	225.6459	6.9004	0.0327	1.5571	4	6,7	2.819
Ex 10	1557.0673	225.6459	6.9004	0.0327	1.5571	4	6,7	2.742

* represents "Failed to distinguish fault".

Table 4. 5 Results obtained by the diagnoser in case of E5.

Executions of E5	P_{Array} (W)	V_{Array} (V)	I_{Array} (A)	$f(N_{sc}, N_{oc}, sc, oc)$ (W)	ε	Detected Fault Position		Response Time (sec)
						OC	SC	
Ex 1	1041.3284	196.5535	5.2979	0.0284	1.0413	3,5	1,10	2.775
Ex 2	1041.3284	196.5535	5.2979	0.0284	1.0413	3,5	1,10	3.351
Ex 3	1041.3284	196.5535	5.2979	0.0284	1.0413	3,5	1,10	3.056
Ex 4	1041.3284	196.5535	5.2979	0.0284	1.0413	3,5	1,10	2.864
Ex 5	1041.3284	196.5535	5.2979	0.0284	1.0413	3,5	1,10	3.272
Ex 6	1041.3284	196.5535	5.2979	0.0284	1.0413	3,5	1,10	3.561
Ex 7	1041.3284	196.5535	5.2979	0.0284	1.0413	3,5	1,10	3.086
Ex 8	1041.3284	196.5535	5.2979	0.0284	1.0413	3,5	1,10	4.061
*Ex 9	1042.9419	196.4979	5.3035	1.6419	0.8447	3,5	7,10	4.996
Ex 10	1041.3284	196.5535	5.2979	0.0284	1.0413	3,5	1,10	2.759

* represents "Failed to distinguish fault".

Table 4. 6 Results obtained by the diagnoser in case of E6.

Executions of E6	P_{Array} (W)	V_{Array} (V)	I_{Array} (A)	$f(N_{sc}, N_{oc}, sc, oc)$ (W)	ε	Detected Fault Position		Response Time (sec)
						OC	SC	
Ex 1	1254.6165	235.2203	5.3337	0.0165	1.254	Nil[a]	1, 2, 3	2.672
Ex 2	1254.6165	235.2203	5.3337	0.0165	1.254	Nil[a]	1, 2, 3	2.735
Ex 3	1254.6165	235.2203	5.3337	0.0165	1.254	Nil[a]	1, 2, 3	3.113
Ex 4	1254.6165	235.2203	5.3337	0.0165	1.254	Nil[a]	1, 2, 3	2.674
Ex 5	1254.6165	235.2203	5.3337	0.0165	1.254	Nil[a]	1, 2, 3	2.945
Ex 6	1254.6165	235.2203	5.3337	0.0165	1.254	Nil[a]	1, 2, 3	2.504
Ex 7	1254.6165	235.2203	5.3337	0.0165	1.254	Nil[a]	1, 2, 3	2.756
Ex 8	1254.6165	235.2203	5.3337	0.0165	1.254	Nil[a]	1, 2, 3	2.694
Ex 9	1254.6165	235.2203	5.3337	0.0165	1.254	Nil[a]	1, 2, 3	3.386
Ex 10	1254.6165	235.2203	5.3337	0.0165	1.254	Nil[a]	1, 2, 3	2.525

* represents "Failed to distinguish fault".

[a] Nil represents normal operation (no fault).

Table 4. 7 Results obtained by the diagnoser in case of E8.

Executions of E8	P_{Array} (W)	V_{Array} (V)	I_{Array} (A)	$f(N_{sc}, N_{oc}, sc, oc)$ (W)	ε	Detected Fault Position		Response Time (sec)
						OC	SC	
Ex 1	347.7530	131.9940	2.6346	0.053	0.3477	2,6,9	Nil[a]	2.673
Ex 2	347.7530	131.9940	2.6346	0.053	0.3477	2,6,9	Nil[a]	2.759
Ex 3	347.7530	131.9940	2.6346	0.053	0.3477	2,6,9	Nil[a]	2.943
Ex 4	347.7530	131.9940	2.6346	0.053	0.3477	2,6,9	Nil[a]	2.552
Ex 5	347.7530	131.9940	2.6346	0.053	0.3477	2,6,9	Nil[a]	2.946
Ex 6	347.7530	131.9940	2.6346	0.053	0.3477	2,6,9	Nil[a]	2.782
Ex 7	347.7530	131.9940	2.6346	0.053	0.3477	2,6,9	Nil[a]	2.713
Ex 8	347.7530	131.9940	2.6346	0.053	0.3477	2,6,9	Nil[a]	2.759
Ex 9	347.7530	131.9940	2.6346	0.053	0.3477	2,6,9	Nil[a]	2.598
Ex 10	347.7530	131.9940	2.6346	0.053	0.3477	2,6,9	Nil[a]	3.173

[a] Nil represents normal operation (no fault).

Table 4. 8 Results obtained by the diagnoser in case of E9.

Executions of E9	P_{Array} (W)	V_{Array} (V)	I_{Array} (A)	$f(N_{sc}, N_{oc}, sc, oc)$ (W)	ε	Detected Fault Position		Response Time (sec)
						OC	SC	
Ex 1	189.9715	60.6296	3.1333	0.0715	0.189	3,4,7	1,9	2.691
Ex 2	189.9715	60.6296	3.1333	0.0715	0.189	3,4,7	1,9	3.541
Ex 3	189.9715	60.6296	3.1333	0.0715	0.189	3,4,7	1,9	2.782
[*] Ex 4	188.8792	60.6149	3.1160	1.0208	0.189	3,7,10	1,9	4.999
Ex 5	189.9715	60.6296	3.1333	0.0715	0.189	3,4,7	1,9	2.943
Ex 6	189.9715	60.6296	3.1333	0.0715	0.189	3,4,7	1,9	3.311
Ex 7	189.9715	60.6296	3.1333	0.0715	0.189	3,4,7	1,9	2.736
Ex 8	189.9715	60.6296	3.1333	0.0715	0.189	3,4,7	1,9	3.035
[*] Ex 9	184.8381	60.8770	3.0363	5.0619	0.189	3,4,6	1,9	4.998
Ex 10	189.9715	60.6296	3.1333	0.0715	0.189	3,4,7	1,9	2.851

[*] represents "Failed to distinguish fault".

Table 4. 9 Results obtained by the diagnoser in case of E11.

Executions of E11	P_{Array} (W)	V_{Array} (V)	I_{Array} (A)	$f(N_{sc}, N_{oc}, sc, oc)$ (W)	ε	Detected Fault Position		Response Time (sec)
						OC	SC	
Ex 1	669.3163	170.1409	3.9339	0.0163	0.6693	7,10	4,8	2.693
Ex 2	669.3163	170.1409	3.9339	0.0163	0.6693	7,10	4,8	3.134
Ex 3	669.3163	170.1409	3.9339	0.0163	0.6693	7,10	4,8	2.924
Ex 4	669.3163	170.1409	3.9339	0.0163	0.6693	7,10	4,8	3.428
Ex 5	669.3163	170.1409	3.9339	0.0163	0.6693	7,10	4,8	2.756
Ex 6	669.3163	170.1409	3.9339	0.0163	0.6693	7,10	4,8	2.841
Ex 7	669.3163	170.1409	3.9339	0.0163	0.6693	7,10	4,8	2.651
Ex 8	669.3163	170.1409	3.9339	0.0163	0.6693	7,10	4,8	3.071
Ex 9	669.3163	170.1409	3.9339	0.0163	0.6693	7,10	4,8	2.861
Ex 10	669.3163	170.1409	3.9339	0.0163	0.6693	7,10	4,8	2.843

Table 4. 10 Results obtained by the diagnoser in case of E12.

Executions of E12	P_{Array} (W)	V_{Array} (V)	I_{Array} (A)	$f(N_{sc}, N_{oc}, sc, oc)$ (W)	ε	Detected Fault Position		Response Time (sec)
						OC	SC	
Ex 1	824.5856	208.7567	3.9500	0.0144	0.8245	8	6	2.693
Ex 2	824.5856	208.7567	3.9500	0.0144	0.8245	8	6	2.861
Ex 3	824.5856	208.7567	3.9500	0.0144	0.8245	8	6	2.882
Ex 4	824.5856	208.7567	3.9500	0.0144	0.8245	8	6	3.134
Ex 5	824.5856	208.7567	3.9500	0.0144	0.8245	8	6	2.735
Ex 6	824.5856	208.7567	3.9500	0.0144	0.8245	8	6	2.924
Ex 7	824.5856	208.7567	3.9500	0.0144	0.8245	8	6	2.885
Ex 8	824.5856	208.7567	3.9500	0.0144	0.8245	8	6	3.407
Ex 9	824.5856	208.7567	3.9500	0.0144	0.8245	8	6	2.987
Ex 10	824.5856	208.7567	3.9500	0.0144	0.8245	8	6	3.113

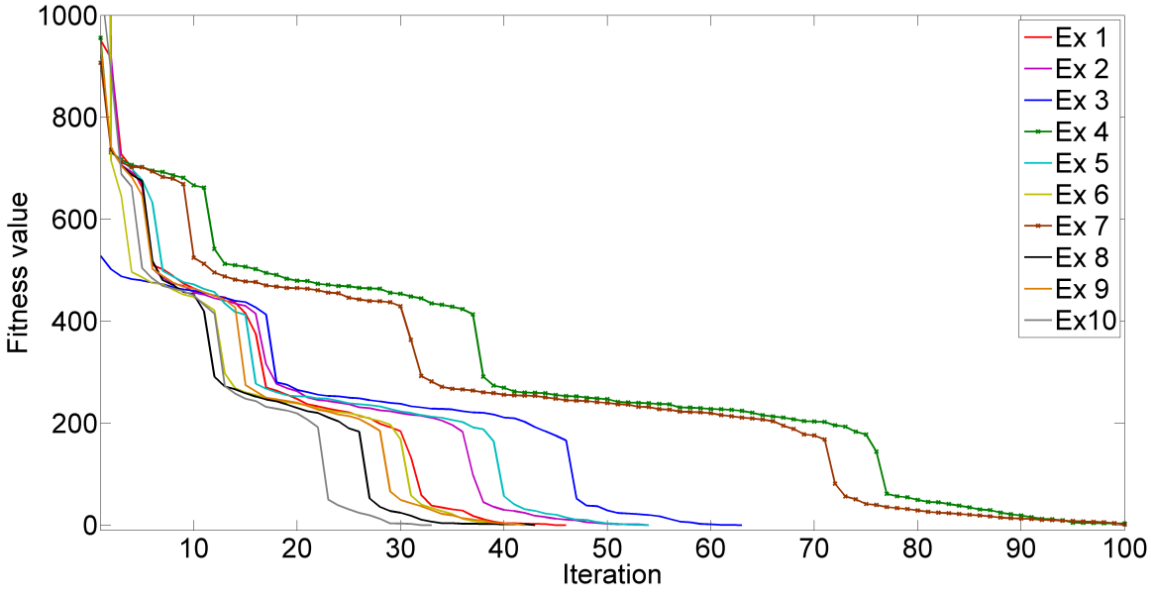

Figure 4. 7 Convergence curves for E2.

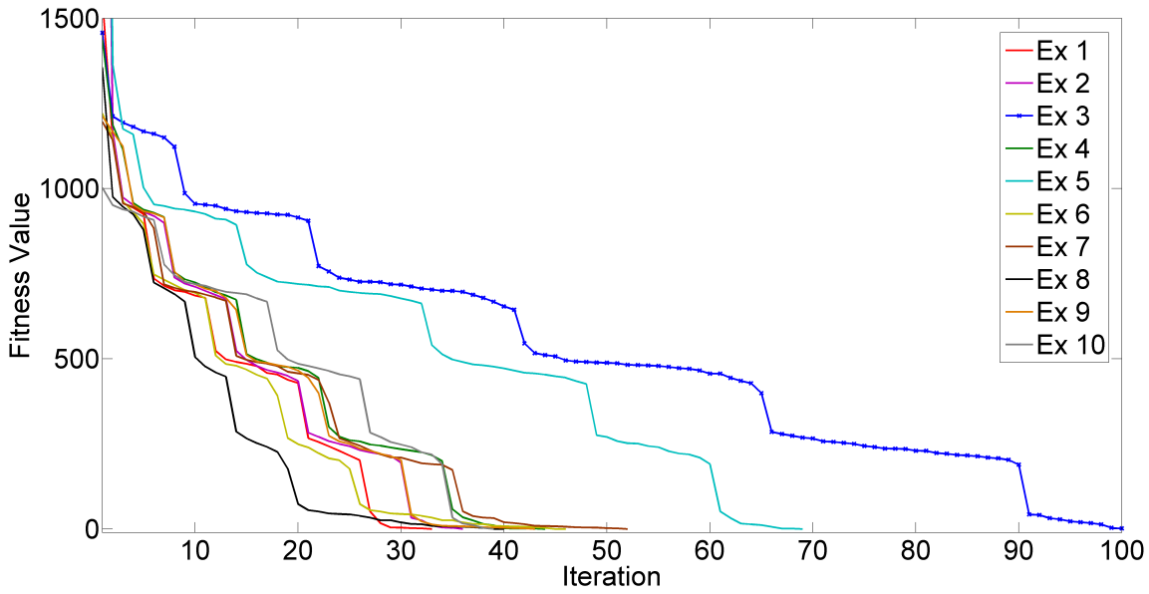

Figure 4. 8 Convergence curves for E3.

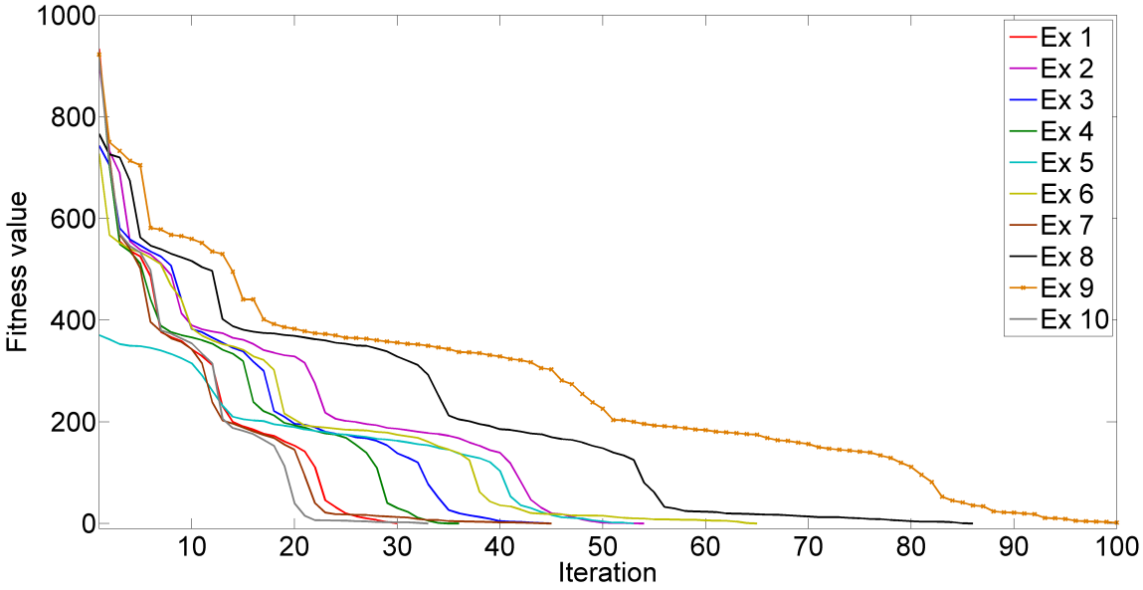

Figure 4. 9 Convergence curves for E5.

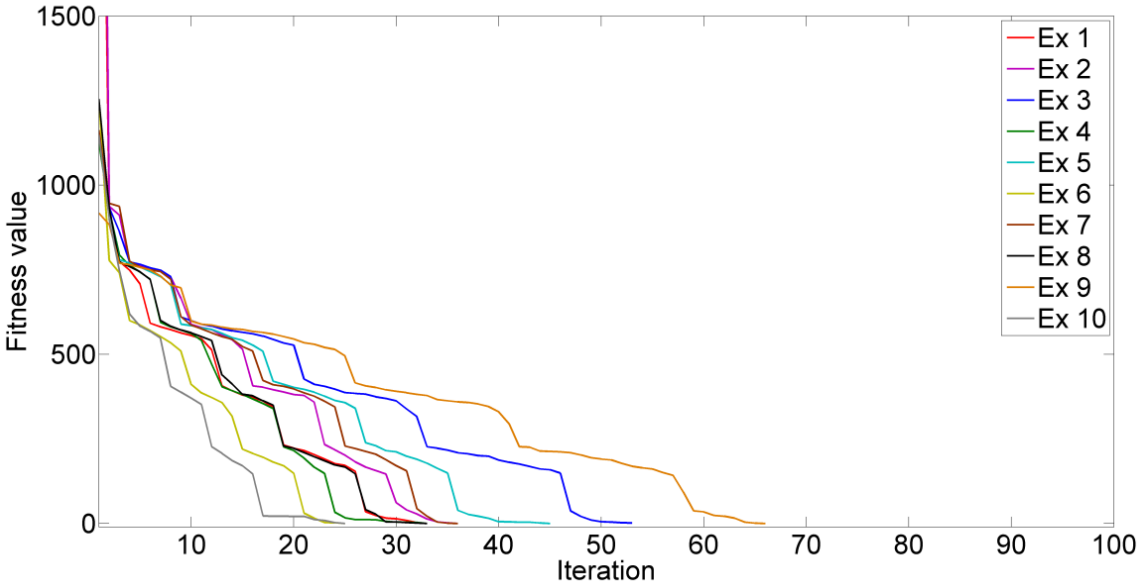

Figure 4. 10 Convergence curves for E6.

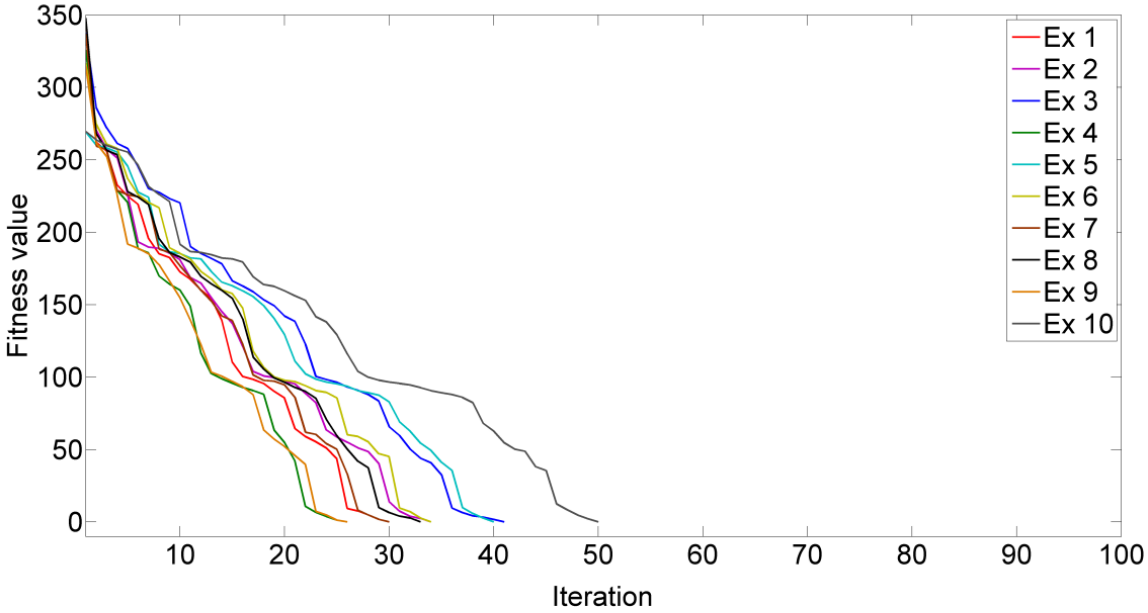

Figure 4. 11 Convergence curves for E8.

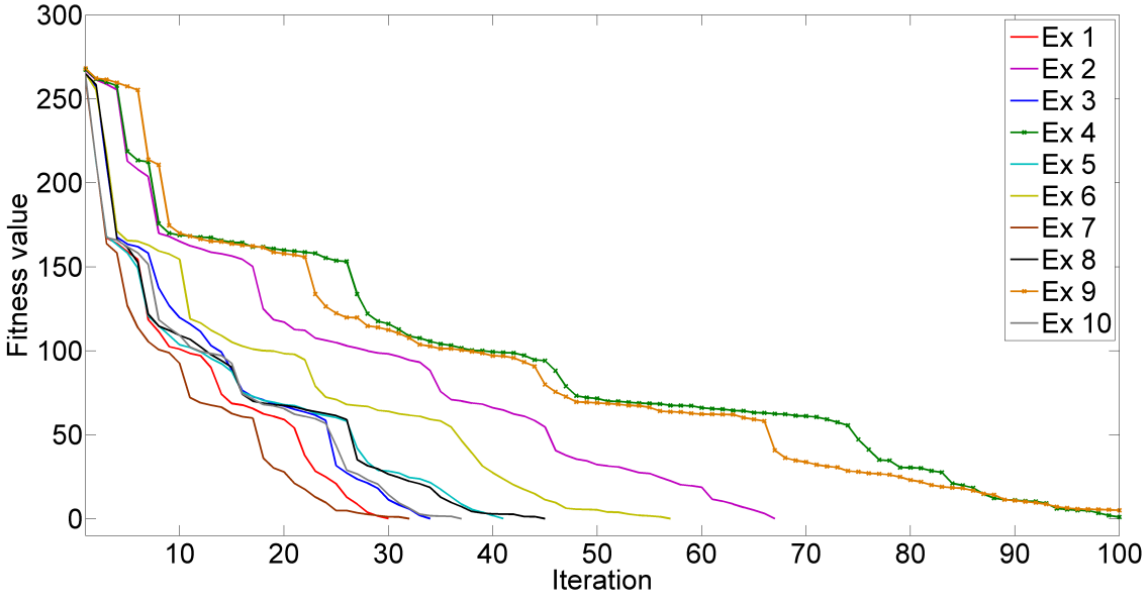

Figure 4. 12 Convergence curves for E9.

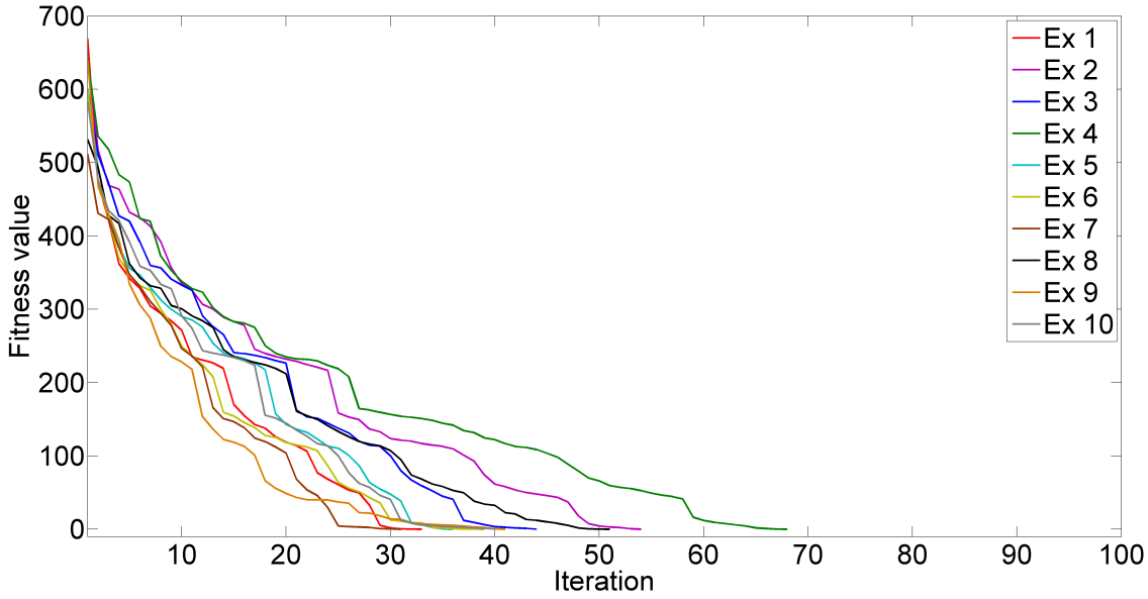

Figure 4. 13 Convergence curves for E11.

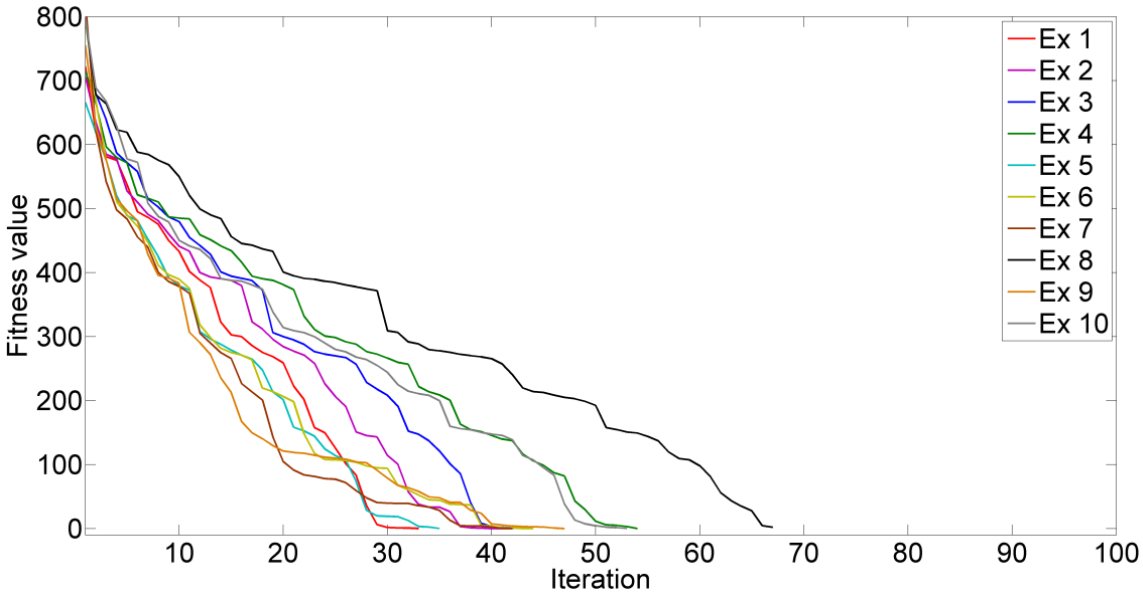

Figure 4. 14 Convergence curves for E12.

From the diagnosis outcomes represented above, it is distinguished that the entire executions of the experiments E1, E4, E6, E7, E8, E10, E11 and E12 are diagnosed successfully. Two executions of E2 and E9 and one execution of E3 and E5 fail to identify fault properly. Out of 120 (10×12) number of executions, 114 executions achieve success. Therefore, experimental results show 95% success rate.

The status of the PV array is monitored online and updated at every 5sec of time step. The results presented in Table 4. 1 to Table 4. 10 verify the successful accomplishment of the proposed fault diagnosis methodology in real-time because the overall response times are within the real-time limit for successful fault diagnosis.

In the cases where the diagnoser detects fault properly, the final values of objective functions, converges below relevant ε before the attainment of *itr_max*, although it is supposed to be zero theoretically for correct fault combination. These may be elucidated considering the following facts. Monitoring units usually have some precision, accuracy, and tolerance errors (at least, it is about ±0.1%). Abrupt variations of irradiation and temperature take place especially in tumultuous ambient operating circumstances. It is very difficult to assess the precise shading percentage with only one irradiation and temperature sensing device per module. If not, it will be unreasonably costly. There also may exist differences of the intrinsic cells proprieties from that as specified by the manufacturer. It is assumed that all the modules have identical electrical behaviors in a simulated PV system, while two practical PV modules may have dissimilar electrical behaviors to some extent.

The cases where the diagnoser fails to distinguish faults properly, it is evident from the above experimentation results and the convergence curves that, the final values of objective functions are not converged under ε, but the program is ended as the iteration counts arrive at *itr_max*. These cases may also capture the accurate fault combination after further iterations. However, that may not be a reasonable option because of the time constraint of an online real-time fault diagnoser. Further, in these failure cases, the fault diagnoser produces a notification as "Failed to distinguish fault". In these cases, a feasible measure is to reload the fault diagnoser by operator for researching the real fault combination until it confirms the successful fault discovery.

4.1.2 Discussion

Founded on the acquired successful results, the projected metaheuristic-based fault diagnosis algorithm seems to be beneficial. It effectively executes the following fault identification operations (O1-O6).

O1: Detect PV array condition (for example, healthy or faulty)

O2: Detect the OC fault

O3: Detect the SC fault

O4: Identify the number of open circuited modules in the faulty PV array

O5: Identify the number of short circuited modules in the faulty PV array

O6: Locate the open circuited modules in the faulty PV array

O7: Locate the short circuited modules in the faulty PV array

While, other methodologies, viz., threshold assessments [8]-[22], fault diagnosis based on neural network [22]-[25], machine learning [26]-[27] and other techniques are plentiful in literature and are able to merely perform a few of the aforementioned operations (O1-O6) and are incapable to diagnose module with open circuit and short circuit faults in an PV array completely regarding identification, differentiate the faults and tracing their respective locations. The performance comparisons of several methods presented in the literature are tabulated in Table 4.11

The planned metaheuristic optimization-based fault diagnosis approach necessitates fewer sensors for each PV array only at the DC side of the array inverter. The projected method does not involve any AC quantities of the PV system, nor does it need any training data for various PV configurations, ambient conditions, and the fault combinations. Training data is extremely case specific. The preparation of the training data is a costly, intricate, and meticulous procedure that needs expertise of human efforts [27]. Conversely, ECM and TDR methods are offline [28]-[33]. Necessary complicated devices, viz., photoluminescence, electroluminescence, thermal imaging cameras and infrared thermographs and their maintenances are extremely expensive particularly for large scale PV systems [35]. While the proposed fault diagnosis method can be implemented online with very simple actions. The PV array output power can be measured directly from the MPPT controller embedded in grid-connected inverter. Thus, the proposed method can be implemented through the installed inverter to monitor online the status of the PV array. Furthermore, the method can be effortlessly generalized and employed in large scale PV plants. For the generalization, it only entails for PV array information, viz., number of modules exist in the PV array and the technical specifications of PV array and modules. Therefore, the projected metaheuristic

optimization-based fault diagnosis approach is a simple, cost effective, online process which is able to diagnose the module outages due to open and short circuit faults in a PV array irrespective of its configurations and sizes.

Table 4. 11 The performance comparison of fault diagnosis methods available in literature.

Sl. no.	Method	Fault diagnosis operations							Average success rate
		O1	O2	O3	O4	O5	O6	O7	
1.	Evaluation of current and voltage indicators [8]	√		√					-
2.	Analysis of current and voltage indicators [9]	√	√	√					-
3.	OPC monitoring [10]	√		√		√			-
4.	Analysis of output power [11]	√	√	√	√	√			92%
5.	Analysis of DC and AC power [12]	√	√						-
6.	Analysis of operating voltage window [13]	√	√	√	√	√			94.6%
7.	Wald test technique and Simple Flash Test Driver [15]	√	√	√					-
8.	Analysis of I-V characteristic [17]	√	√	√					72.72%
8.	Hybridization of SVM and NN [18]	√	√		√				92.5%
9.	Analysis of I-V characteristic [19]	√	√	√					-
10.	Analysis of DC current and voltage [20]	√	√	√					-
11.	Analysis of array electrical parameters [21]	√							-
12.	ANN [22]	√	√	√					90.3%
13.	TFFNN [23]	√		√		√		√	-
14.	WNN [24]	√	√	√					96%
15.	Multilayer NN [25]	√	√	√					90%
16.	Hybridization of SVM and k-NN [26]	√		√					68%-75.8%
17.	GSSL [27]	√	√	√		√			99.6%-100%
18.	ECM [28]	√	√				√		-
19.	Thermography-Based Temperature Distribution Analysis [34]	√	√	√		√		√	-
20.	Metaheuristic optimization-based fault diagnosis strategy [86]	√	√	√	√	√	√	√	95%

√ represents the ability to execute that fault diagnosis operation.

- represents data unavailability in the literature.

4.1.3 Limitations

Although the proposed fault diagnosis technique shows high success rate, some limitations still exist. The limitations are listed as follows:

- Here only two fault categories (open circuit and short circuit) have been considered. There are chances of incidences of other related module faults such as partial shading, delamination, bypass diode failure, failure of balance of system etc. These failures cannot be diagnosed using the proposed technique.
- Other PV module failure can also influence the power output of PV array and may cause placebo open circuit and short circuit fault pattern and may lead the projected technique to false diagnosis of open circuited and short circuited module outages.

4.2 Performance assessment of optimal bidding plan of microgrid under uncertainties and outages

4.2.1 Illustrative implementation

The proposed bidding plan is experienced on a grid-connected microgrid as shown in Fig 4.15. The microgrid model consists of three GT systems, one PV system, one WT system and one ESS unit. The technical specifications at STC and the economic data [87], [88] are given in Table 4.12, Table 4.13, Table 4.14 and Table 4. 15 respectively. The local load demand of the microgrid can be grouped as the critical load and the non-critical load or the flexible load. The flexible load acts as resources for demand response since they are comprised of the fixed load and the shiftable load. Therefore, the local consumers with flexible load can partake in DRP while planning the day-ahead bidding strategy. The DRP data is presented in Table 4. 16. The maximum power transaction amount between the main grid and the microgrid is 50 MW.

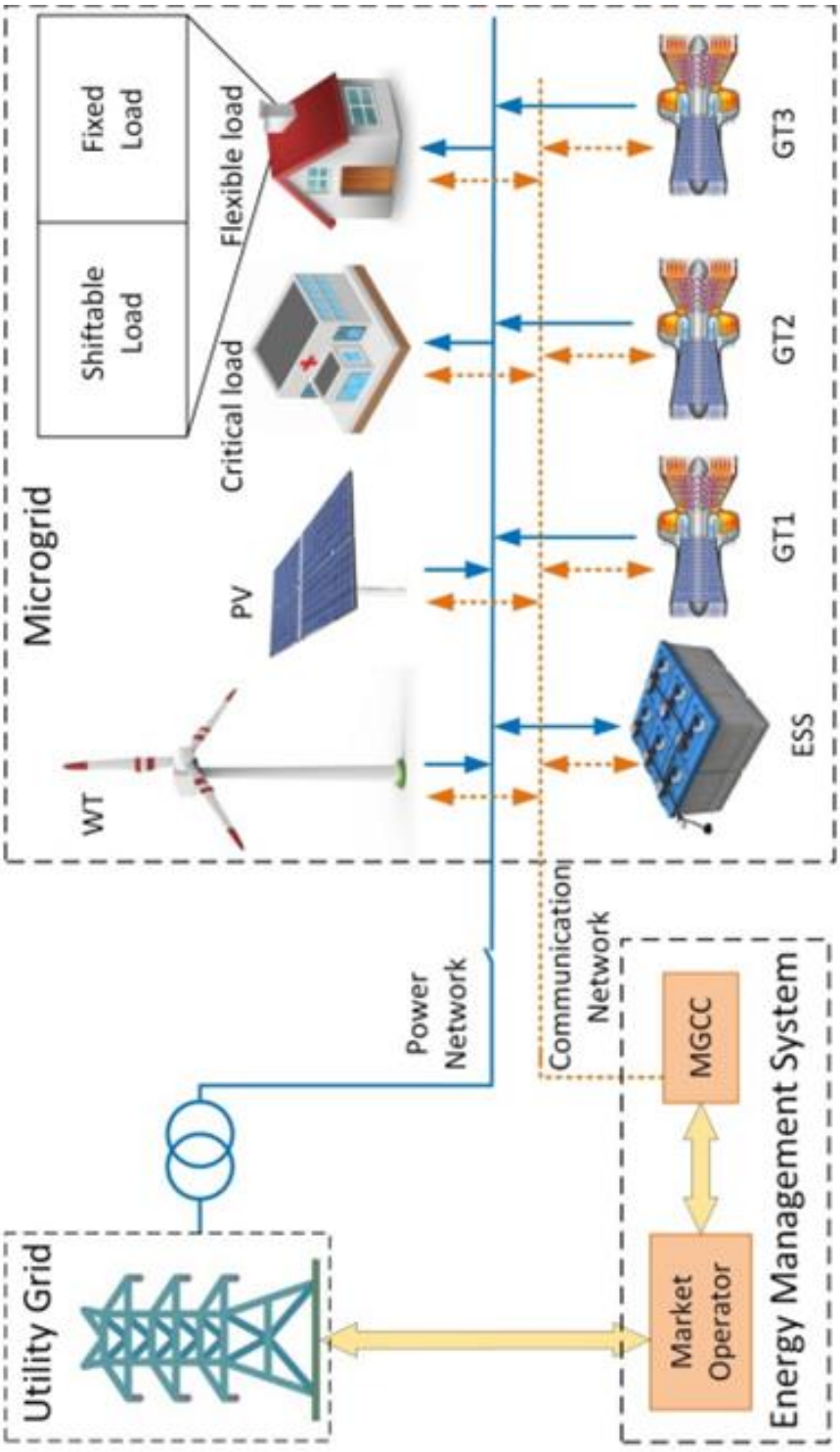

Figure 4. 15 The microgrid test system with various energy resources.

Table 4. 12 Data of GT systems.

Parameter	First GT	Second GT	Third GT	Unit
$P_{GT_{i,t}}^{max}$	8	8	10	MW
$P_{GT_{i,t}}^{min}$	0	0	0	MW
MUT_i	1	1	1	h
MDT_i	1	1	1	h
R_{U_i}	4	4	5	MW
R_{D_i}	4	4	5	MW
$S_{GT_{i,t}}$	1	1	1	-
c_{GT_i}	68	68	68	$/MWh

Table 4. 13 Data of PV system.

Parameter	Value	Unit
P_{PVr}	10	MW
Irradiation at STC	1000	W/m^2
Temperature STC	25	℃
NOCT	44	℃
μ_{Log}	5.2	-
σ_{Log}	0.6	-
F	33	Failure times/year
$MTTR$	63	Days
Life span	15	years
T	5	years
μ_{Norm}	13	-
σ_{Norm}	3	-
F_{PV}	0.6	-
d_{PV_j}	36	$/MWh
o_{PV_j}	80	$/MWh
u_{PV_j}	20	$/MWh

Table 4. 14 Data of WT system.

Parameter	Value	Unit
P_{WTr}	15	MW
v_{in}	2	m/s
v_r	14	m/s
v_{out}	25	m/s
α	9	-
β	2	-
F	54	Failure times/year
$MTTR$	96	Days
Life span	20	years
T	5	years
μ_{Norm}	17	-
σ_{Norm}	4	-
F_{WT}	0.6	-
d_{WT_k}	29	$/MWh
o_{WT_k}	80	$/MWh
u_{WT_k}	20	$/MWh

Table 4. 15 Data of ESS system.

Parameter	Value	Unit
P_{Charge}^{max}	5	MW
P_{Disc}^{max}	5	MW
E^{max}	10	MWh
E^{min}	1	MWh
ζ	90	%
η	90	%
c_{ESS}	382	$/MWh

Table 4. 16 Data for DRP.

Parameter	Value	Unit
DRP^{max}	20	%
c_{DRP}	30	$/MWh

The climate data of Kolkata, India on 6th May 2018 is considered for the case studies of the projected microgrid bidding strategy [89]. Weibull, lognormal, normal and exponential PDFs are employed to estimate the trend and forecasting error of wind velocity, solar irradiation, load utilization and the failure rate of renewable energy systems respectively. Figure 4. 16(a-f) demonstrates the forecast load demand profile, wind velocity, solar irradiation, day-ahead market prices of energy, energy prices in the retail market, prices of the positive and the negative imbalances and the failure rates of renewable systems respectively.

Turbulence occurrences in weather are observed at 12th, 15th to 17th hour in Figure 4. 16(b). Such winds with towering velocity may destroy various components of renewable energy unit and usually cause power interruption due to outages of renewable systems. Such powerful wind is commonly accompanied by intense cloud formation, heavy rain or serious dust particles which partially or completely shed or cover the solar panels. These in addition corrode turbine blades of WT system. The hourly based failure rates of renewable systems, as displayed in Figure 4. 16 (e) to Figure 4. 16 (f), are determined by the units' operators based on hourly forecast of weather condition and earlier failure data. After that weather dependent FOPs of renewable systems are computed as expressed in equation (2.27). The weather dependent and the cumulative FOPs of WT and PV systems for the forecast failure rates are portrayed in Figure 4. 17(a-b). The FOP limits of WT and PV systems are also specified in the Figure 4. 17(a-b). The FOP limits are set at 0.6 for both the systems. It is seen in Figure 4. 17 (a) that during the 12th, 15th, 16th and 17th hours the cumulative FOPs are 0.6471, 0.6779, 0.6394 and 0.6805 respectively and violate the FOP limit. Therefore, the forecasted outage periods for WT system are 12th, 15th, 16th and 17th hours. Likewise, in Figure 4. 17 (b) it is noticed that during the 15th and 17th hours the cumulative FOPs are 0.6695 and 0.6759 respectively which exceed the FOP limit (0.6). Hence, the forecasted outage periods for PV system are 15th and 17th hour.

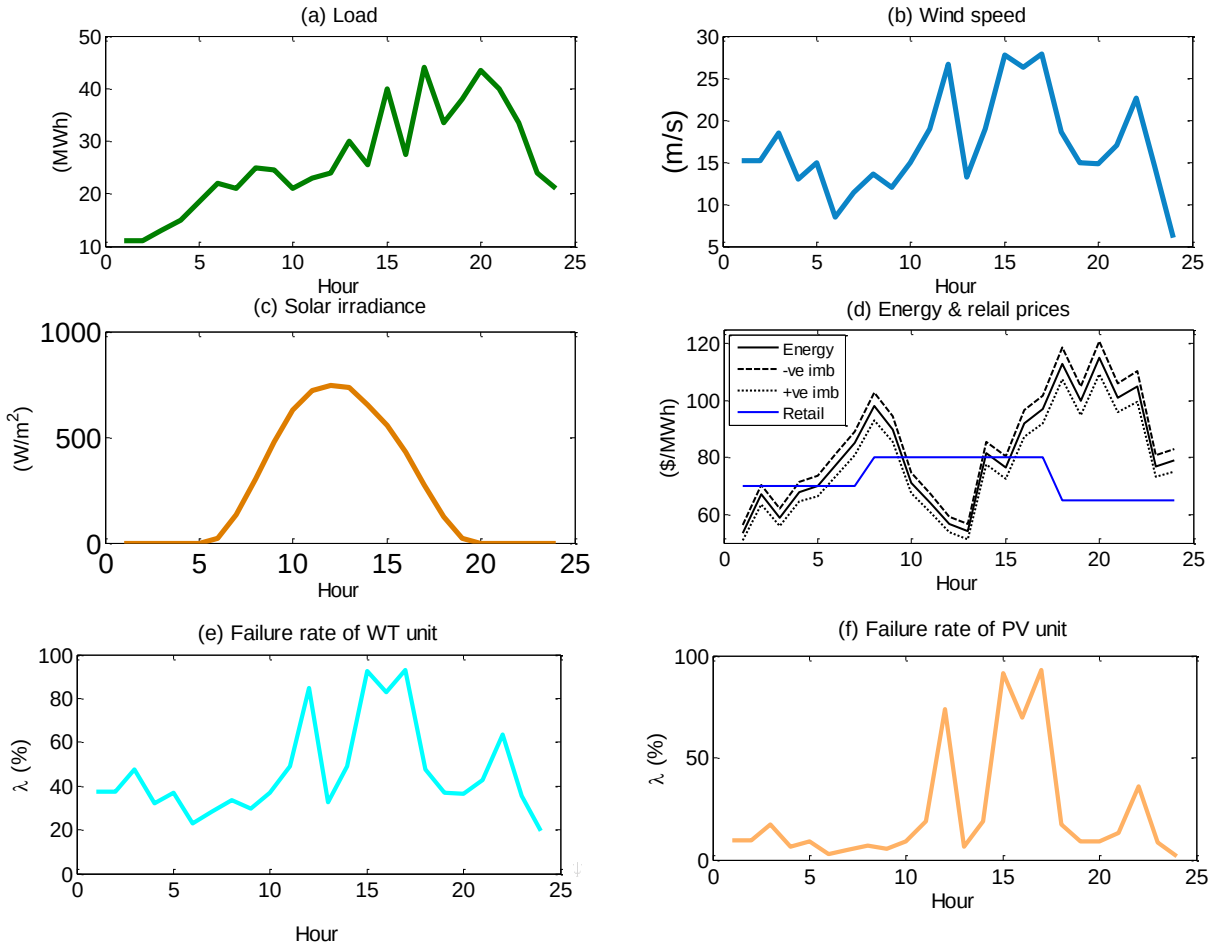

Figure 4. 16 Day-ahead forecasted load profile, wind speed, solar irradiation ,energy prices for next day, positive and negative imbalances' prices and retail prices and failure rates of WT and PV systems.

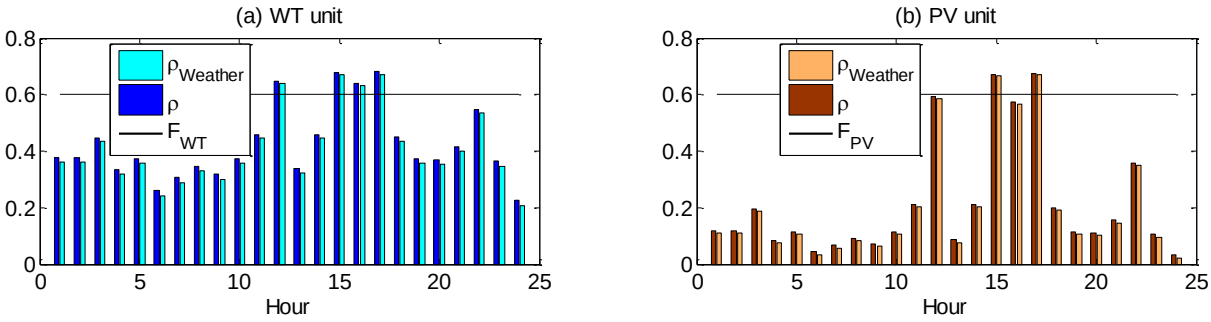

Figure 4. 17 The weather dependent FOPs and the cumulative FOPs of WT and PV systems for the forecasted failure rates.

Afterward, six scenarios of load demand, wind velocity, solar irradiation and the failure rates for WT and PV systems are produced using Tent mapping technique within 90% confidence intervals. The $ctrl$ is taken to be 2. The Figure 4. 18 (a-f) exhibit the produced scenarios of the base load demand, wind velocity, solar irradiation, the failure rates within confidence intervals and the DRP modified load scenarios respectively. Figure 4. 19(a) and Figure 4. 19(b) demonstrate six scenarios of hourly based power yields respectively from WT and PV systems. These figures also characterize the outage scenarios for considering the FOP limit as 0.6. The generated set of scenarios are supplied to the twofold SP to resolve the MINLP modeled optimal bidding problem of microgrid in the day-ahead electricity market with the ability to compensate imbalances produced due to the uncertainties regarding the decision variables and the outages of the renewable systems. The projected bidding model is optimized using LINDOGlobal solver in GAMS 27.1 platform. The objective function value is evaluated to be 8007.72 with $\omega = 0.4$. The optimal bidding profit and the CVaR are found to be respectively 8276.87$ and 7604.01$. The optimum energy bids in the day-ahead market are illustrated in Figure 4. 20. Throughout the hours 1 to 11 the hourly load demands are comparatively low. Throughout the hours 1 to 5, 10 and 11 the hourly wind power generations are convincingly good. From the 7th hour, the hourly generations from the PV system also raise to a good quantity. Consequently, microgrid trades surplus energy to the market during the hours 1 to 5 and 7 to 11. As it is evident from Figure 4. 17(a) and Figure 4. 17 (b), the forecasted outage hours of WT systems are 12, 15, 16 and 17 and that of PV systems are 15 and 17, the microgrid buys energy from the grid at those hours. During the hours 18 to 22 the forecasted power outcome from both the WT system and PV system are less while load demand is relatively high, thus at the hours 18 to 22 the microgrid has to buy energy from the grid. As, one single optimal bid is offered to the energy market for every hour, hourly energy imbalances, power dispatch from the GTs and ESS energy states for the six scenarios are dissimilar. The positive and the negative imbalances for the subsequent day are depicted in Figure 4. 21. Figure 4. 22 (a-b) correspond to the power dispatches of three GT systems for six scenarios for the subsequent day. Figure 4. 23 (a-b) illustrate respectively the energy states and the charging and the discharging

status of ESS through six scenarios for the next day. The outage periods of every scenario are discussed and explained as follows.

- Scenario 1: The outages of WT system happen at the 12th, 15th, 16th and 17th hours. The outages of PV system are evident at the 15th and 17th hours. Therefore, battery discharges at the 12th, 15th and 16th hours. At 16th hour, the ESS attains to its minimum energy level. Along with high energy procurement from the grid, the GT2 and GT3 systems are also functioning at their full rating during the 15th and 17th hours and at half rating during the 12th hour. Thus, small positive imbalances take place at the 12th, 15th and 17th hours. The total energy output from the WT system and the PV system are 217.19 MWh and 48.32 MWh respectively. The profit for the scenario is 8700.62$.

- Scenario 2: The outages of WT system take place at the 15th, 16th and 17th hours. The outages of PV system occur during the 15th and 17th hours. So, ESS has to discharge at the 15th and 16th hours. At 16th hour, the ESS arrives at its minimum energy level. As no outage takes place at 12th hour, it causes more positive imbalance at 12th hour than the first scenario. At the 15th hour, GT2 system is not dispatching and GT3 system is operating at its half rating. Thus, with the increment in the load utilization the microgrid has to purchase the deficit energy from the real-time market at the outage hour 15th, resulting into negative imbalance. The GT1 system and GT2 system are operating at their full rating at the 16th hour ensuing in positive imbalance. Along with high energy purchase from the grid, the GT1 system and the GT2 system are also functioning at their full rating during the 17th hours. Accordingly, positive imbalances take place at the 17th hour. The total energy output from the WT system and the PV system are 212.55 MWh and 47.08 MWh respectively. The profit for this scenario is 7610.11$.

- Scenario 3: The outages of the WT system take place during the 15th and 17th hours. The outage of the PV system happens at the 15th hour. As a result, the ESS discharges during the 15th and 17th hours. Besides, at the 15th hour, the GT1 system and the GT3

system are not generating. So, with the raise of load consumption, microgrid has to procure the deficit energy from the real-time market at the outage hour 15th ensuing negative imbalance. Along with elevated energy procurement from grid, the GT1 system, the GT2 system and the GT3 system are also running at their full rating at the 17th hour. So, positive imbalances take place at the hour 17. The total energy outcome from the WT system and the PV system are respectively 217.22 MWh and 47.65 MWh. The profit for this scenario is 8856.64$.

- Scenario 4: The outages of both the WT and the PV systems happen at 15th hour. So, the battery discharges at the 15th hour. Furthermore, at the 15th hour, the GT2 system and the GT3 system are not generating. Hence, with the increment in the load demand the microgrid has to purchase the deficit energy from the online market at the outage hour 15th ensuing in negative energy imbalance. The total energy output from the WT system and the PV system are respectively 234.10 MWh and 43.75 MWh. The profit for this scenario is 8952.73$.

- Scenario 5: In this scenario both the WT and the PV systems do not face any outages. The total energy outcome from the WT system and the PV system are respectively 220.58 MWh and 49.57 MWh. The profit for this scenario is 7397.59$.

- Scenario 6: In the 6th scenario also both the WT and the PV systems are not experiencing any outages. The total energy outcome from the WT system and the PV system are respectively 209.99MWh and 48.66 MWh. The profit for this scenario is 8143.50$.

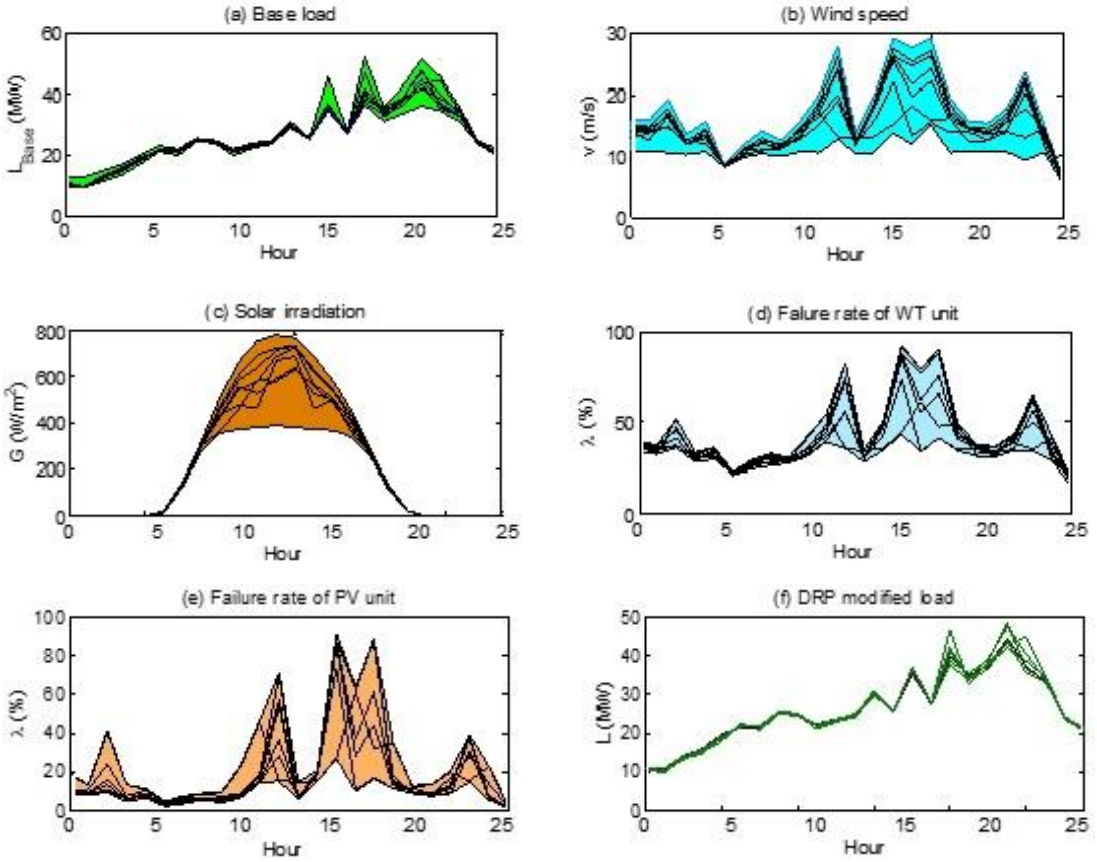

Figure 4. 18 Generated scenarios for base load, wind speed, solar irradiation, and failure rates within confidence intervals and DRP based load scenarios.

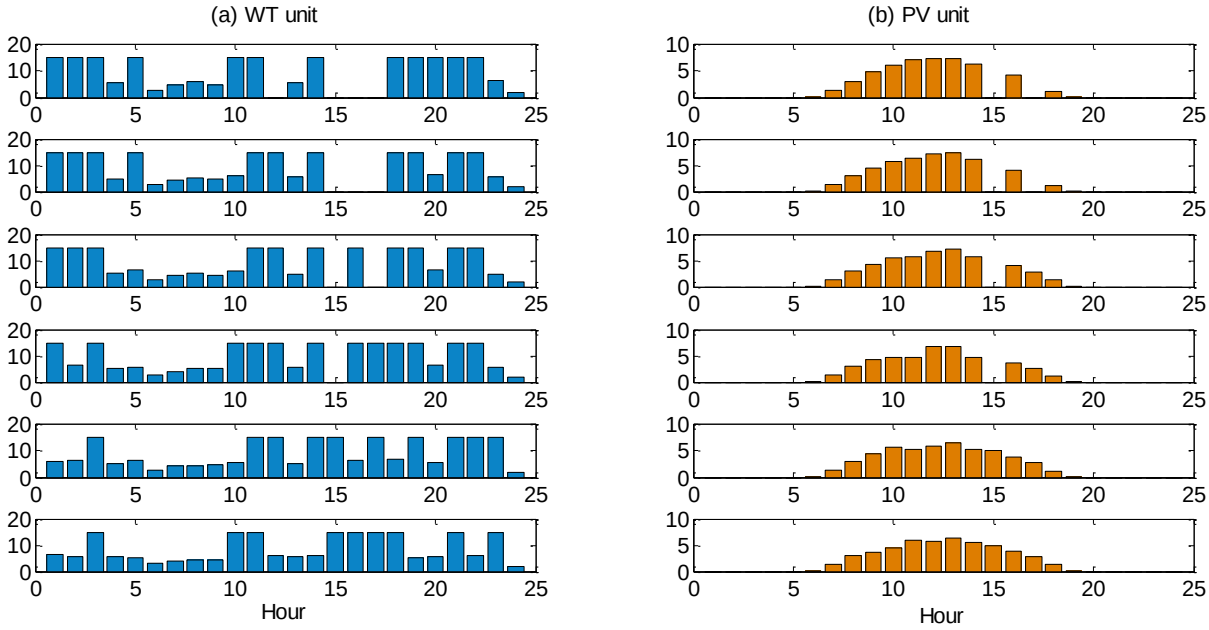

Figure 4. 19 Power output of WT system and PV system for the 6 scenarios for the next day.

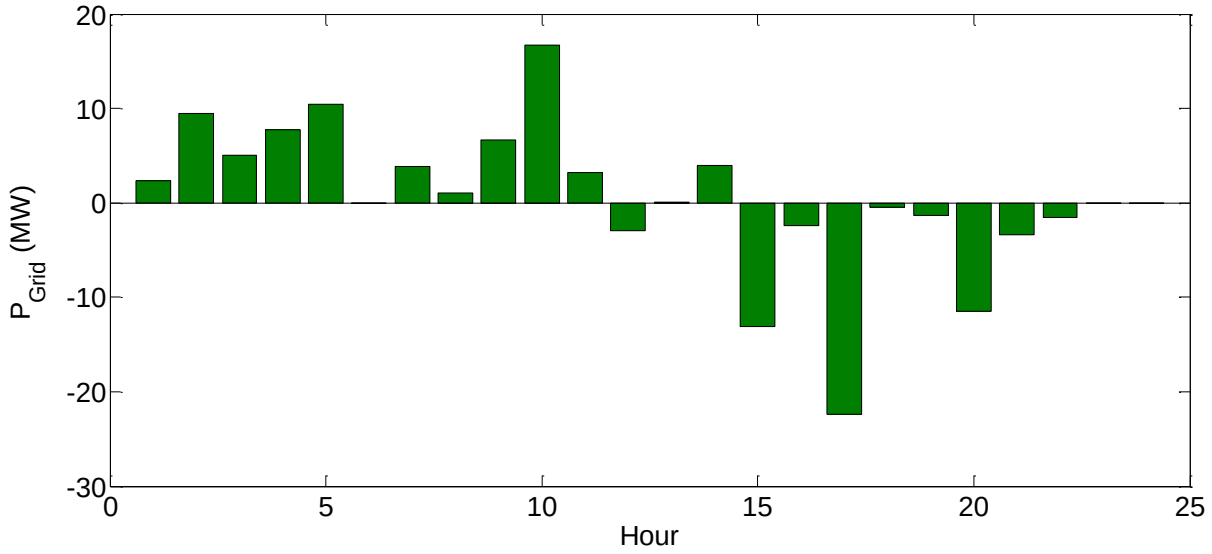

Figure 4. 20 The energy bids for the next day.

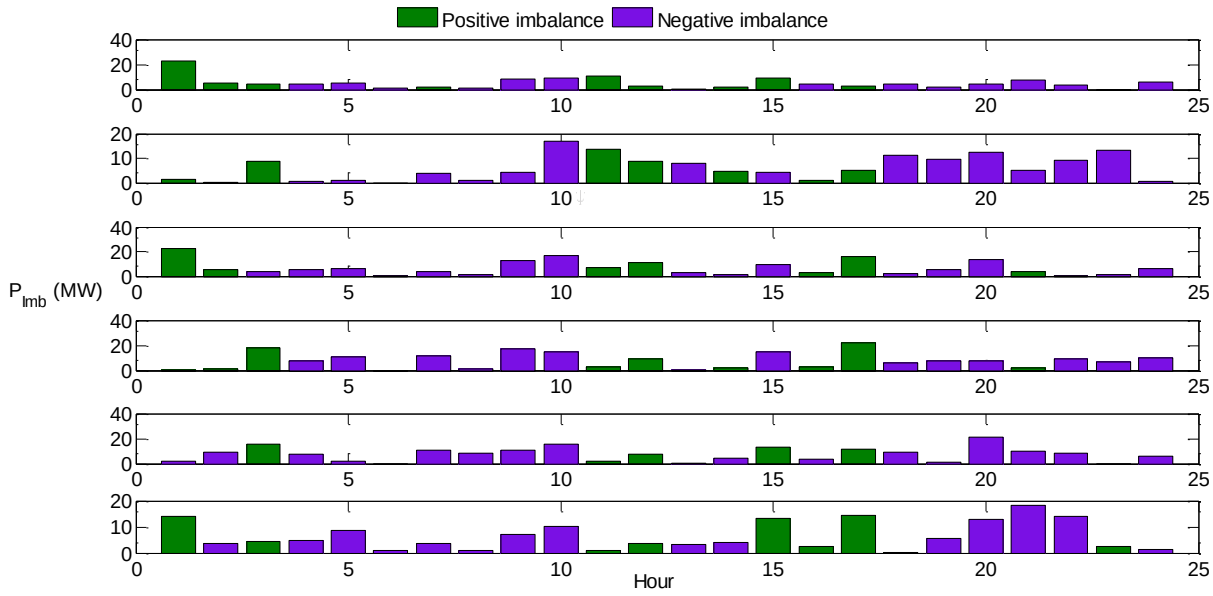

Figure 4. 21 Positive and negative imbalances for the 6 scenarios for the next day.

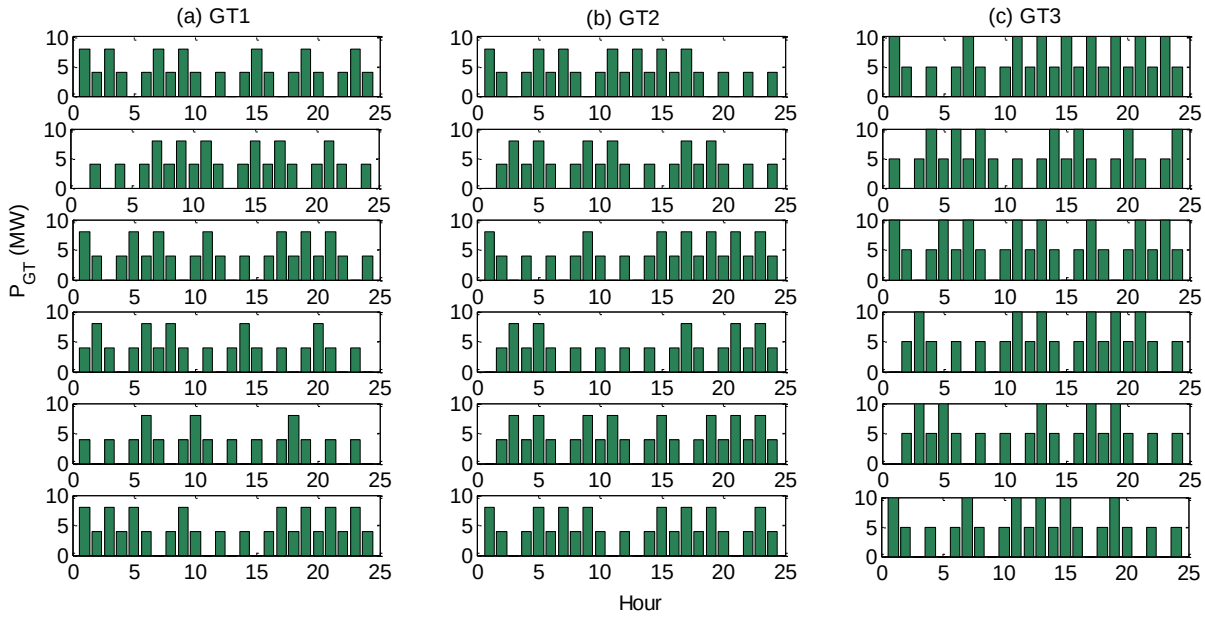

Figure 4. 22 Power output of 3 GT systems for the 6 scenarios for the next day.

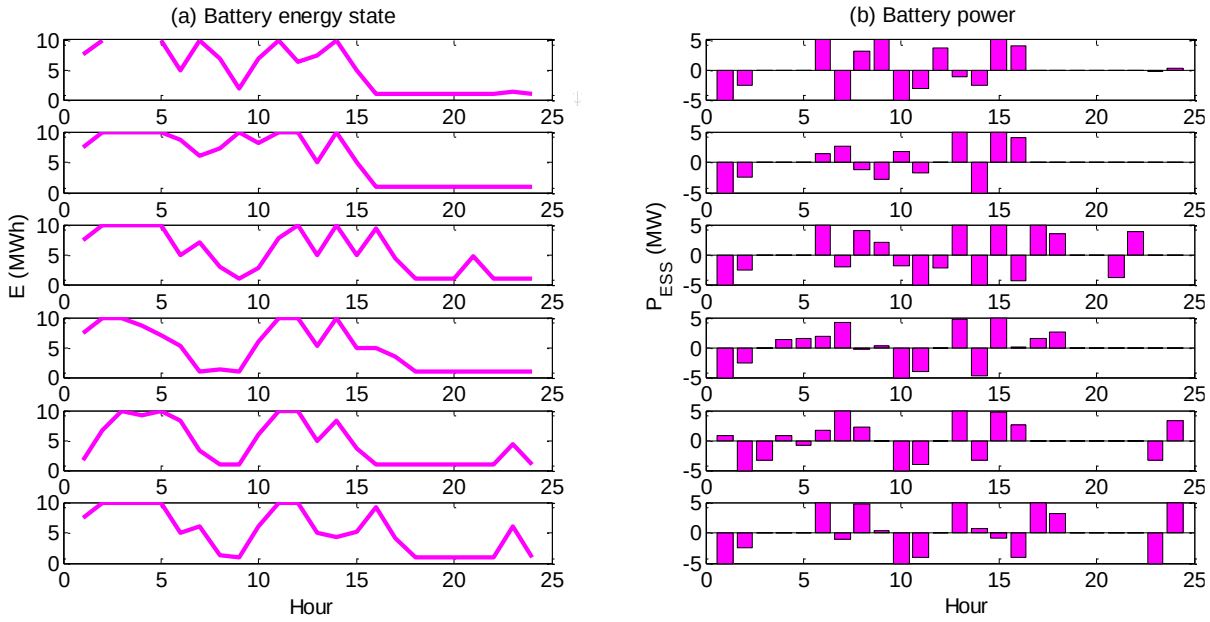

Figure 4. 23 Energy state and power output of energy storage system for the 6 scenarios for the next day.

To decide the quality of the optimum stochastic solution, the parameter 'value of stochastic solution' (VSS) is evaluated as (2.70), $VSS = 8573.38 - 8276.87 = 296.51$. The VSS is adequately high to justify the application of the SP in uncertainty modeling. For further assurance that the expected value of the profit fall under 10% of the worst scenarios, the CVaR is calculated for different values of weight (ω) as presented in Figure 4. 24.

Moreover, to study the sensitivity of the planned bidding strategy with different outage situations, the variations of renewable energy outcome, expected profit of microgrid from day-ahead bidding and the reserve and the penalty costs with a range of values of FOP are depicted in Figure 4. 25 ((a)-(d)) respectively. It is marked that renewable energy production; the outage probabilities and risk of uncertainties directly influence the profit from participation in energy market.

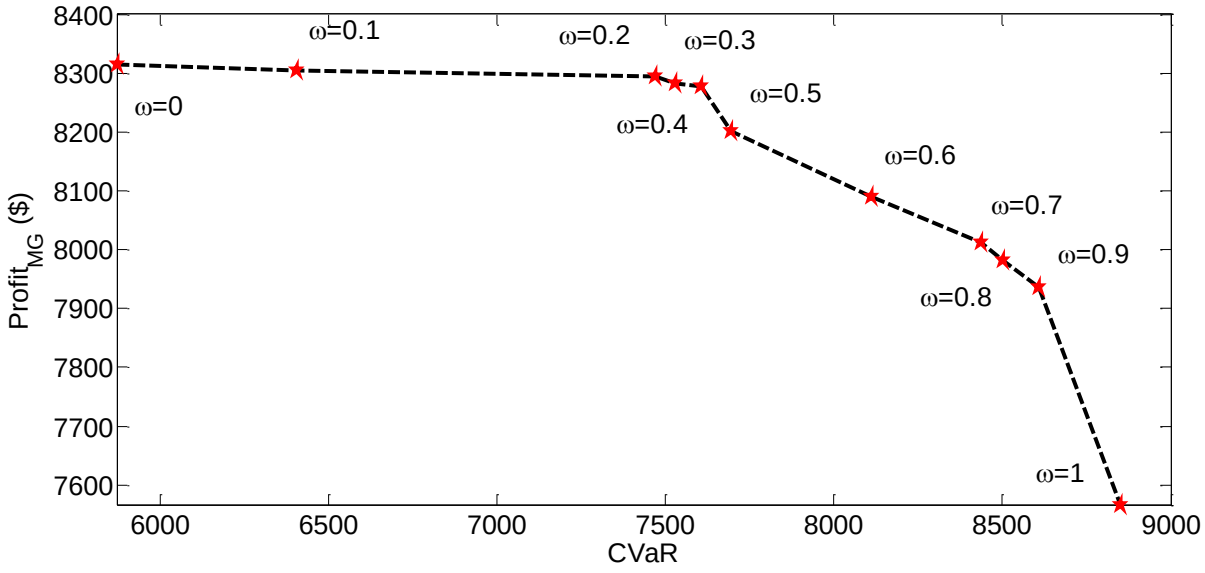

Figure 4. 24 Risk analysis of expected bidding profits for different values of weight (ω).

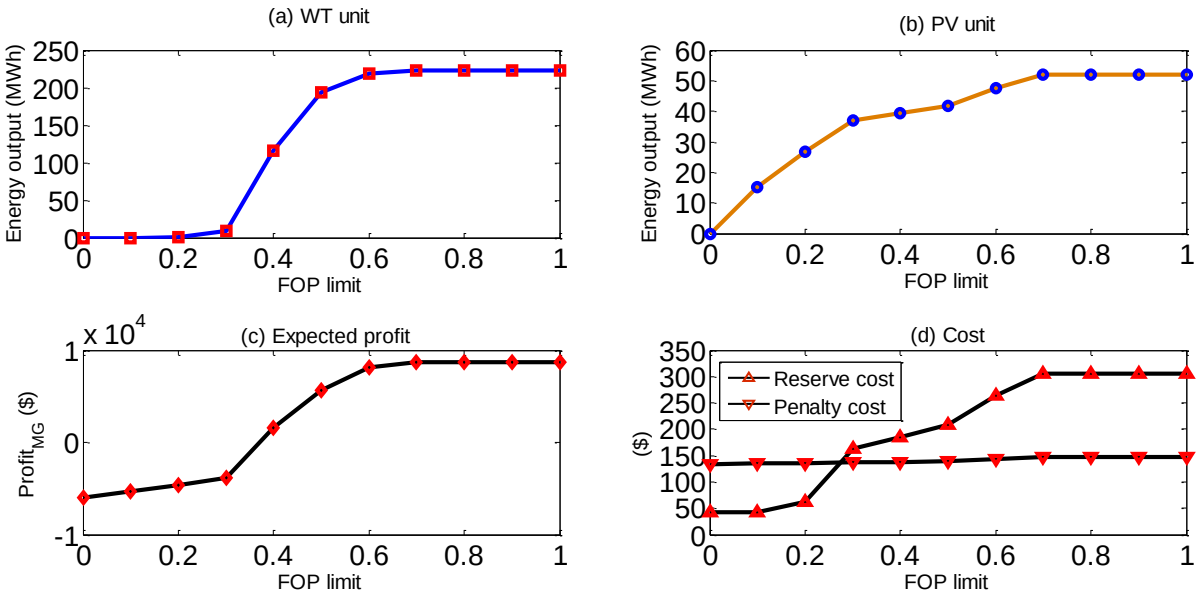

Figure 4. 25 The variations of the RERs' production, profit and reserve and penalty costs regarding to FOPs.

4.2.2 Discussion

The uncertainties associated with renewable energy resources and their outages are considered in the depicted case study [90]. VSS justify the decency of the expected profit from bidding since the profit (8573.38$) of deterministic solution is satisfactorily higher than the profit (8276.87$) of stochastic solution. From the CVaR estimation it is evident that, the expected profit of the worst 10% scenarios of the next day energy market is 7604.01$, which is also reasonably high to guarantee the efficiency of the projected bidding formulation. Besides, sensitivity analysis is studied to demonstrate the consequences of renewable system outages on generations, the microgrid profit and the reserve and the penalty costs. Figure 4. 25 ((a)-(d)) show that, with the increment of the value FOP limit setting, the energy outcome from renewables, the profit and reserve and penalty costs also amplify. The consequent increase in the reserve and the penalty costs aids the microgrid operator to decide the effective FOP limits and the outage models to condense the impact of renewable energy integration into the system. The cumulative FOPs of this case study remain below 0.7. Beyond the FOP limit of 0.7, the energy output from renewable systems, profit and the reserve and the penalty costs stay constant.

4.2.3 Limitations

Even though DRP inclusion can result in successful bidding strategy planning, several limitations may prevent appropriate outage modeling and complete implementation of DRP in real-time market. In real life the climate conditions are very vacillating and sometimes significantly deviate from the prior forecast. All these poses enormous challenge to the microgrid operators to realize failure rate of renewable energy systems. However efficient outage modeling of day-ahead bidding strategy planning can secure the power system from severe blackouts.

Conversely, the major difficulties for efficient DRP accomplishment in online market are the inelasticity in load demand and negligible customer involvement due to irregularities in information. In addition, slow deployments of the technical infrastructures, for instance, smart metering and other essential telecommunication platforms, are the additional hindrances in full implementation of DRP. Nevertheless, outage based DRP modeling integration in microgrid bidding operation facilitate to lessen the energy procurement cost during the renewable energy outage periods.

4.3 Summary

The performance of both the works has been assessed using results of several case studies. The efficiency of the proposed fault diagnosis method has to found around 95%. The comparison of the technique with other available techniques in literature has been also presented. From the scenario-based case study of the proposed bidding strategy also yield better profit with lower risk. This is achieved due to incorporation of outage and uncertainty modeling and risk assessment. A few limitations have come into view while discussing the performance assessment of the works. Hence, some inferences to overcome these restraints are proposed in the following chapter for the future practice.

This page is left blank intentionally.

Chapter 5

Concluding remarks

5.1 Overall conclusion

This dissertation is revolved around the application of soft computing technique in power system security analysis. The power system security problems which are demonstrated here deal with research advancements concerning outages of power system components and uncertainties.

Regarding component outage, PV module outages due to short circuit fault and open circuit fault under non-uniform irradiation and their diagnosis based on soft computing technique is accomplished. The diagnosis procedure has been developed as a mathematical search problem to identify the faults, location of the faulty modules and type of module fault. Improved Real Coded Genetic Algorithm is employed successfully as metaheuristic search technique. For performance validation, twelve fault patterns concerning the open circuit fault and the short circuit fault of the PV systems are experimented. The experiments are executed under non-uniform irradiation and temperature allotment to validate the projected approach. The diagnosis results show that the proposed scheme can independently recognize, locate and differentiate between the short circuited and the open circuited modules in a PV array. Furthermore, this fault diagnosis algorithm effectively differentiates between the healthy PV array and faulty PV array experiencing heterogeneous irradiation and temperature. Lesser number of sensor requirements makes the scheme cost effective. As the diagnosis algorithm can be implemented along with the inverter, it can be used as an online diagnosis tool. Besides, it can be employed for diagnosis operation in any PV systems of different configurations and sizes. But as stated earlier the proposed fault diagnosis method can not find other PV module related failure except open circuit and short circuit faults. So, remaining major failures can also be researched and mathematically modelled into fitness function, so that it can be solve using soft computing approaches. If the solution is achieved in near future,

the incidences of other related module faults can be diagnosed. Their influences on the power output of PV array can be easily determined and the placebo effect of open circuit and short circuit fault pattern can be mitigated. Despite having the above mentioned limitations, being economic, flexible, and fast functioning, it is conclusive that the proposed procedure can be implemented as a proficient fault diagnoser for PV systems which aids to restore the system security quickly.

Considering both component outages and system uncertainties, a bidding strategy model is proposed for renewable integrated microgrid for effective participation in day-ahead energy market. The outages of renewable systems and the uncertainties related to load, renewable systems and their outages are incorporated in this study. The uncertainties are evaluated by means of specific probability distribution functions. In addition, Tent chaos mapping is used to create the uncertain scenarios adaptively and non-repeatedly within 90% confidence level. These uncertainties are dealt with dual phase stochastic programming (SP). Moreover, both price-based and emergency-based demand response programming is employed, specially allowing for outage periods along with period of peak load/energy prices to boost security of microgrid and its profit maximization. The microgrid is supposed to be capable of compensating energy imbalances in the balancing market. The reserve cost for overestimation and the penalty cost for underestimation of renewable generations are considered in the cost modeling to further reduce the energy imbalances. All these ensure secure operation and management of microgrid in real-time energy market and enhance economic security of microgrid operators as well as consumers. The precise modeling of the microgrid components, numerous technical and management constraints, and intricate uncertainties results into a complex MINLP bidding strategy problem with a lot of binary variables. Hence, the bidding optimization is solved using the soft computing solver LINDOGlobal in GAMS. The risk of competing in day-ahead and real-time energy markets is investigated through the CVaR and sensitivity analysis of expected profit for several values of ω. Moreover, the VSS indicator is evaluated to validate the efficacy of the stochastic solutions of the proposed bidding of microgrid. Sensitivity analysis of the market participation profit with the variation of force outage probability is also performed to indicate the significance of renewable energy capacity on bidding schedules.

The outage and uncertainty modeling and their incorporation for power system security analysis during bidding is a vast field. It can not be completely researched in a single work. Some limitations still persist regarding the works as stated earlier in the section 4.2.3. As a result, the proposed bidding strategy modeling and the outage-based sensitivity analysis have the following inferences for the future practice.

- To trounce the climatic fluctuations and consequences on the efficacy of the bidding strategy planning for microgrids, the projected DRP modeling based on uncertainties and outages of renewable energy resources may be applied.
- Market operators and MGCC can comprehend the efficient models to diminish the consequences of outages of renewable energy resources into the network.
- Outage dependent sensitivity analysis can be deployed by system operators to compare the variation of FOP limits by which microgrid operators can compare the impact of implementation of different FOP limits as required.

5.2 Future scope of the work

There exist countless scopes to research in the area of power system security presently. With the drastic gain in renewable energy share in energy sector in near future unknown and complex security issues may arise which may need serious attention. Need of more secure power system design, generation-load scheduling and planning, energy market modeling, operation and management planning and policy making considering component outages and uncertainties of renewable energy systems, is evident.

The designing of renewable integrated power system involves many socio-techno-economic security parameters, *viz.*, human development index, job creation, emission, renewable fraction, loss of power supply probability, economic security, and many others. The outage and uncertainties of renewable energy can fail the long-term design planning, management and operation of the system. Hence, after precise long-term forecasting, uncertainties related to renewable generations and their outages can be modelled and incorporated in system design. Reserve and penalty cost can also be considered for cost modelling.

As noted earlier, efficient demand side management can facilitate better economic performance of bidding strategy and operation of the system which can be achieved through proficient load shedding scheme. Modern power system is based on dense incorporation of distributed generations (DG). But for the shake of under frequency load shedding (UFLS), if DG connected buses are isolated from the system that can cause more adverse situation. In that case, supplied power from DGs connected with the shed buses will also be separated from the main system. Thus, further loss of generation from the system by conventional UFLS methods can further reduce the frequency of the system. So, new load shedding scheme considering proper bus selection can be modelled in future.

Therefore, different power system contingency phenomenon likes load shedding, frequency errors, harmonic injection, power quality issues, faults analysis of different power system components and so on also necessitate more research for overall socio-techno-economic security of power system. Research on these power system security areas (alongside with several others) may be executed extending the basis of the works presented in this thesis.

This page is left blank intentionally.

References

[1] Billinton R, Allan RN, Salvaderi L (1991). *Applied reliability assessment in electrical power systems*. IEEE Press, New York.

[2] Li, W. (2014). Outage models of system components.

[3] Lin, J., Cheng, L., Chang, Y., Zhang, K., Shu, B., & Liu, G. (2014). Reliability based power systems planning and operation with wind power integration: A review to models, algorithms and applications. *Renewable and Sustainable Energy Reviews*, *31*, 921-934.

[4] Zadeh, L. A. (1996). Soft computing and fuzzy logic. In *Fuzzy Sets, Fuzzy Logic, and Fuzzy Systems: Selected Papers by Lotfi a Zadeh* (pp. 796-804).

[5] Iea. (n.d.). Renewables 2020 – Analysis. Retrieved from https://www.iea.org/reports/renewables-2020.

[6] Hare, J., Shi, X., Gupta, S., & Bazzi, A. (2016). Fault diagnostics in smart micro-grids: A survey. *Renewable and Sustainable Energy Reviews*, *60*, 1114-1124.

[7] Platon, R., Martel, J., Woodruff, N., & Chau, T. Y. (2015). Online Fault Detection in PV Systems. *IEEE Transactions on Sustainable Energy*, *6*(4), 1200-1207.

[8] Silvestre, S., da Silva, M. A., Chouder, A., Guasch, D., & Karatepe, E. (2014). New procedure for fault detection in grid connected PV systems based on the evaluation of current and voltage indicators. *Energy Conversion and Management*, *86*, 241-249.

[9] Silvestre, S., Kichou, S., Chouder, A., Nofuentes, G., & Karatepe, E. (2015). Analysis of current and voltage indicators in grid connected PV (photovoltaic) systems working in faulty and partial shading conditions. *Energy*, *86*, 42-50.

[10] Silvestre, S., Mora-López, L., Kichou, S., Sánchez-Pacheco, F., & Dominguez-Pumar, M. (2016). Remote supervision and fault detection on OPC monitored PV systems. *Solar Energy*, *137*, 424-433.

[11] Gokmen, N., Karatepe, E., Celik, B., & Silvestre, S. (2012). Simple diagnostic approach for determining of faulted PV modules in array based PV arrays. *Solar energy*, *86*(11), 3364-3377.

[12] Chine, W., Mellit, A., Pavan, A. M., & Kalogirou, S. A. (2014). Fault detection method for grid-connected photovoltaic plants. *Renewable Energy*, *66*, 99-110.

[13] Gokmen, N., Karatepe, E., Silvestre, S., Celik, B., & Ortega, P. (2013). An efficient fault diagnosis method for PV systems based on operating voltage-window. *Energy conversion and management*, *73*, 350-360.

[14] Stellbogen, D. (1993, May). Use of PV circuit simulation for fault detection in PV array fields. In *Photovoltaic Specialists Conference, 1993., Conference Record of the Twenty Third IEEE* (pp. 1302-1307). IEEE.

[15] Davarifar, M., Rabhi, A., El Hajjaji, A., & Dahmane, M. (2013, October). New method for fault detection of PV panels in domestic applications. In *3rd International Conference on Systems and Control* (pp. 727-732). IEEE.

[16] Rezgui, W., Mouss, N. K., Mouss, L. H., Mouss, M. D., Amirat, Y., & Benbouzid, M. (2014, November). Modeling the PV generator behavior submit to the open-circuit and the short-circuit faults. In *Environmental Friendly Energies and Applications (EFEA), 2014 3rd International Symposium on* (pp. 1-6). IEEE.

[17] Rezgui, W., Mouss, H., Mouss, N., Mouss, D., Benbouzid, M., & Amirat, Y. (2015, June). Photovoltaic module simultaneous open-and short-circuit faults modeling and detection using the I–V characteristic. In *2015 IEEE 24th International Symposium on Industrial Electronics (ISIE)* (pp. 855-860). IEEE.

[18] Rezgui, W., Mouss, N. K., Mouss, L. H., Mouss, M. D., Amirat, Y., & Benbouzid, M. (2015, May). Smart diagnosis algorithm of the open-circuit fault in a photovoltaic generator. In *Control, Engineering & Information Technology (CEIT), 2015 3rd International Conference on* (pp. 1-5). IEEE.

[19] Chine, W., Mellit, A., Pavan, A. M., & Lughi, V. (2015, June). Fault diagnosis in photovoltaic arrays. In *Clean Electrical Power (ICCEP), 2015 International Conference on* (pp. 67-72). IEEE.

[20] Silvestre, S., Chouder, A., & Karatepe, E. (2013). Automatic fault detection in grid connected PV systems. *Solar Energy*, *94*, 119-127.

[21] Hariharan, R., Chakkarapani, M., Ilango, G. S., & Nagamani, C. (2016). A Method to Detect Photovoltaic Array Faults and Partial Shading in PV Systems. *IEEE Journal of Photovoltaics*, *6*(5), 1278-1285.

[22] Chine, W., Mellit, A., Lughi, V., Malek, A., Sulligoi, G., & Pavan, A. M. (2016). A novel fault diagnosis technique for photovoltaic systems based on artificial neural networks. *Renewable Energy*, *90*, 501-512.

[23] Karatepe, E., & Hiyama, T. (2011, September). Controlling of artificial neural network for fault diagnosis of photovoltaic array. In *Intelligent System Application to Power Systems (ISAP), 2011 16th International Conference on* (pp. 1-6). IEEE.

[24] Li, X., Yang, P., Ni, J., & Zhao, J. (2014, June). Fault diagnostic method for PV array based on improved wavelet neural network algorithm. In *Intelligent Control and Automation (WCICA), 2014 11th World Congress on* (pp. 1171-1175). IEEE.

[25] Jiang, L. L., & Maskell, D. L. (2015, July). Automatic fault detection and diagnosis for photovoltaic systems using combined artificial neural network and analytical based methods. In *2015 International Joint Conference on Neural Networks (IJCNN)* (pp. 1-8). IEEE.

[26] Rezgui, W., Mouss, L. H., Mouss, N. K., Mouss, M. D., & Benbouzid, M. (2014, March). A smart algorithm for the diagnosis of short-circuit faults in a photovoltaic generator. In *2014 First International Conference on Green Energy ICGE 2014* (pp. 139-143). IEEE.

[27] Zhao, Y., Ball, R., Mosesian, J., de Palma, J. F., & Lehman, B. (2015). Graph-based semi-supervised learning for fault detection and classification in solar photovoltaic arrays. *IEEE Transactions on Power Electronics*, *30*(5), 2848-2858.

[28] Takashima, T., Yamaguchi, J., Otani, K., Oozeki, T., Kato, K., & Ishida, M. (2009). Experimental studies of fault location in PV module arrays. *Solar Energy Materials and Solar Cells*, *93*(6), 1079-1082.

[29] Takashima, T., Otani, K., Sakuta, K., Yamada, T., Igarashi, T., Hasegawa, K., ... & Yamaguchi, T. (2003, May). Electrical detection and specification of failed modules in PV array. In *Photovoltaic Energy Conversion, 2003. Proceedings of 3rd World Conference on* (Vol. 3, pp. 2276-2279). IEEE.

[30] Takashima, T., Yamaguchi, J., Otani, K., Kato, K., & Ishida, M. (2006, May). Experimental studies of failure detection methods in PV module arrays. In *2006 IEEE 4th World Conference on Photovoltaic Energy Conference* (Vol. 2, pp. 2227-2230). IEEE.

[31] Schirone, L., Califano, F. P., Moschella, U., & Rocca, U. (1994, December). Fault finding in a 1 MW photovoltaic plant by reflectometry. In *Photovoltaic Energy Conversion, 1994., Conference Record of the Twenty Fourth. IEEE Photovoltaic Specialists Conference-1994, 1994 IEEE First World Conference on* (Vol. 1, pp. 846-849). IEEE.

[32] Takashima, T., Yamaguchi, J., & Ishida, M. (2008, May). Fault detection by signal response in PV module arrays. In *Photovoltaic Specialists Conference, 2008. PVSC'08. 33rd IEEE* (pp. 1-5). IEEE.

[33] Alam, M. K., Khan, F., Johnson, J., & Flicker, J. (2013, September). PV ground-fault detection using spread spectrum time domain reflectometry (SSTDR). In *2013 IEEE Energy Conversion Congress and Exposition* (pp. 1015-102). IEEE.

[34] Hu, Y., Cao, W., Ma, J., Finney, S. J., & Li, D. (2014). Identifying PV module mismatch faults by a thermography based temperature distribution analysis. *IEEE Transactions on Device and Materials Reliability*, *14*(4), 951-960.

[35] Zou, Z., Hu, Y., Gao, B., Woo, W. L., & Zhao, X. (2014). Study of the gradual change phenomenon in the infrared image when monitoring photovoltaic array. *Journal of Applied Physics*, *115*(4), 1-11.

[36] Photovoltaics and Electricity. Photovoltaics and Electricity - Energy Explained, Your Guide To Understanding Energy - Energy Information Administration.

[37] Smith, M., & Ton, D. (2013). Key connections: The U.S. department of energy? Microgrid initiative. IEEE Power and Energy magazine, 11(4), 22-27.

[38] Zheng, Y., Jenkins, B. M., Kornbluth, K., Kendall, A., & Træholt, C. (2018). Optimization of a biomass-integrated renewable energy microgrid with demand side management under uncertainty. *Applied Energy*, *230*, 836-844.

[39] Fazlalipour, P., Ehsan, M., & Mohammadi-Ivatloo, B. (2019). Risk-aware stochastic bidding strategy of renewable micro-grids in day-ahead and real-time markets. *Energy*, *171*, 689-700.

[40] Salkuti, S. R. (2019). Day-ahead thermal and renewable power generation scheduling considering uncertainty. *Renewable energy*, *131*, 956-965.

[41] Kaviani, A. K., Riahy, G. H., & Kouhsari, S. M. (2009). Optimal design of a reliable hydrogen-based stand-alone wind/PV generating system, considering component outages. *Renewable energy*, *34*(11), 2380-2390.

[42] Lim, Y., & Kim, H. M. (2014). Strategic bidding using reinforcement learning for load shedding in microgrids. *Computers & Electrical Engineering*, *40*(5), 1439-1446.

[43] Shayeghi, H., & Sobhani, B. (2014). Integrated offering strategy for profit enhancement of distributed resources and demand response in microgrids considering system uncertainties. *Energy conversion and management*, *87*, 765-777.

[44] Ferruzzi, G., Cervone, G., Delle Monache, L., Graditi, G., & Jacobone, F. (2016). Optimal bidding in a Day-Ahead energy market for Micro Grid under uncertainty in renewable energy production. *Energy*, *106*, 194-202.

[45] Wang, J., Zhong, H., Tang, W., Rajagopal, R., Xia, Q., Kang, C., & Wang, Y. (2017). Optimal bidding strategy for microgrids in joint energy and ancillary service markets considering flexible ramping products. *Applied Energy*, *205*, 294-303.

[46] Mehdizadeh, A., & Taghizadegan, N. (2017). Robust optimisation approach for bidding strategy of renewable generation-based microgrid under demand side management. *IET Renewable Power Generation*, *11*(11), 1446-1455.

[47] Shi, L., Luo, Y., & Tu, G. Y. (2014). Bidding strategy of microgrid with consideration of uncertainty for participating in power market. *International Journal of Electrical Power & Energy Systems*, *59*, 1-13.

[48] Nguyen, D. T., & Le, L. B. (2014). Optimal bidding strategy for microgrids considering renewable energy and building thermal dynamics. *IEEE Transactions on Smart Grid*, *5*(4), 1608-1620.

[49] Liu, G., Xu, Y., & Tomsovic, K. (2016). Bidding strategy for microgrid in day-ahead market based on hybrid stochastic/robust optimization. IEEE Transactions on Smart Grid, 7(1), 227-237.

[50] Zhao, T., Pan, X., Yao, S., Ju, C., & Li, L. (2018). Strategic Bidding of Hybrid AC/DC Microgrid Embedded Energy Hubs: A Two-stage Chance Constrained Stochastic Programming Approach. *IEEE Transactions on Sustainable Energy*.

[51] Fazlalipour, P., Ehsan, M., & Mohammadi-Ivatloo, B. (2019). Risk-aware stochastic bidding strategy of renewable micro-grids in day-ahead and real-time markets. *Energy*, *171*, 689-700.

[52] An, D., Yang, Q., Yu, W., Yang, X., Fu, X., & Zhao, W. (2017). Sto2auc: A stochastic optimal bidding strategy for microgrids. *IEEE Internet of Things Journal*, *4*(6), 2260-2274.

[53] Faqiry, M. N., & Das, S. (2018). Double auction with hidden user information: Application to energy transaction in microgrid. *IEEE Transactions on Systems, Man, and Cybernetics: Systems*, (99), 1-14.

[54] Pei, W., Du, Y., Deng, W., Sheng, K., Xiao, H., & Qu, H. (2016). Optimal bidding strategy and intramarket mechanism of microgrid aggregator in real-time balancing market. *IEEE Transactions on Industrial Informatics*, *12*(2), 587-596.

[55] Rezaei, N., Ahmadi, A., Khazali, A., & Aghaei, J. (2018). Multi-objective risk-constrained optimal bidding strategy of smart microgrids: An IGDT-based normal boundary intersection approach. *IEEE Transactions on Industrial Informatics*.

[56] Zhang, D., Li, S., Zeng, P., & Zang, C. (2014). Optimal microgrid control and power-flow study with different bidding policies by using powerworld simulator. *IEEE Transactions on Sustainable Energy*, *5*(1), 282-292.

[57] Dupačová, J., Gröwe-Kuska, N., & Römisch, W. (2003). Scenario reduction in stochastic programming Mathematical programming, 95(3), 493-511.

[58] Dupačová, J., Gröwe-Kuska, N., Römisch, W.: "Scenario reduction in stochastic programming"*Mathematical Programming*, 2003, **95**, (3), pp. 493–511.

[59] Schuster HG. Deterministic chaos: an introduction. 2nd revised ed. PhysickVerlag Gmnh; 1988. D 6940 Weinheim, Federal Republic of Germany.

[60] Gokhale, S. S., & Kale, V. S. (2016). An application of a tent map initiated Chaotic Firefly algorithm for optimal overcurrent relay coordination. *International Journal of Electrical Power & Energy Systems*, *78*, 336-342.

[61] May, R. M. (1976). Simple mathematical models with very complicated dynamics. Nature, 261(5560), 459.

[62] Li, W. (2014). Risk assessment of power systems: models, methods, and applications. John Wiley & Sons.

[63] Hu, Y., Zhang, J., Cao, W., Wu, J., Tian, G. Y., Finney, S. J., & Kirtley, J. L. (2015). Online two-section PV array fault diagnosis with optimized voltage sensor locations. *IEEE Transactions on Industrial Electronics*, *62*(11), 7237-7246.

[64] Hachana, O., Hemsas, K. E., & Tina, G. M. (2015, March). Fault diagnosis of building integrated PV generator: A metaheuristic technique. In *Renewable Energy Congress (IREC), 2015 6th International* (pp. 1-6). IEEE.

[65] Hachana, O., Tina, G. M., & Hemsas, K. E. (2016). PV array fault DiagnosticTechnique for BIPV systems. *Energy and Buildings*, *126*, 263-274.

[66] Chang, W. D. (2006). An improved real-coded genetic algorithm for parameters estimation of nonlinear systems. *Mechanical Systems and Signal Processing*, *20*(1), 236-246.

[67] Lin, C. H., Huang, C. H., Du, Y. C., & Chen, J. L. (2011). Maximum photovoltaic power tracking for the PV array using the fractional-order incremental conductance method. *Applied Energy*, *88*(12), 4840-4847.

[68] Mattei, M., Notton, G., Cristofari, C., Muselli, M., & Poggi, P. (2006). Calculation of the polycrystalline PV module temperature using a simple method of energy balance. *Renewable energy*, *31*(4), 553-567.

[69] Sinapis, K., Tzikas, C., Litjens, G., van den Donker, M., Folkerts, W., van Sark, W. G. J. H. M., & Smets, A. (2016). A comprehensive study on partial shading response of c-Si modules and yield modeling of array inverter and module level power electronics. *Solar Energy*, *135*, 731-741.

[70] Reddy, S. S., Bijwe, P. R., & Abhyankar, A. R. (2015). Real-time economic dispatch considering renewable power generation variability and uncertainty over scheduling period. *IEEE Systems journal*, *9(4)*, 1440-1451.

[71] Seguro, J. V., & Lambert, T. W. (2000). Modern estimation of the parameters of the Weibull wind speed distribution for wind energy analysis. *Journal of Wind Engineering and Industrial Aerodynamics*, *85(1)*, 75-84.

[72] Javed, F., Arshad, N., Wallin, F., Vassileva, I., & Dahlquist, E. (2012). Forecasting for demand response in smart grids: An analysis on use of anthropologic and structural data and short term multiple loads forecasting. *Applied Energy*, *96*, 150–160.

[73] Xiao, H., Gao, J., Li, Q., Ma, F., Su, L., Feng, Y., & Zhang, A. (2019). Towards confidence interval estimation in truth discovery. *IEEE Transactions on Knowledge and Data Engineering*, *31*(3), 575-588.

[74] Hajibandeh N, Shafie-Khah M, Talari S, Dehghan S, Amjady N, Mariano SJPS, et al. (2019). Demand Response-Based Operation Model in Electricity Markets With High Wind Power Penetration. *IEEE Transactions on Sustainable Energy*, *10*, 918–30.

[75] Wang, Y., & Li, L. (2013). Time-of-use based electricity demand response for sustainable manufacturing systems. *Energy*, *63*, 233-244.

[76] Dehnavi, E., & Abdi, H. (2016). Optimal pricing in time of use demand response by integrating with dynamic economic dispatch problem. *Energy*, *109*, 1086-1094.

[77] "Annual Report, Prepared by Summit Blue Consulting, Submitted to Ameren Illinois Utilities. Power Smart Pricing 2009," 27-Apr-2010. [Online]. Available: https://www.illinois.gov/sites/ipa/Documents/CUB-Comments-Appendix-D-2009-Navigant-Power-Smart-Pricing-Annual-Report.pdf. [Accessed: 01-Nov-2017].

[78] Aalami, H, Moghaddam, M. P., & Yousefi, G. (2010). Demand response modeling considering Interruptible/Curtailable loads and capacity market programs. *Applied Energy, 87(1);* 243–250.

[79] Holland, J. H. (1975). *Adaptation in natural and artificial systems: an introductory analysis with applications to biology, control, and artificial intelligence*. U Michigan Press.

[80] Golberg, D. E. (1989). Genetic algorithms in search, optimization, and machine learning. *Addion wesley*, *1989*, 102.

[81] Deb, K., & Agrawal, R. B. (1994). Simulated binary crossover for continuous search space. *Complex Systems*, *9*(3), 1-15.

[82] Herrera, F., Lozano, M., & Verdegay, J. L. (1998). Tackling real-coded genetic algorithms: Operators and tools for behavioural analysis. *Artificial intelligence review*, *12*(4), 265-319.

[83] Bussieck, M. R., & Vigerske, S. (2010). MINLP solver software. *Wiley encyclopedia of operations research and management science*.

[84] Lin, Y., & Schrage, L. (2009). The global solver in the LINDO API. *Optimization Methods & Software*, *24*(4-5), 657-668.

[85] Introduction. (n.d.). Retrieved from https://www.gams.com/latest/docs/S_LINDO.html

[86] Das, S., Hazra, A., & Basu, M. (2018). Metaheuristic optimization based fault diagnosis strategy for solar photovoltaic systems under non-uniform irradiation. *Renewable energy*, *118*, 452-467.

[87] Lazard's Levelized Cost of Energy Analysis - Version 12.0. *Lazard*. 2018-11-02.

[88] Lazard's Levelized Cost of Storage Analysis - Version 4.0. *Lazard*. 2018-11-02.

[89] Bara Bazar Monthly Weather Forecast. The Weather Channel 2018. https://weather.com/en-IN/weather/monthly/l/INWB0120:1:IN (accessed May 6, 2018).

[90] Das, S., & Basu, M. (2020). Day-ahead optimal bidding strategy of microgrid with demand response program considering uncertainties and outages of renewable energy resources. *Energy*, *190*, 116441.

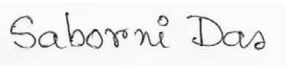

Signature of the Candidate:

Date: 29.06.2021